The Water Trimer

Frank N. Keutsch,† Jeffery D. Cruzan,† and Richard J. Saykally*

Department of Chemistry, University of California, Berkeley, California 94720

Received November 25, 2002

Contents

I. Introduction

Non-pairwise-additive or cooperative intermolecular forces may account for up to 25% of the cohesive energy of bulk-phase water, most of which result from three-body effects.[1] Because the isolated water trimer is not affected by higher-order nonadditive interactions, it is the obvious prototype for a detailed examination of the three-body forces operative in liquid water and ice, even though cyclic structures resembling the water trimer are not themselves an important constituent of liquid water and ice. Many sophisticated simulation efforts have shown that inclusion of non-pairwise-additive intermolecular forces is crucial in order to faithfully reproduce all of the enigmatic properties of water. Efforts to properly incorporate cooperativity into the model potential functions have recently been aided by a profusion of experimental data on gas-phase water clusters.[2] Ultimately, a major goal of this water cluster research is the determination of a "universal" intermolecular potential energy surface (IPS) that is both sufficiently accurate to reproduce the high-resolution cluster spectra and sufficiently general to yield reliable bulk-phase water simulations, wherein computational time constraints restrict the complexity that can be tolerated in a potential function.

The early theoretical work of Frank and Wen[3] predicted that formation of a single hydrogen bond (H-bond) in liquid water should facilitate formation of additional adjacent H-bonds, and that the cohesive energy gained from H-bonding should be proportional to the number of adjacent H-bonds in a network. Although the detailed picture presented by those early authors has evolved substantially, there is modern consensus that liquid water exists as a continuously rearranging H-bonded network and that inclusion of many-body forces into the model potentials is necessary to arrive at a realistic simulation.[1,4−15] Indeed, it has recently been shown that energy ordering of the various possible equilibrium structures of water clusters larger than the pentamer (a quasiplanar ring) is strongly dependent upon inclusion of three-body forces in the model potentials.[16]

The water trimer IPS can be broken down into a sum of two- and three-body interactions:

$$V_{\text{trimer}} = V_{\text{AB}} + V_{\text{BC}} + V_{\text{AC}} + V_{\text{ABC}} \qquad (1)$$

where A, B, and C label the monomers, and V_{XY} and V_{ABC} are two- and three-body terms, respectively. More recent efforts have approached the problem of determining the water dimer IPS (V_{XY}) by comparing a variety of parametrized trial IPS's to the dimer spectra and iteratively adjusting those parameters to achieve a faithful reproduction of the experimental data. Ultimately, convergence to the full experimental precision (<0.001 cm^{-1} in some experiments) is

* Corresponding author. Phone: (510) 642-8269. E-mail: saykally@uclink4.berkeley.edu.
† Present address: Department of Chemistry and Chemical Biology, Harvard University, Cambridge, MA 02138.

10.1021/cr980125a CCC: $44.00
Published on Web 06/10/2003

Frank Keutsch received his Diplom in chemistry from the Technical University of Munich, Germany, in 1997, under the supervision of Vladimir E. Bondybey. He received his Ph.D. in physical chemistry from the University of California at Berkeley in 2001. His graduate research was conducted under the direction of Richard J. Saykally and focused on vibration–rotation–tunneling spectroscopy and hydrogen-bond-breaking dynamics in water clusters. At present, he is a research associate in the Department of Chemistry and Chemical Biology at Harvard University (Cambridge, MA) under the direction of James G. Anderson.

Born in Rhinelander, Wisconsin, and educated at University of Wisconsin–Eau Claire and University of Wisconsin–Madison, Saykally has been a professor at the University of California–Berkeley since 1979. He and his students pioneered important advances in laser spectroscopy, including velocity modulation spectroscopy of ions, terahertz laser vibration–rotation–tunneling spectroscopy of clusters, infrared photon counting spectroscopy, and infrared cavity ringdown spectroscopy. These have permitted the first detailed study of important textbook molecules, including the hydronium (H_3O^+), hydroxide (OH^-), and ammonium (NH_4^+) ions, small water clusters, and carbon clusters. Recent work includes the spectroscopic determination of the water pair potential, the development of femtosecond nonlinear molecular imaging microscopy, and X-ray spectroscopy of liquid surfaces. A coauthor of over 250 publications and the recipient of over 30 honors and awards, Saykally is a member of the National Academy of Sciences and the American Academy of Arts and Sciences, and has recently received the Langmuir Prize in Chemical Physics from the American Chemical Society and the Centenary Medal of the UK Royal Society of Chemistry. He is a UC–Berkeley Distinguished Teacher, has been active at the national level in science education, and has mentored over 100 Ph.D.'s and postdocs. Saykally currently holds the Class of 1932 Distinguished Chair in the Department of Chemistry.

sought. By employing a multidimensional scattering Hamiltonian in which all six of the global intermolecular coordinates (rigid monomers) are fully coupled and can be fully sampled, the complete "anharmonicity" of the intermolecular potential is rigorously treated. The approach to constructing the trimer IPS is necessarily different, since a similar 12-D trimer calculation is not presently feasible due to the unfavorable size scaling of the Hamiltonian matrix. Therefore, determining the IPS's of the trimer and larger water clusters may involve first extracting the pairwise-additive components of eq 1 and then quantifying the remaining three-body terms from the experimental results and theoretical predictions.

A quantitative understanding of how induction, dispersion, and exchange intermolecular forces contribute to the nonadditive part of the potential functions of aqueous systems constitutes the essence of these efforts. For the most part, theoretical studies of small water clusters have shown that expansions of the IPS's in terms of 3-, 4-, ... n-body forces is rapidly convergent, with the four-body term accounting for only about 1% of the total cohesive energy of cyclic tetramers and pentamers. In contrast, three-body interactions probably contribute as much as 20% toward the total stabilization of the trimer.[17]

Gas-phase spectroscopy has proved to be a key source of experimental data on the structures, energetics, and dynamics of weakly bound clusters and has led directly to determination of reliable IPS's for several dimer systems (an excellent overview is also given in the review by Wormer and van der Avoird[18]).[19−23] In particular, terahertz (THz) vibration−rotation−tunneling (VRT) spectroscopy has proved to be a valuable tool for direct interrogation of the intermolecular vibrational eigenstates supported by H-bonds in water clusters, and for measurement of the H-bond network rearrangement (HBNR) dynamics.[24] Nonadditivity in cluster potentials has directly observable consequences in high-resolution spectroscopic data. For example, a number of high-level calculations of small water cluster properties have predicted a sequential contraction of the interoxygen separation (R_{OO}), as well as a significant increase in the per-monomer binding energy ($\Delta E^{(mon)}$), as a function of increasing cluster size. The interoxygen contraction in cyclic water clusters has been predicted to converge to the liquid-phase values by $n = 5$ or 6.[25,26] Indeed, when the water cluster VRT data are viewed together,[24] not only is the predicted structural contraction observed, but the number of spectral features indicative of floppy dynamics (vide infra) is also reduced as the cluster size increases, implying sequentially more tightly bound complexes.

The nature of the low-frequency VRT data, which constitute the bulk of the experimental water trimer measurements, has been a source of considerable experimental and theoretical confusion since the initial VRT study.[27] Experimentally, the spectra are characterized by a variety of strong perturbations in the form of energy level shifts and/or splittings, due to interactions of internal HBNR dynamics with overall rotation of the complex. Those effects substantially hindered efforts to assign the first water trimer VRT spectrum. Theoretical efforts to rationalize the data have also been impeded by the complexity of the exact Hamiltonian for a weakly bound trimer of three-dimensional monomers,[25] and specifically by the high density of, and lack of experimentally established connections between, the VRT energy levels. The recent work of van der Avoird and

co-workers has been vital for the global analysis of all of the existing trimer VRT spectroscopic data, providing much of the basis for the last part of this review.[28,29]

This article is intended to provide an overview of the extensive water trimer literature, beginning with the earliest theoretical studies and experimental observations. In addition to theoretical efforts focused explicitly on water clusters, theoretical simulations of liquid water have also been instrumental in motivating water cluster research by establishing the importance of nonadditive intermolecular forces in water. Those studies will be briefly reviewed. A more detailed survey of theoretical studies directly relevant to the water trimer, including the development of both empirical and ab initio potential energy surfaces, will be presented in the following section. The second half of this article will focus mainly on efforts designed to untangle the facile HBNR dynamics that have characterized the high-resolution THz-VRT data. A brief summary of the salient group-theoretical results will precede a discussion of efforts to model the low-frequency H-bond torsional dynamics, which are responsible for the high density of low-frequency states observed in the trimer spectra.

II. Theoretical Studies

A. Bulk-Phase Simulations

Beginning with the "flickering clusters" model of Frank and Wen,[3] many studies have sought to characterize the structural nature of liquid water. This early theory predicted that water H-bonding is highly cooperative and characterized liquid water as having localized regions of H-bonded monomers surrounded by regions of relatively unassociated monomers. While the notion of H-bond cooperativity has survived, the view of liquid water as comprising networks of small clusters has evolved considerably. Employing a lattice statistical model, Perram and Levine[30] concluded that the opposite of the flickering clusters model must be more accurate, viz. that regions of unassociated waters must be rare amid regions of dense H-bonding. That conclusion is consistent with simple thermodynamic arguments showing that only about 10% of the H-bonds in ice are broken in the solid-to-liquid-phase transition at 0 °C.

Simplified empirical potential functions are obviously attractive for modeling purposes, wherein calculation of the potential energy must occupy as little computational time as possible. In work that has constituted a large part of more recent modeling efforts, numerous groups have constructed empirical water potentials, many of which will be discussed in the next section. Using one such potential, the pairwise-additive ST2 function,[31,32] Rahman and Stillinger[33] examined distributions of identifiable H-bonded clusters, defined as non-short-circuited polygons traceable in a simulated H-bonded water network. They found that for reasonable energetic and geometric definitions of a H-bond, small polygons, particularly pentamers and hexamers, dominated the distributions, with cyclic trimers playing an insignificant role. They concluded that, "liquid water consists of a spatially homogenous, random hydrogen-bonded network in which no recognizable crystal patterns (are) resolved." In a series of contributions, Scheraga and co-workers[34−39] developed additive statistical thermodynamic simulations of water using cluster models, considering the properties of liquid water and of water as a solvent for both hydrophilic and hydrophobic solutes. They also observed a preponderance of five- and six-membered clusters in most simulations.

Many subsequent simulations, notably those of Ohmine,[40−46] Sceats,[47−52] and Speedy[53,54] and their co-workers, built upon those early studies, incorporating H-bond rearrangement dynamics into the analyses. Ohmine's review article[41] gives an excellent overview of structure and HBNR dynamics in both simulated water and experiments. Using classical Monte Carlo simulations, Jorgensen and co-workers compared several early effective pair potentials constructed with point charge models.[55] They found reasonable agreement with several liquid water observables for the TIP(S2, 3P, 4P),[56,57] SPC, and ST2[31,32] potentials. Further improvements of these models were introduced in the SPC/E[58] and more recent TIP5P[59] potentials. These are considered two of the best current simple potentials. Studies by Clementi and co-workers[4−12] and others[13−15] showed that the geometric pair correlation functions, g_{OO}, g_{OH}, and g_{HH}, as well as other liquid properties, including the anomalous heat capacity of supercooled water, are better simulated by model potentials that include three-body contributions to the potential energy.

B. Structure and Energetics of Water Clusters

Both empirical- and ab initio-calculated potential functions have been employed to model the structures and properties of water clusters. The first goal of such calculations has usually been to determine the equilibrium structures. In pointing out difficulties with ab initio cluster calculations, Schütz and co-workers[60] noted that molecular cluster geometry optimizations suffer from three main problems as the number of subunits increases: (1) the number of local IPS minima grows approximately exponentially with the number of constituents in the complex, (2) the coupling of inter- and intramolecular degrees of freedom slows convergence of the calculations, and (3) basis set superposition errors (BSSE) are a significant contaminant of the resultant energies at levels of theory higher than Hartree−Fock (HF). The first point argues for simplified potential functions. Therefore, calculations using empirical potentials, based either on bulk-phase properties or on a set of ab initio-calculated points, emerged early as a way to search the configuration spaces efficiently. Nevertheless, the most detailed structural and energetic information on water clusters to date has come from high-level ab initio methods, sometimes guided by results of empirical optimizations. In turn, the ab initio calculations, along with the experimental data, serve to evaluate the accuracy of the empirical IPS's. The following sections will review the development of empirical potentials and ab initio theory as they have applied to the water trimer and three-body

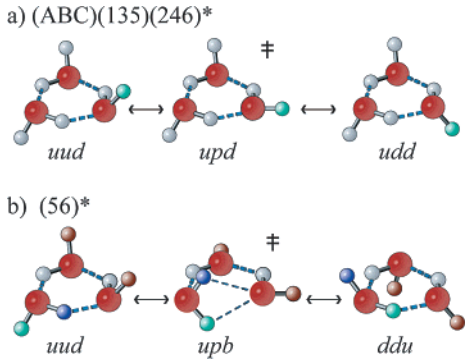

Figure 2. The H-bond network rearrangement (HBNR) dynamics that feature prominently in high-resolution FIR spectra of the water trimer include (a) H-bond torsion, flipping of the non-H-bonded protons between sides of the O−O−O plane via the *upd* transition state, and (b) bifurcation or donor tunneling, an exchange of the H-bonded and free protons of one monomer. H-bond torsion (a) occurs on a femtosecond time scale, such that many periods are averaged during any intermolecular vibration. The calculated ab initio barrier for flipping is ca. 63−133 cm^{-1} (see Table 2), which is close to or below the ZPE of the trimer. H-bond torsion has been shown to generate a manifold of low-frequency pseudorotational states, which superimpose upon any other intermolecular vibration. The transition state, referred to as *upb*, for bifurcation tunneling (b) is one in which the H-bond formed by the water in question is bifurcated. The calculated ab initio barrier for bifurcation tunneling is ca. 640−760 cm^{-1} (see Table 2), which is close to or below the ZPE of the trimer. The bifurcation pathway shown here is in agreement with the analysis of experimental splittings (see section III.B.1.4)[192] and includes a double flip (of the other water molecules), but high-level ab initio calculations do not agree on how many flipping motions occur on the low-energy pathway.

Figure 1. (a) The gas-phase water trimer adopts a cyclic, homodesmic, quasiplanar ring structure with C_1 symmetry (n.b. and is therefore chiral). The interoxygen separation R_{OO}, the out-of-plane H-bond angle χ, the H-bond out-of-plane angle γ (MP2/aug-cc-pVQZ)[170], and the H-bonding angle δ (MP2/aug-cc-pVDZ)[17] are defined. Throughout this review, the notation of Schütz et al.[61] is adopted to describe the free H positions: The equilibrium configuration is (*uud*), where "*u*" and "*d*" denote a free proton above and below the O−O−O plane, respectively. Similarly, the notation "*p*" denotes a free proton in the O−O−O plane (see Figure 2a), and "*b*" refers to a water monomer, which acts as a double hydrogen bond donor (see Figure 2b). The arrangement (*uud*) actually belongs to a set of six such equivalent conformations. (b) The planar reference geometry (C_{3h} symmetry, *ppp*) and coordinate system of van der Avoird et al.[28] are adopted for all discussions in this review. The centers of mass (μ_X) of each water monomer are exaggerated from their real positions. The axes $\{h_n\}$, connecting the water monomer centers of mass with the centers of the H-bonded protons, define the H-bond torsional or "flipping" axes described by the coordinates $\{\chi_{A,B,C}\}$.

forces in water. A nomenclature that was first introduced by Schütz et al.[61] for important torsional minima and transitions states of the cyclic water trimer will be introduced here (and explained in detail in section II.C). The global minimum corresponds to the cyclic C_1 structure shown in Figure 1a, with two hydrogens above the plane (up or "*u*") defined by the oxygens and one hydrogen below this plane (down or "*d*"). This torsional reference structure will be referred to as *uud*. Similarly, a structure with all hydrogens on the same side of the plane (crown) will be referred to as either *uuu* or *ddd*, and the structure with one hydrogen above the plane, one hydrogen in the plane ("*p*"), and one hydrogen below the plane (flip transition state, see Figure 2a) will be referred to as *upd*. Finally, the structure with one hydrogen in the plane, one water molecule acting as a double H-bond donor, and one water molecule acting as a double H-bond acceptor with the free hydrogen in the plane (bifurcation-tunneling transition state, see Figure 2b) will be referred to as *upb*. Even though the exact details of the transition state vary according to the level of theory, the bifurcation transition state will be referred to as *upb*.

1. Empirical Potentials

Whereas the requisite theoretical framework for explicitly inverting the VRT data for trimers and larger water clusters to obtain the corresponding potential surfaces has not yet been developed, an important function of the spectroscopic results is simply to test and calibrate the many ab initio approaches and semiempirical methods currently used in simulations and models for liquid water. Perhaps the most important of these are the density functional approaches that underlie the very popular ab initio molecular dynamics methods.[62] It is generally acknowledged that the improper treatment of dispersion inherent in these methods engenders some errors in the calculated results, although there is some evidence that some GGA functionals (like PW91 and PBE) that obey the Lieb−Oxford bound can represent dispersion forces in an effective manner.[63,64]

The transferable intermolecular potential surfaces (TIPS) of Jorgensen[56,57] are typical of many of the simplest empirical water potentials, incorporating many-body forces in an effective manner by fitting adjustable parameters of a pairwise-additive function to liquid water properties. The TIPS model comprises a rigid water monomer with parametrized charges, q on oxygen and $^1/_2\,q$ on each hydrogen, located at the atomic centers. A Coulomb force is calculated between charges, and repulsion and dispersion are modeled using a Lennard-Jones (LJ) formula. The charge and the two LJ parameters were adjusted to reproduce the density and heat of vaporization of water. Berendsen et al.[65,66] reparametrized the TIPS model to better fit the same liquid water properties, finding that reproduction of secondary peaks in the O−O autocorrelation function (g_{OO}) of liquid water is very sensitive to the choice of parameters. The resulting simple point charge (SPC) model gave an effective water molecule dipole moment of 2.27 D, compared with the gas-phase value of 1.85 D. These authors later incorporated a polarization correction in the SPC/E potential,[58] gaining better agreement with diffusion coefficients and autocorrelation functions. Ferguson introduced a modified SPC potential that included flexibility.[67] Torres et al.[68] used a simulated annealing algorithm, which they called "Boltzmann simplex" simulated annealing, for global optimization of water clusters $(H_2O)_n$, $n = 2-6$, using Ferguson's flexible modification of the SPC potential. The method, which is not a very good global optimization scheme, predicted the correct minimum energy structures for all water clusters except for the water hexamer, for which a distorted cyclic structure with six H-bonds was found. A later reparametrization of TIPS (TIP3P) failed to reproduce the second g_{OO} peak, indicating the high sensitivity of such simple potentials to the choice of parameters.[55] Jorgensen et al. later developed the TIPS2 and TIP4P (a reparametrization of TIPS2) potentials. To better model the oxygen lone electron pairs, they moved the oxygen partial charge a parametrized distance (M) along the monomer C_2 axis, away from the hydrogens. In a comparison of several empirical potentials, they showed that TIP4P reproduced many of the properties of liquid water, including the density (+0.2% error from experimental), internal energy (+1.5%), enthalpy of vaporization (+1.4%), and heat capacity (+7.3%).[55] In a further extension of the TIPnP class of potentials, Mahoney and Jorgensen studied a five-site potential, which retained the computationally efficient Coulomb and LJ forms.[59] The main distinction of the TIP5P potential from TIP4P is that two negatively charged interaction sites were placed symmetrically along the lone-pair directions. The authors argued that TIP5P forces tetrahedral arrangements to be more attractive than in real water, but result in an improved temperature-dependent density and temperature of maximum density. The model underestimated the oxygen−oxygen distance, which is typical for nonpolarizable models, resulting from the expression of many-body terms in the two-body potential. The temperature-dependent density and energy were reproduced with an average error of less than 1% (−37.5 to 62.5 °C), and the dielectric constant was near 80 and had the correct temperature dependence.

The empirical potential using electrons and nuclei (EPEN) method of Owicki et al.[69] placed partial charges on both the rigid monomer O−H bond centers and the lone pairs at parametrized distances from the O atom. Those distances, the magnitude of the charge (all equal), and parameters from exponential repulsion and $1/R^6$ attraction terms were all fitted to reproduce liquid water data. Employing their simple model, they calculated a cyclic trimer structure remarkably similar to later estimates made using electron-correlated levels of ab initio theory. Their equilibrium trimer (see Table 1) had a per-monomer binding energy $\Delta E^{(mon)} = -4.94$ kcal/mol, with an average interoxygen separation of 2.9 Å and equilibrium H-bond torsional angles (see Figure 1) very near more recent estimates. Moreover, Owicki et al. were able to search their IPS for transition states on low-energy H-bond network rearrangement pathways, finding the transition state to the H-bond torsional or "flipping" motion to lie only 0.6 kcal/mol above the global minimum (see Table 2). Other optimizations employing empirical additive potentials have produced similar results. Schröder[70] used a modified EPEN surface (QPEN/B2), obtained by fitting the parameters of EPEN to quantum-mechanical water dimer calculations, to compute $\Delta E^{(mon)} = -5.44$ kcal/mol for a cyclic C_1 trimer, with one H-bond torsional variant lying within 0.6 kcal/mol of the global minimum. Including zero-point energy (ZPE), Owicki et al. calculated a barrier to H-bond torsion of 0.04 [0.12] kcal/mol for $(H_2O)_3$ [$(D_2O)_3$], and hypothesized that the experimentally measured (time-averaged) free proton positions would be highly averaged, even for a trimer at 0 K. They were also the first to comment on the interconnectivity of structurally degenerate minima on the trimer IPS, partitioning the 96 possible minima corresponding to a C_1 cyclic structure into groups of 16, connected by rearrangement pathways whereby the H-bonded and free protons of a given monomer exchange coordinates. That rearrangement, they predicted, should have an effective barrier of several kilocalories per mole. As has been noted more recently,[70] and is evident in the water tetramer and pentamer optimizations of Owicki et al., the EPEN model has a tendency to maximize the number of H-bonds made by a given monomer. Thus, three-dimensional structures are predicted for the tetramer and pentamer in the same work, whereas cyclic, quasiplanar structures are found in both the experimental data[71−73] and more recent calculations. Nevertheless, the work of Owicki et al. is remarkable both for its numerical accuracy using a simple additive potential and for its insight into the HBNR dynamics of small clusters that anticipated features later observed in the high-resolution spectroscopic data. Schütz et al. subsequently refitted the EPEN potential to a set of ab initio-calculated points along the H-bond torsional coordinate in order to reproduce some of the experimentally measured intermolecular vibrational frequencies arising from H-bond torsional motion.[74]

Table 1. Calculated Water Trimer Average Bond Lengths (Å), Angles (deg), and Energies (kcal/mol)

method	basis set	ref	$r_{OH}^{bounded}$	r_{OH}^{free}	∠HOH	R_{OO}	δ	$\lvert\chi\rvert$	$\lvert\gamma\rvert$	$\Delta E^{(mon)}$ (BSSE corr.)	% E_{ABC}
gas-phase monomer		264	(0.957)	0.957	104.5						
BGLK[a]		78				~2.9		~58.5			*b*
EPEN[a]		69				2.897	28.3	58.0		−4.94	*b*
MCY[a]		77								−5.28	*b*
POL1[a]		124				2.78				−4.86	*b*
POL2[a]		124				2.86				−4.75	*b*
RWK-2		265				2.817				−5.07	*b*
TIP3P[a]		266								−5.81	*b*
TIP3P[a]		124				2.75				−5.97	*b*
TIP4P[a]		157								−5.57	*b*
TIP4P[a]		104				2.761					*b*
TIP4P[a]		266								−5.57	*b*
ASP-W2[a]		104				2.722					
ASP-W2[a,c]		105								−5.29	16.1
ASP-W4[a]		104				2.851					
ASP-W4[a,c]		105								−4.91	14.5
ASP-W4[a]		266								−5.16	
DIM[a]		123				2.85	~30			−5.77	
NEMO[a]		91				2.779	21	42.9	3.3	−4.84	12.5
PIMO[a]		122				2.841				−5.83	12
TCPE		94	0.96	0.96	103.0	2.83	20.6	39.3		−5.56	15.2
TTM[a]		116				2.804				−5.56	38.7
TTM2-R[a]		117				2.804				−5.20	33.0
TTM2-F		119	0.9695	0.921	105.72	2.800				−5.30	
VRT(ASP-W)[a]		108				2.756				−5.22	
DFT/PP		149	0.990	0.971	106.1	2.782	28.8	76.2	2.0		
DFT/B-LYP	6-31+G(d,p)	166	0.992			2.793				−5.63	
DFT/B-LYP	6-311++G(3df,2dp)	166								−4.60	27.7
DFT/B-LYP	aug-cc-pVDZ	25	0.992	0.975	105.5	2.809	28.8	62.3	6.6	−4.57	
DFT/B3-LYP	6-31+G(d,p)	166	0.98			2.775				−5.97	
DFT/B3-LYP	6-311++G(3df,2dp)	166								−4.93	22.9
DFT/B3-LYP	6-311++G**	267				2.784				−5.78 (5.15)	22.9
SCF	6-31G*	142	0.956	0.947	106.0	2.868			2.7	−5.81	
SCF	aug-cc-pVDZ	17, 26	0.950	0.943	106.6	2.927	31.0	49.3	3.6	−3.89 (−3.67)	11.2 (12.5)
MP2	6-311+G(d,p)	95	0.970	0.958	105.0	2.794	31.8				
MP2	6-311++G(d,p)	61	0.971	0.959		2.797		41.4		−4.64	
MP2-R12[d]	6-311++G(d,p)	158	0.971[d]	0.959[d]		2.797[d]		41.4[d]		−5.44	14.1
MP2[e]	aug-cc-pVDZ[e]	105								(−4.75)	(17.2)
MP2[f]	aug-cc-pVDZ[f]	170	0.978	0.965	105.2	2.803		47.0	2.13	−5.45 (−4.63)	
MP2	aug-cc-pVDZ	17, 26	0.978		105.2	2.799	29.7	56.6	6.13	−5.52 (−4.62)	13.7 (17.6)
MP2[f]	aug-cc-pVDZ[f]	160				2.803				−5.45 (−4.63)	
MP2[f]	aug-cc-pVTZ[f]	170	0.974	0.961	105.4	2.787		47.0	1.93	−5.43 (−4.99)	
MP2[h]	aug-cc-pVTZ[h]	170	0.973	0.960	105.6	2.784		46.4	1.90		
MP2[f]	aug-cc-pVTZ[f]	175								−5.43 (−4.99)	
MP2[f]	aug-cc-pVTZ[f]	160				2.787				−5.43 (−4.99)	
MP2[f]	aug-cc-pVQZ[f]	170	0.972	0.958	105.6	2.782		46.3	1.91	−5.37 (−5.15)	
MP2[g]	aug-cc-pVQZ[g]	175								−5.37 (−5.15)	
MP2[i]	aug-cc-pV5Z[i]	170								−5.32 (−5.2)	
MP2[g]	aug-cc-pV5Z[g]	175								−5.32 (−5.2)	
MP2[i]	aug-cc-pV6Z[i]	170								−5.30 (−5.23)	
CCSD	DZP	155	0.977	0.966	105.1	2.819	28.9	51.8		−5.97	
CCSD	DZP+diff.	155	0.976	0.966	105.3	2.830	31.7	42.9		−5.57	
CCSD	aug-cc-pVDZ	170	0.974	0.963	105.3	2.837		46.7	1.80		
CCSD(T)[i]	aug-cc-pVDZ no CPC[i]	170								−5.45	
MP4	6-311+G(d,p)	95								−5.23	
MP4[j]	aug-cc-pVDZ	17, 153	0.978[j]	0.964[j]	105.2[j]	2.807	29.7[j]	56.6[j]	6.1[j]	−5.53 (−4.55)	13.3 (17.6)

[a] Monomer coordinates fixed to gas-phase values. Note that these coordinates are irrelevant for the TIP*n*P and EPEN potentials. [b] Pair-additive potential. [c] At MP2 geometry. [d] At MP2/6-311++G(d,p) geometry. [e] BSSE-corrected, rigid monomers. [f] 1s orbitals frozen. [g] 1s orbitals frozen at aug-c-pVTZ geometry. [h] No orbitals frozen. [i] 1s orbitals frozen at aug-cc-pVQZ geometry. [j] Calculated at MP2/aug-cc-pVDZ geometries except for R_{OO}.

Their mod-EPEN potential was designed to be useful only for examining the torsional subspace of the full IPS and will be discussed in a later section, along with a similar torsional potential developed by van Duijneveldt and van Duijneveldt-van de Rijdt (henceforth being referred to as BGLK and DD potentials, following van der Avoird et al.[28]).[75]

Matsuoka, Clementi, and Yoshimine[76] developed a pairwise-additive potential function (MCY) based on a point-charge model with a charge distribution similar to that of the TIP4P function, but a significantly more sophisticated treatment of induction, dispersion, and exchange repulsion via exponentials. They fitted 10 parameters to a set of points calculated in a configuration-interaction (CI) ab initio model of the water dimer. The model predicts the correct minimum energy structure for the trimer with a binding energy of $\Delta E^{(mon)} = -5.44$ kcal/mol.[77] Bürgi

Table 2. Energies (kcal/mol) of Important Stationary Points on the Trimer IPS

method	ref	{*uud*}[a]	{*upd*}[b]	{*uuu*}	{*uup*}	{*upp*}	(*ppp*)	*upb*[c]
EPEN	69	0	0.62					
EPEN	104	0	0.61	0.65	1.02	not	2.75	0.71
TIP4P	104	0	0.01	not	not	not	0.17	1.92
EFP	121	0	0.25					1.72
EPEN[d]	78	0	0.93	0.67	0.94[e]	2.04	3.43	
TIP4P[d]	78	0	−0.09	0.87	0.78[e]	0.28	−0.1	
MCY[d]	78	0	0.10	0.82	0.80[e]	0.60	0.56	
SPC[d]	78	0	−0.43	1.29	1.05[e]	−0.18	−1.38	
BGLK	78	0	0.27	0.86	0.90	1.04	1.65	
NEMO	91	0	0.24	0.99			1.17	
ASP-W2	104	0	1.15	0.96	1.72	2.78	4.38	2.57
ASP-W4	104	0	0.72	0.84	1.24	1.77	2.67	1.91
DIM	123	0		0.4				
TCPE	94	0	0.54	0.46			1.87	3.93
SAPT	171	0	0.137	0.677			0.956	1.8
MP2/EZPPBF	75	0	0.26	0.79	0.81	0.94	1.44	
MP2/6-311++G(d,p)	61	0		0.61			0.29	
MP2/R-12[f]	158	0	0.22	0.79			1.22	
MP2/aug-cc-pVDZ	160	0	0.24	0.73	0.76			2.18
MP2/aug-cc-pVTZ	160	0	0.28	0.75	0.80			2.34
CCSD/DZP	155	0	0.38	1.23			2.20	1.96
CCSD/DZP+diff	155	0	0.30	0.85			1.67	2.06
CCSD(T)/aug-cc-VDZ	158	0	0.18	0.72			1.22	
CCSD(T)/aug-cc-pVDZ[g]	83	0	0.18	0.72			1.22	
CCSD(T)/aug-cc-pVDZ	171	0	0.255	0.771			1.412	1.837

[a] Equilibrium structure reference energy (see Table 1 for trimerization energies). [b] Flipping transition state (see Figure 2a). [c] Bifurcation transition state (see Figure 2b). [d] At torsional angles for BGLK stationary points. [e] The p proton is not quite in the plane in this stationary point. [f] At the geometries of ref 61. [g] At the geometries calculated with 6-311++G(d,p) and 6-311++G(2d,2p).

et al. calculated the relative energies of various torsional structures corresponding to stationary points on their BGLK potential with the MCY potential (Table 2) and found that the MCY gives the same energy ordering as the BGLK potential except for the *ppp* structure, which is significantly more stable on the MCY surface.[78]

Building on the earlier work of Watts,[79] Reimers, Watts, and Klein designed the more robust RWK potential, comprising Coulomb, exponential repulsion, and Morse terms, plus an empirical dispersion energy.[80] They fitted seven parameters to second virial coefficients of steam, lattice energies of ice, and bulk-phase water densities, as well as the gas-phase water dimer structure. In the RWK-1 potential, the negative charge was shifted away from the protons along the C_2 axis. In another version (RWK-2), the dispersion energy of Douketis et al.[81] was incorporated. Watts's original potential[79] was the first empirical function to include intramolecular relaxation of the water monomers, incorporated as an anharmonic potential with 16 adjustable force constants, all fitted to the gas-phase monomer data and HF calculations. They calculated $\Delta E^{(\mathrm{mon})} = -5.07$ kcal/mol for a cyclic, C_1 trimer (Table 1). Cieplak and co-workers[82] later reparametrized the RWK-2 potential and included a classical polarization term, iterated to convergence, to form the CKL potential. They fit 13 adjustable parameters to second virial coefficients and the densities of ice I_h and ice VII, calculating the gas-phase dimer structure as a final check on the parametrization. Guiang and Wyatt later refit the torsional subspace of the CKL potential to four different high-level ab initio water trimer IPS's (cc-PVDZ and DZP calculations with and without counterpoise BSSE correction), calculating the binding energies of several H-bond torsional variants of the equilibrium structure, as well as intermolecular vibrational frequencies.[83] They found $\Delta E^{(\mathrm{mon})} = -4.18$ to -5.88 kcal/mol over the range of ab initio calculations and were able to reproduce the experimental frequencies to within 20% with the cc-PVDZ + counterpoise fitted CKL potential.

A number of potential surfaces have attempted to avoid the problems associated with incorporating many-body forces in an effective manner. Barnes and co-workers[13] emphasized the need for inclusion of nonadditivity in potentials used for bulk water simulations. They noted that, in addition to the role of three-body forces in stabilizing gas-phase clusters, isolated water molecules are neither very good H-bond donors nor acceptors, and that the average monomer dipole moment in hexagonal ice is greater than 2.6 D, more than 1 D larger than the gas-phase value.[84] In their polarizable electrupole (PE) model, Barnes et al. included H-bond cooperativity by incorporating classical polarization of the monomers in a potential consisting of point multipoles and a spherical LJ-type function. They argued that because electron cloud distortion dominates electron transfer as the size of the basis set is increased, a classical polarization model is adequate to describe the polarizable monomers. They essentially used a self-consistent-field procedure wherein the electric field of the monomer multipole moments and the response to it, calculated using classical polarizability tensors, were iterated to convergence to yield the polarization contribution. Stone has written extensively on iterated many-body polarization or induction models.[85] As tests of the model, which contained no adjustable parameters, Barnes et al. noted good agreement with the second virial coefficients of steam ($T = 100-400$

°C), with previous calculations of the water dimer equilibrium structure, with the experimental dipole moment of monomers in ice I_h (PE = 2.88 ± 0.3 D, experiment = 2.45−3.0 D), and with the measured internal energy of this form of ice. Their treatment produced a cyclic trimer repulsive by 10.5 kcal/mol, although the exact geometry used in the calculation is unclear. Also inconsistent with more recent results, the per-monomer binding energies computed for clusters up to the cyclic hexamer were quite large; e.g., Barnes and co-workers calculated a cyclic pentamer that was 38% more stable than the ab initio value of Del Bene and Pople,[86] which is itself larger than more recent estimates.

In an effort to develop more transferable potentials, Dykstra constructed a similar cluster model (MMC: molecular mechanics of clusters) based on classical electrostatic interactions and classically calculated multipole polarization.[87] He justified a classical approach by noting that permanent multipolar interactions dominate cluster energetics at long range, while polarization-dependent readjustments — evolution of charge density due to multipole moment−charge cloud interactions — make up the balance and are cooperative by definition. A LJ-type interaction was included to account for the effects of dispersion and repulsion, and mutual polarizations were iterated to convergence. The resulting optimized water trimer structure had $\Delta E^{(\mathrm{mon})} = -5.27$ kcal/mol, with a water center-of-mass separation of 2.94 Å. The energy without polarization was −4.25 kcal/mol, while that including the noniterated polarization (the pairwise-additive energy) was −5.08 kcal/mol per monomer. The nonadditive polarization therefore accounted for 3.5% of the total MMC energy. Dykstra's model incorporated the quantum mechanical effects of dispersion and exchange repulsion using only a LJ function. Nevertheless, its portability and its accuracy compared to more recent calculations are striking.

In work that contributed considerable insight into the origin of nonadditivity in water, Belford and Campbell[88] studied $(H_2O)_n$, $n = 3, 4, 6$, using a model potential they had developed previously.[89] Like those of Barnes et al.[13] and Dykstra,[87] their model comprised a high-order multipole expansion (additive), a long-range additive + nonadditive induction term, and a $(1/R^9 + 1/R^{12})$ additive repulsion formula, but also included an additive C_6/R^6 dispersion energy. Their optimized water trimer (cyclic, C_1 symmetry) had $R_{OO} = 2.79$ Å, with $\Delta E^{(\mathrm{mon})} = -6.14$ kcal/mol, E_{ABC} constituting 8.7% of the total. In similar computations, E_{ABC} accounted for 16% and 25% of the tetramer and (cyclic) hexamer energies, respectively, and their structural optimizations agreed with previous conclusions for the trimer, tetramer, and hexamer. Belford and Campbell calculated a systematic contraction of R_{OO} as a function of increasing the number of waters in cyclic clusters. They attributed this mainly to the approach to linearity of the H-bonding angles in successively larger clusters, which decreases the angle between the electric field of any monomer dipole acting on the permanent moment of its neighbor, affording a more attractive electrostatic configuration. Inclusion of the additive dispersion interaction, 18% of the total trimer energy, produced −0.071 Å shifts in R_{OO}. This decrease, they reasoned, led to an increase in the nonadditive induction energy. Belford and Campbell argued that failure to include dispersion in geometry optimizations will yield longer R_{OO} values, and thus smaller two- and three-body induction interactions. This point seems particularly important in light of the fact that dispersion interactions are difficult to represent accurately using ab initio techniques, especially for density functional methods.

Wallqvist and co-workers developed the NEMO potential in an effort to reproduce the stationary points on ab initio-calculated trimer IPS's.[90,91] Their potential is based on a perturbation expansion of the monomer SCF electron density. The electrostatic and induction energies were computed from a multipole expansion of the SCF charge density. The electrostatic energy was then calculated as a Coulomb interaction between partial charges, while the induction was modeled by the interaction of local polarizabilities with the same multipoles. The exchange repulsion was modeled by an orbital overlap function, and dispersion was given by a simple London-type formula. They calculated $\Delta E^{(\mathrm{mon})} = -4.84$ kcal/mol, with the three-body induction accounting for 12% of the total and exchange repulsion constituting over half of the absolute value of the total energy at the trimer equilibrium geometry (Table 1).

Dang and Chang used molecular dynamics simulation techniques to develop a polarizable, rigid, four-site potential for water.[92] The general form of the potential was similar to the TIP4P potential, using the gas-phase monomer geometry, and charges on the hydrogen atoms and on the M site, located on the bisector of the H−O−H angle. The charges were placed to match the monomer dipole and quadrupole moments, as well as the ab initio-calculated dimer energy and distance. A LJ potential was assigned to the oxygen atoms to account for short-range interactions, and the M site carried a polarizability to describe nonadditive interactions. These parameters were optimized in molecular dynamics simulations by comparison with bulk water properties and the dimer interoxygen distance and dimer energy. For the water trimer, the model gave the correct minimum energy structure with three nonequivalent oxygen−oxygen distances of 2.837, 2.846, and 2.883 Å. The authors state that the total binding energy agreed well with the ab initio values, whereas the three-body contribution was 8% (ca. half as large as that for ab initio results), although they did not give values for either. The calculated water monomer dipole moment in the water trimer was ca. 2.2 D, which compares well with the results of Gregory et al.[93]

Masella and Flament studied the importance of many-body interactions for the stability of water clusters, comparing three different flexible model potentials.[94] All potentials were created to reproduce the ab initio water dimer IPS and had the same general form. The CMP model included a classical molecular many-body polarization term, and the

TCPE potential included an additional term for topological effects[95] by expressing two of the parameters of the CMP potential as functions of the hydrogen bond strength for a molecule when it acts as an acceptor of one or two H-bonds, to reproduce ab initio results for the water trimer. The PW model was derived from the CMP potential by leaving out the nonpairwise effects. The binding energy and geometry of the cyclic water trimer ground-state structure calculated from the TCPE ($\Delta E^{(\mathrm{mon})} = -5.56$ kcal/mol) model agreed well with ab initio results, which is expected, as ab initio water trimer results were explicitly included in this model. The difference in binding energy between the PW and TCPE models showed that the nonpairwise interactions account for ca. 15% of the total binding energy, and the difference between the CMP and PW models showed that the many-body polarization term accounts for ca. 40% of the total nonpairwise energy for the water trimer. The authors also calculated the energies of the torsional (*upd*) and bifurcation-tunneling (*upb*) transition states (Table 2). The TCPE energies were a factor of 2 larger than the ab initio results for both of these transition states. The model reproduced the energetic ordering of various states (including the *ppp* structure), except for the *uuu* structure, which it predicted at lower energy than the *upd* transition state of the torsional flipping pathway.

In an effort to produce the most physically realistic water potential, Millot and Stone have developed a family of anisotropic site potentials (ASP), based on ab initio intermolecular perturbation theory (IMPT)[96] calculations. In several incarnations of the ASP, they have addressed the electrostatic, induction, dispersion, and exchange-repulsion contributions to the water−water interaction in detail. Electrostatic energy in the ASP surfaces is calculated by using distributed multipoles computed in high-level ab initio calculations. Charge and dipole terms on each hydrogen and charge, dipole, and quadrupole terms on each oxygen are summed over to arrive at the Coulomb energy.[97,98] The exchange repulsion, an empirical term in the ASP surfaces, was essentially a "soft-sphere" model formed by superimposing spherical harmonics on the atomic centers. Two types of dispersion terms were used. The first, given by Rijks and Wormer,[99] contained an anisotropic dispersion energy used in conjunction with the Tang−Toennies[100] spherically symmetric damping function. The damping term was included because the short-range dispersion is modeled poorly due to exchange effects with the same interaction range. Because of doubts about the validity of the isotropic damping term, Millot and Stone also formed an ASP variant using the isotropic dispersion term of Szczesniak,[101] in conjunction with an anisotropic damping function based on the sum of atomic radii. Finally, induction was calculated using the effects of the fields of the point multipoles on point atomic polarizations.[85,102] In early versions of the ASP surfaces, induction was not iterated, but later models were iterated to convergence in the interest of modeling many-body effects. By adding the Axilrod−Teller[103] triple-dipole interaction to those versions, Gregory and Clary were able to reproduce the experimentally measured moments of inertia of $(H_2O)_3$ and $(D_2O)_3$ to within 5% using diffusion quantum Monte Carlo (DQMC) methods. Walsh and Wales[104] compared the TIP4P, EPEN, ASPW2, and ASPW4 potentials, noting significant differences in the energies of the transition states for torsion about a single H-bond ("flipping") and bifurcation tunneling. Of the four, the TIP4P surface best reproduced the high-level ab initio results, although, as will be shown, those details are also quite sensitive to basis set size. Hodges, Stone, and Xantheas compared the contribution of many-body terms to the energy of $(H_2O)_n$, $n = 2-5$, for the ASP-W2 and ASP-W4 potentials with results from ab initio calculations.[105] They studied the importance of many-body forces for the cyclic structure and two open-chain structures of the water trimer (all energy calculations were made at fully optimized MP2/aug-cc-pVDZ geometries). Three-body contributions were found to significantly stabilize the cyclic structure, whereas they are slightly repulsive for the open structures. The ASP-W2 and ASP-W4 potentials both gave larger two-body contributions than the ab initio results, whereas the three-body terms compared reasonably well, with ASP-W2 being closer to the ab initio results. However, the opposite was found for the two-body contributions, and as a result the ASP-W4 total energy is closer to the ab initio value. In the same study, a 3-D cage structure for the pentamer was found to be more stable than the cyclic form for both the ASP-W2 and ASP-W4 potentials, primarily due to the overestimate of the two-body contributions. An extension of this study to the water hexamer, with slightly different values for the trimer, can be found in ref 106. The most recent version of the ASP potential includes an exponential attraction term to model charge transfer.[107]

Fellers et al. determined a potential of spectroscopic quality using the split Wigner pseudo-spectral algorithm[108,109] to fit a small number (4 or 6) of the 72 parameters of the ASP-W potential to 13 microwave transitions and tunneling splittings of the $J = 0$ and $J = 1$ dimer ground state and 8 $J = 0$ terahertz transitions in three observed dimer vibrational bands (J is the total angular momentum quantum number). The equilibrium $R_{OO} = 2.756$ Å, the ground-state $R_{OO} = 2.843$ Å, and $\Delta E^{(\mathrm{mon})} = -5.22$ kcal/mol calculated from this potential for the trimer are in good agreement with the ab initio complete basis set limit values. Whereas no three-body terms were explicitly added to the VRT(ASP-W) potential, the proper inclusion of the tensorial induction interaction implicitly includes the leading many-body terms.

Groenenboom et al. calculated the torsional flipping levels using the SAPT-5s potential with the DVR method and torsional Hamiltonian developed by van der Avoird et al. for these states.[110] The SAPT-5s potential represents a pair plus three-body potential (including formulas for second- and third-order induction, third-order induction−dispersion, third- and fourth-order dispersion with neglect of intramonomer correlation from the three-body polarization expansion, first-order intramonomer correlation to third

order, and first- and second-order exchange energies),[111] and was fitted to a large number (>2500) of ab initio data points computed by symmetry-adapted perturbation theory (SAPT). The potential was further improved by adjusting it to reproduce the experimentally observed acceptor switching tunneling (the exchange of the protons of the hydrogen bond acceptor) splitting of $(H_2O)_2$. The lower torsional levels within the first torsional manifold were in excellent agreement with experiment for both $(H_2O)_3$ and $(D_2O)_3$, whereas the second torsional manifold of $(D_2O)_3$ showed bigger deviations. The agreement, in fact, was the best for any tested global water potential, even the VRT(ASP-W) potential, which the authors argued produced an excessively large flipping barrier. The discrepancies for the second manifold of $(D_2O)_3$ could result from the approximate method of calculating the energy levels rather than inaccuracies in the potential, as studies have shown[112−114] that accurate calculations for the higher torsional levels require inclusion of at least the symmetric stretch coordinate.

Burnham et al. presented a polarizable model for water using Thole's method[115] for the molecular polarizabilities, which uses smeared-out charges and dipoles to mimic the electron distribution.[116] The potential is a four-site potential, using gas-phase monomer geometry and a site distribution similar to that of the TIP4P model. The potential was parametrized by fitting to the ab initio (MP2/aug-cc-pVTZ) potential energy along the oxygen−oxygen distance of the ab initio minimum energy geometry. Although the overall binding energy of the water trimer, $\Delta E^{(\mathrm{mon})} = -5.56$ kcal/mol, was in fairly good agreement with ab initio results, the three-body contribution was 38.7%, considerably larger than the ab initio values. The dipole moment obtained for the trimer was 0.8 D, and that of the individual monomers was 2.322 D. Later, Burnham and Xantheas[117] presented a reparametrization of the existing TTM potential, in this case to the water dimer C_s-symmetry-constrained optimized energies along the oxygen−oxygen distance, rather than the energy along the intermolecular oxygen−oxygen distance of the minimum energy geometry. The second virial coefficients of this potential agreed well with theory and are within 1% of the SAPT-5s model,[118] which was fit to over 2500 ab initio data points, whereas TTM2-R was fit to only 25 ab initio points. The authors argued that a small number of appropriately chosen points was adequate for reproducing the second virial coefficients (whereas SAPT-5s was specifically developed to reproduce the intricate VRT splitting patterns observed by experiment). However, both the ASP-W4 and VRT(ASP-W) potentials exhibit closer agreement to experimental virial coefficients. Regarding water clusters larger than trimer, the TTM2-R potential energies were closer to the MP2/CBS estimate than are those of the ASP-W4 or VRT(ASP-W) potentials. For the water trimer, the binding energies of the ASP potentials and TTM2-R ($\Delta E^{(\mathrm{mon})} = -5.20$ kcal/mol) were found to be similar, and the three-body dipole energy component for the water trimer with the TTM2-R was about 35% (Table 1), similar to the TTM2 value. Burnham and Xantheas extended the TTM2-R potential to the flexible, all-atom polarizable TTM2-F and TTM2-F(L) potentials by incorporating ab initio-derived, geometry-dependent charges.[119] The TTM2-F(L) potential included a linear and the TTM2-F a nonlinear dipole moment surface. The calculated binding energies for the TTM2-F model were in excellent agreement with the ab initio MP2/CBS limit for the water dimer through hexamer, with an RMS deviation of 0.05 kcal/mol per H-bond. For the water trimer, the calculated per-monomer binding energy was $\Delta E^{(\mathrm{mon})} = -5.30$ kcal/mol. The increase in the bend angle of the water monomers in $(H_2O)_n$, $n = 2-6$, predicted by TTM2-F model also was in excellent agreement with ab initio results, whereas the TTM2-F(L) model predicted a decrease. The authors argued that models that include a linear dipole moment surface cannot predict the increase in the bend angle correctly. The TTM2-F model, however, predicted only a small red-shift of the bound OH stretch vibrations for $(H_2O)_n$, $n = 2-6$, which was reflected in shorter $r_{\mathrm{OH}}^{\mathrm{b}}$ than the ab initio values or those predicted by TTM2-F(L). It should be noted that the TTM2-F potential is unusual in that it contains a geometry-dependent electronic polarizability tensor.

2. Ab Initio/Empirical Potential Hybrid Calculations

Long et al. studied the conformation and binding energies of $(H_2O)_n$, $n = 2-4$, using a combined density functional theory/molecular mechanics method (DFT/MM).[120] A modified flexible TIP3P potential[55] was used for the MM part and both the DZVP or aug-cc-pVDZ basis set with the BP and mixed BP (MBP) functional (nonlocal) or VWN (local) form. The conditions for the DFT part were chosen as the authors assumed that the effects of the MM part were larger than the effects of basis set size or functional form. The authors showed that the local density approximation generally resulted in an overestimate of the binding energy, with correspondingly short R_{OO} values, for both pure DFT clusters and the water molecules treated with DFT in the mixed DFT/MM clusters. The DFT/MM coupling term was found to be geometry-dependent and thus has to be chosen with care. In general, the authors found good agreement between the DFT/MM and the pure DFT results for the nonlocal functionals. For DFT calculations on the trimer with the MBP functional and the BP functional with the DZVP basis set, binding energies of $\Delta E^{(\mathrm{mon})} = -5.82$ and -5.80 kcal/mol, and $R_{\mathrm{OO}} = 2.746$ and 2.744 Å, respectively, were found. The pure DFT trimers calculated with the BP functional and the aug-cc-pVDZ basis set had a binding energy of $\Delta E^{(\mathrm{mon})} = -5.11$ kcal/mol and $R_{\mathrm{OO}} = 2.764$ Å. For the pure MM trimer, the authors found a binding energy of $\Delta E^{(\mathrm{mon})} = -5.09$ kcal/mol and $R_{\mathrm{OO}} = 2.733$ Å. An increased trimer binding energy from the pure DFT trimer to the trimer with two MM molecules using the BP functional and aug-cc-pVDZ basis set was observed, whereas with the MBP and BP functionals and the DZVP basis set the binding energies for the pure DFT, trimer with two DFT, and trimer with two MM molecules were fairly constant. Similar differences in trends for R_{OO} were also found,

and for the trimer with two MM molecules one short and one long DFT/MM R_{OO} value were found. As expected, the value of R_{OO} of the two MM molecules was close to that for the pure MM water trimer. This highlights the importance of the term coupling the DFT and MM regions in such calculations.

Merrill and Gordon[121] compared the energies and structures of $(H_2O)_n$, $n = 3-5$, calculated with the effective fragment potential (EFP) model with ab initio results. The effective fragment potential model separates the system into two regions, the "active" and the "spectator" regions, thus being computationally more efficient than pure ab initio methods, and only a factor of 3 slower than for the TIP3P potential. The active region, consisting of solute and solvent molecules directly participating in hydrogen-bond-making or -breaking processes, was treated with an ab initio Hamiltonian. The spectator region was treated with three one-electron terms — electronic, polarization, and exchange repulsion/charge transfer — which included interactions between each fragment and the electrons and nuclei of the active region. The EFP model predicted the trimer *upd* transition state to lie 0.25 kcal/mol and the *upb* transition state 1.72 kcal/mol above the global minimum, which the authors compared to the *upb* transition-state value of 1.66 kcal/mol for HF/DZP+ results reported by Walsh and Wales.[104] The ordering of stationary points on the water tetramer IPS, as well as most of the investigated transition states for the pentamer, agreed with ab initio results. Unfortunately, the authors do not give a value for the binding energy of the minimum energy structures.

Kitaura et al. calculated the binding energies of the cyclic water trimer, two open trimer structures, and some tetramer structures with a pair interaction molecular orbital method.[122] The method reduces the computational requirements by performing MO calculations on the molecules and molecular pairs only, thus avoiding supermolecular calculations. The calculations were performed at the HF/6-31G** level with rigid monomers. The authors compared their value for $\Delta E^{(mon)} = -5.83$ kcal/mol to $\Delta E^{(mon)} = -5.8$ kcal/mol for the ab initio calculation at the same level of theory. The PIMO method predicted a 12% contribution of three-body interactions to the binding energy, compared to 11% for the ab initio results (Table 1). As the three-body polarization term contributed about 45% of the total three-body energy for the cyclic structure, the authors argued that the PIMO method included not only the full many-body polarization term but also other many-body terms within their pair approximation. The agreement for the open structures was not as good as for the cyclic one.

In a related approach designed to circumvent the need for supermolecule calculations, Grigorenko et al. used the diatomics-in-molecules (DIM) method in an attempt to improve some of the shortcomings of other hybrid quantum mechanics/molecular mechanics (QM/MM) methods.[123] The DIM method computes the PES of a polyatomic system by combining the potential energy curves of diatomic fragments in specific electronic states, including ionic states. The model used rigid water monomer structures and included a LJ potential assigned to the O_2 diatomic fragment with parameters adjusted to approach the energy dependence of $(H_2O)_2$ along R_{OO}. The method reproduced the correct cyclic minimum energy structures for the water trimer and tetramer. The per-monomer binding energy of the trimer was $\Delta E^{(mon)} = -5.77$ kcal/mol (Table 1), and the authors estimated that energies could be calculated to within 1−2 kcal/mol, and argued that calculation of spectroscopic properties requires further adjustments of flexible parameters within the model. The average trimer oxygen−oxygen distance, $R_{OO} = 2.85$ Å, differed significantly from the MP2/aug-cc-pVDZ ab initio value of 2.80 Å.[25]

Aida et al.[124] calculated the minimum energy structures of $(H_2O)_n$, $n = 2-5$, with a QM/MM method and the TIP3P,[57] POL1,[125] and POL2[92] potentials containing vibrational energy terms for all water molecules. The method used the established QM/MM method to systematically study the effect of replacing QM (HF/6-31G** or HF/6-31G*) water molecules one at a time with MM molecules, reoptimizing the structures, and calculating the energy. The results showed that, as expected, R_{OO} was too short for all three potentials for the pure MM water trimer, even shorter than Dang's original POL2 results for the trimer. Interestingly, trimers with two MM water molecules showed two quite long R_{OO} (ca. 3 Å) and one short R_{OO} between the two MM water molecules, similar to the pure MM bond length. For the trimers with one MM water molecule, all three R_{OO} distances were distinctly longer than for both the pure QM or pure MM trimers. Similar results were obtained for the other water clusters, indicating that interactions between MM molecules are too strong, and repulsion between the QM and MM molecules too large. The authors argued that a different choice of potential or modification of the potentials used would improve the results significantly.

3. Ab Initio Calculations

Although the more computationally tractable water dimer has received far more theoretical attention in terms of electronic structure calculations (see Scheiner's review[126]), the trimer has recently been addressed with many ab initio methods. Calculations of the equilibrium geometry have converged to the cyclic C_1 structure shown in Figure 1. Many transition-state structures and rearrangement pathways have also been explored in detail, providing valuable information on the details of the IPS relevant to recent experimental measurements. High-level ab initio calculations have also provided tests for DFT methods, which promise to reduce the complexity of calculations of larger cluster properties. Several studies have calculated intramolecular vibrational frequencies of water clusters with the aim of interpreting the results of IR experiments and understanding changes in intramolecular geometries in the pairwise and nonadditive approximations. Calculations of intermolecular frequencies via empirical or ab initio potentials have suffered from the necessity of applying harmonic approximations.

In view of the highly anharmonic water cluster IPS, other methods, such as DQMC, have been developed for calculating the vibrational properties.[127−129] Because the DQMC methods accurately account for ZPE effects, they are also more directly comparable to experimental data of all types.

Quantum mechanical studies of the water trimer began at uncorrelated levels of ab initio theory with minimal basis sets, e.g., STO-*n*G.[130] Later, improvements were made using larger basis sets and more sophisticated calculations that included electron correlation, converging the structural predictions to the modern consensus. More recent efforts have characterized not only the magnitudes of the nonadditive interactions but also their physical origins and anisotropies. The important concept of H-bond strain obviously arises from the anisotropies of the respective intermolecular forces. Because H-bonds are known to be highly directional, favoring linear configurations in a pairwise-additive approximation, an important question arose early on: does the binding energy gained by closing a noncyclic trimer to form a third H-bond overcome the decrease in the individual H-bond stabilization energies resulting from strain? In particular, the role of cooperative forces became the focus of arguments in favor of one or the other configuration as the equilibrium structure.

The earliest ab initio characterization of the trimer IPS was that of Del Bene and Pople,[86,131] who examined small water clusters up to the hexamer in SCF calculations using a minimal (STO-4G) basis set. They found that the equilibrium trimer geometry was similar to that shown in Figure 1, with a per-monomer stabilization energy of −6.17 kcal/mol, but with an interoxygen separation (R_{OO}) nearly 0.2 Å (7%) less than more modern theoretical and experimental estimates. A sequentially bonded (OH···OH···OH) linear structure was found to be 2.2 kcal/mol less stable than the cyclic form.

The ab initio trimerization energy can be decomposed into components using

$$\Delta E = -3E_{H_2O(free)} + E_A + E_B + E_C + (E_{AB} + E_{AC} + E_{BC} + E_{ABC}) \quad (2)$$

where $E_{H_2O(free)}$ is the free monomer energy, the E_X are the monomer energies in the water trimer, the E_{XY} are the pairwise-additive interactions, and E_{ABC} is the nonadditive (three-body) term. In what follows, ΔE will usually be expressed as the per-monomer stabilization energy, $\Delta E^{(mon)} = \Delta E/3$. In calculating ΔE in this manner, Del Bene and Pople concluded that the decreased stabilization due to bent H-bonds in the cyclic trimer [δ(O−H···O) angle 19° from linear] was more than compensated for by the E_{ABC} term and the extra (but reduced) E_{AB} contribution gained by closing the ring. Despite the strain, their trimer was stable by an amount approximately equal to three linear dimer bonds, −6.09 kcal/mol per bond. E_{ABC} accounted for 49% of the total trimer energy, a very large fraction compared to more recently calculated values. In a Mulliken-type analysis of the charge distribution in the optimized cyclic trimer, Del Bene and Pople provided some insight into the nature of the principal three-body interaction by noting that the negative charge density of the H-bonded protons decreased as a function of cluster size for cyclic clusters, while the O atoms of a given monomer became more negative. They suggested that mutual polarization leads to the increased stability of the cyclic forms, wherein the effect is larger because of cyclic reinforcement.[1]

Equation 2 also underscores an important point with regard to such "supermolecule" ab initio calculations, namely that the cluster stabilization energy is a small fraction of the total energy so obtained. It is therefore subject to large errors unless (1) large basis sets with full accounting for basis set superposition error (BSSE), typically using the counterpoise (CP) procedure, are used, or (2) fortuitous cancellation of errors in the results for the complex and subunits occurs. The latter situation is clearly less preferable, while the former increases the complexity of the calculations and its exact use has been called into question in a few cases.[65,83,132]

In 1973, Del Bene and Pople[133] revised their calculations using the larger 4-31G basis set. They compared the results to calculations using the STO-4G and minimal LEMAO-4G[134] bases, again finding cyclic, sequentially H-bonded trimers to be consistently more stable than open-chain forms. The nonadditive energy was not calculated for a C_1 cyclic structure, but for a planar (C_{3h}) structure the 4-31G basis yielded $\Delta E^{(mon)} = -8.16$ kcal/mol, with E_{ABC} accounting for 12% of the total at $R_{OO} = 2.69$ Å.

Hankins, Moscowitz, and Stillinger,[135,136] performing Hartree−Fock (HF) calculations with a larger basis set (O:1s,2s,2p,3d/H:1s,2p), studied three quasilinear trimer structures identifiable in the ice I_h lattice, noting that triangular trimers with strained H-bonds are not observed in ordered ice (it is interesting to note, however, that in one phase of crystalline ice — ice XII — some of the H-bonds in each unit cell are as nonlinear as those of the experimentally measured trimer H-bonds[137]). For those structures, they found E_{ABC} contributions to the cluster energy of 12%, 0.8%, and 3% (calculated at $R_{OO} = 3.0$, 3.15, and 3.15 Å, respectively) for a sequentially H-bonded (OH···OH···OH) trimer. They concluded that substantial nonadditivity is present in sequentially H-bonded small water clusters due to polarization effects. They calculated $\Delta E^{(mon)} = -2.76$ kcal/mol for the open, sequentially bonded structure, considerably smaller than the cyclic trimer energy of Del Bene and Pople, but 25% more stable than the next most stable open structure. Hankins et al. also considered the anisotropy of E_{ABC} as a function of R_{OO} for each of the three quasilinear trimers. They found that for the double-donor (HHO···HOH···OHH) and double-acceptor (HOH···O[HH]···HOH) structures, the three-body energy was repulsive at short range, while that of the sequential geometry was attractive for all values of R_{OO} down to 2.7 Å. Additionally, the E_{ABC} term of the sequential structure was relatively invariant to H-bond torsional angle, predicting that three-body forces are in general attractive, resulting in shorter H-bonds, and are thus compressive in the bulk phases of water.

Lentz and Scheraga[138] in 1973 asserted that it was impossible to reproduce many thermodynamic properties of liquid water using the stabilization energies of Del Bene and Pople.[86,131] In a SCF calculation performed to verify the results, they calculated the equilibrium structures of water trimers and tetramers using the basis set used by Hankins et al.[135,136] They computed $\Delta E^{(\mathrm{mon})} = -6.52$ kcal/mol for a cyclic trimer with E_{ABC} accounting for 13.6% of the total, much smaller than the nonadditive contribution predicted by Del Bene and Pople, and only slightly more than the fractional contribution of E_{ABC} to the open sequential structure of Hankins et al.[135] They concluded that cyclic water clusters have no "special stability", rationalizing the large difference between their calculated nonadditivity and that of Del Bene and Pople by noting that the minimal basis used in the latter calculation was insufficient to fully account for intermolecular repulsion. The attractive effects of three-body forces, which Lentz and Scheraga showed to follow an approximate $1/R_{\mathrm{OC}}^9$ law, were much greater at the interoxygen separation of 2.56 Å found by Del Bene and Pople. They calculated that three-body attraction in the cyclic trimer accounted for 35.6%, 13.6%, and 7.5% of the total interaction energy at $R_{\mathrm{OO}} = 2.81$, 3.00, and 3.25 Å, respectively; their cyclic trimer was repulsive by 4.98 kcal/mol at the R_{OO} of Del Bene and Pople, with $E_{\mathrm{ABC}} = -3.55$ kcal/mol.

Kistenmacher and co-workers[139] employed a least-squares fit of an analytical expression to over 250 ab initio (Hartree−Fock) water dimer points (AFHF: "analytic fit to Hartree−Fock points") in order to more efficiently explore the configuration spaces of the dimer, trimer, and larger clusters. Although pairwise additivity was implicit in their model, it predicted cyclic trimer and tetramer equilibrium structures. After structural optimization with the AFHF potential, they recalculated the trimer binding energy at the HF level, finding $\Delta E^{(\mathrm{mon})} = -4.45$ kcal/mol, compared to −4.1 kcal/mol from the AFHF. The corresponding AFHF per-monomer energy for the quasilinear structures of Hankins et al.[135,136] and Lentz and Scheraga[138] was −3.24 kcal/mol. The three-body contribution to the energy of the C_1 cyclic form was 8.5% of $\Delta E^{(\mathrm{mon})}$. The AFHF potential was the precursor to the well-known MCY water pair potential later developed by Matsuoka, Clementi, and Yoshimine.[76] Later versions of that potential, incorporating three- and four-body corrections, have successfully reproduced many liquid water properties, such as pair correlation functions (g_{OO}, g_{OH}, g_{HH}), diffusion coefficients, and IR spectra.[7−9,12] Kistenmacher et al. showed that simple semiempirical potentials can accurately predict the structures of small water clusters, but more recent studies have shown that nonadditive forces must be considered in order to rationalize the structures of water clusters larger than the pentamer.[16,140]

Habitz et al. studied the convergence of three-body interactions of three cyclic C_{2v} trimers as a function of electron correlation in ab initio theory,[7] comparing SCF and configuration interaction (CI) calculations. They found that the three-body components of the stabilization energies were essentially accounted for in SCF calculations, with minor corrections at the correlated level. Those CI corrections contained the three-body dispersion interaction, which correlates at long range to the Axilrod−Teller triple dipole energy.[103,141] While the three-body CI correction differed as a function of structure, it typically accounted for about 5% of the SCF three-body energy.

In an ab initio study of the structures and intramolecular vibrational frequencies of water clusters, Honegger and Leutwyler optimized the cyclic trimer structure in SCF calculations using the 4-31G and 6-31G* bases.[142] The 4-31G basis predicted $R_{\mathrm{OO}} \leq 2.7$ Å, confirming the results of Del Bene and Pople.[133] The larger basis predicted an average R_{OO} value of 2.87 Å, with $\Delta E^{(\mathrm{mon})} = -5.81$ kcal/mol. Relaxing the monomer geometries, they found that bridged O−H bond lengths ($r_{\mathrm{OH}}^{\mathrm{b}}$) increased by approximately 0.01 Å in the optimized structures of both calculations, while a decrease in length of the free O−H bonds ($r_{\mathrm{OH}}^{\mathrm{f}}$) by 0.008 Å was observed only using the smaller basis.

Clementi and co-workers[6] studied nonadditivity in the trimer as a function of basis set size and geometry at the SCF level. They calculated pairwise-additive and nonadditive contributions to the stabilization of 29 trimer configurations, including the equilibrium structure, using four contracted bases comprising minimal (O:7s,3p/H:3s) and extended (O:13s,8p,1d/H:7s,1p) sets. Their BSSE-corrected energies for the equilibrium structure were $\Delta E^{(\mathrm{mon})} = -4.32$ and −4.24 kcal/mol for the smallest and largest basis sets, respectively, with three-body contributions of 8.9% and 9.7% of the respective totals. All four basis sets gave nonadditive contributions in the range 8.8−9.7%, while the total energies differed by as much as 1.5 kcal/mol per H-bond. From their comparisons, Clementi et al.[6] concluded that there is no justification for using the intermediate bases when conditions allow use of larger ones, but noted that well-chosen minimal bases with BSSE corrections gave energies within 2% of the extended basis result. They also proposed a perturbation approximation of the SCF energies in the form of

$$\Delta E = E_{\mathrm{es}} + E_{\mathrm{exch}}^{(1)} + E_{\mathrm{ind}}^{(2)} + E_{\mathrm{disp}}^{(2)} + E_{\mathrm{exch}}^{(2)} + \ldots \quad (3)$$

where E_{es} and $E_{\mathrm{disp}}^{(2)}$ are the additive electrostatic and dispersion contributions, and $E_{\mathrm{ind}}^{(n)}$ and $E_{\mathrm{exch}}^{(n)}$ are the nth-order induction and exchange energies, which contain nonadditive components. They noted that the nonadditive part of $E_{\mathrm{exch}}^{(1)}$, like the analogous term in rare gas trimers (e.g., see ref 141), should be small for R_{OO} near 3 Å (long range); therefore, the principal nonadditivities in second order arise from the $E_{\mathrm{ind}}^{(2)}$ and $E_{\mathrm{exch}}^{(2)}$ terms. They approximated $E_{\mathrm{nadd}}^{(2)}$, the nonadditive part of $E_{\mathrm{ind}}^{(2)}$, using a bond polarizability model. The principal polarization anisotropy in their approach was accounted for by separation into bond polarizabilities. They found that this simple model accounted for about half of the equilibrium structure (SCF) nonadditivity calculated with either the minimal or extended bases. Because no dispersion inter-

action is present in SCF calculations, Clementi et al. also calculated London-type dispersion energies using experimental bond polarizabilities, finding a −2.7 kcal/mol contribution (0.9 kcal/mol per monomer) for the equilibrium configuration, or approximately 20% of the total interaction energy. For some configurations, they noted that the dispersion and SCF repulsion contributions nearly cancel, emphasizing the need for accurate accounting of electron correlation and reinforcing the conclusions of Belford and Campbell.[88]

Laasonen et al.[143] studied the energetics and conformations of water clusters using DFT. In a study of clusters as large as the octamer, using the Car−Parrinello[62] method with gradient-corrected DFT, they determined that the cyclic, C_1 trimer was the most stable, with $\Delta E^{(\mathrm{mon})} = -5.14$ kcal/mol and $R_{OO} = 2.8$ Å. The R_{OO} was much shorter ($R_{OO} = 2.57$ Å) in the uncorrected results. This method also predicted the correct tetramer structure, whereas a cyclic hexamer was determined to be most stable, followed by a nearly isoenergetic book like structure. Lee and co-workers[144] extended that study to clusters of up to 20 waters, comparing three functionals, obtaining $\Delta E^{(\mathrm{mon})} = -5.58$ kcal/mol for the trimer with the BLYP functional,[145] one that has proven to reproduce most MP2 results with reasonable fidelity (see Table 1).[25] Interestingly, they found "magic numbers", i.e., clusters showing special stability when the per-monomer stabilization energy was compared with those of clusters of smaller size. Clusters $(H_2O)_n$, $n = 8$, 12, 16, 20, showed such special stability, the tetramer being the fundamental building block of each (for example, the quasicubic octamer is composed of two stacked tetramers). However, these calculations found the most stable hexamer to be a cyclic structure. Liquid water simulations[53,54,146] have tended to focus on pentamers as the fundamental repeating unit in cluster−liquid models, with the notable exception of the work by Benson and Siebert,[147] who modeled liquid water with a simple two-state model, the states being composed of the tetramer and octamer described by Lee et al.[144] They were able to reproduce the anomalously high heat capacity of water to within ±2% between 0 and 100 °C. In a more recent DFT contribution, Estrin and co-workers used the PP functional (see ref 148) and moderate-sized basis sets to calculate the structures and vibrational frequencies of water clusters as large as octamers.[149] Consistent with HF and electron-correlated ab initio results, they observed R_{OO} contraction and r^{b}_{OH} elongation converging to stable values by $n = 6$, although they predicted somewhat shorter values of R_{OO} ($R_{OO} = 2.78$ Å) for the trimer. Their trimer was stable by $\Delta E^{(\mathrm{mon})} = -6.17$ kcal/mol. Estrin et al. also calculated ZPE-corrected binding energies of −4.24, −6.05, and −6.43 kcal/mol per monomer for the cyclic trimer, tetramer, and pentamer, respectively, again reflecting a self-consistent increase in per-monomer binding energies with increasing cluster size. The disparity evident in the DFT equilibrium energies (see Table 1) seems to indicate a lack of convergence to the appropriate functionals for representation of weakly bound clusters, although DFT cluster studies are an active area of research. As with ab initio methods, one particular concern about the DFT method is its ability to properly model dispersion interactions, which are consistently shown to constitute ca. 20% of the total attractive energy, and which may have a stronger parametric effect on the nonadditive energies. Indeed, as Schütz et al. pointed out, the variation in binding energies for a variety of complexes, including water clusters, is of the order of the correlation energies themselves.[60]

In a defining ab initio study, Chalasinski and coworkers[150] dissected the two- and three-body electrostatic, induction, dispersion, and exchange trimer energies using a combination of supermolecular Møller−Plesset perturbation theory (MPPT) and intermolecular (I)MPPT, reviewed in refs 151 and 152. In their method, the cluster energy was calculated from the perturbation series

$$\Delta E = E^{\mathrm{SCF}} + E^{(2)} + E^{(3)} \tag{4}$$

where E^{SCF}, $E^{(2)}$, and $E^{(3)}$ are the SCF energy and the second- and third-order IMPPT corrections to it, respectively. Each term was broken into a sum of two- and three-body energies. The electrostatic contributions, all pairwise additive, arose in each of the three terms. The two-body dispersion energy was a second-order term with a third-order correction that also included three-body dispersion. Chalasinski et al. showed that both electrostatic and dispersion energies were strongly basis-set-dependent, in a comparison of the 6-31G** basis with a larger contracted version of the basis (O:10s,6p,2d/H:5s,2p). In contrast, exchange and induction energies were not as basis-set-dependent. In their treatment, the exchange energy was calculated at the SCF level, with second- and third-order corrections to both the two- and three-body terms. They pointed out that an accurate quantum calculation cannot allow unrestricted deformation of the electron densities, but must comply with the Pauli exclusion principle. Therefore, the induction term of Chalasinski et al., $\Delta E^{\mathrm{SCF}}_{\mathrm{def}}$, included exchange effects. The two- and three-body $\Delta E^{n}_{\mathrm{def}}$ terms arose at each level in the perturbation expansion, but the corrections at the second and third orders were not well defined. However, as Habitz et al. showed, the induction is already well represented by moderate-sized bases at the SCF level.[7]

A few of the salient results of Chalasinski et al. are reproduced in Figures 3−5. In studies of the anisotropy of a planar, cyclic trimer, they showed that the H-bonding angle δ(OH···O) is largely determined by the electrostatic and exchange terms, while induction and dispersion favor a H-to-H cyclic geometry (see Figure 3). The two- and three-body induction, dispersion, and exchange energies are compared in Figure 4, from which it is clear that three-body induction constitutes about 26% of the total induction energy, $\Delta E^{\mathrm{SCF}}_{\mathrm{def}}$, at the equilibrium monomer orientations, while three-body dispersion and exchange forces are much less significant as a function of monomer orientation. All of the angular anisotropy

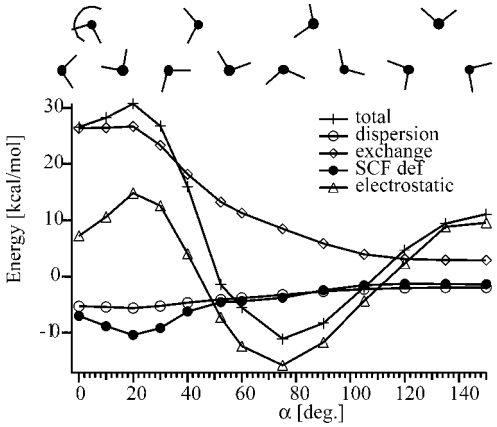

Figure 3. Electrostatic, induction, dispersion, and exchange intermolecular forces (2 + 3-body) calculated by Chalasinski et al.[150] The energies are plotted as a function of the angle α (defined at the top of the figure) for a cyclic, planar trimer. The interoxygen separation R_{OO} was fixed at 3.0 Å in these calculations. The equilibrium trimer has α = 75°.

studies were carried out with R_{OO} fixed at 3.0 Å, while the equilibrium trimer interoxygen separation is closer to 2.9 Å in high-level calculations. Figure 5 shows the behavior of a few of the terms as a function of R_{OO}, including the polarization energy from the RWK2 potential of Reimers et al. Both the three-body SCF energy and the RWK2 polarization estimate drop off rapidly with $1/R_{OO}$. Therefore, the three-body parts of the dispersion and exchange forces would be expected to be larger at the actual trimer interoxygen separation than that shown in Figure 3.

In a series of four articles, Xantheas and Dunning[26,153] and Xantheas[17,25] computed the equilibrium structures of cyclic water clusters up to the hexamer in high-level ab initio calculations. They quantified the many-body interactions in a classical decomposition scheme and compared DFT results using a variety of functionals with correlated ab initio second-order Møller−Plesset perturbation theory (MP2) results. At the fourth-order (MP4) level (aug-cc-pVDZ basis) with BSSE (CP) correction, Xantheas calculated $\Delta E^{(mon)} = -4.36$, -4.55, and -5.95 kcal/mol for the dimer, trimer, and tetramer, respectively. While the three-body contribution constituted 17.6% of the trimer energy, the sum of three-body contributions accounted for 26% of the tetramer energy. The MP4 four-body contribution to the tetramer energy was 2.3% and attractive. The interoxygen separation in Xantheas's (MP2) tetramer was 0.056 Å shorter than the corresponding R_{OO} in the trimer, which may account for a fraction of the added E_{ABC} contribution, but it is more likely due to the more favorable tetramer H-bond angle [δ_{tri}(O−H···O) = 150.3°, δ_{tetra}(O−H···O) = 167.7°], which increases both two- and three-body cohesive forces.

Mó and co-workers performed MP2 and MP4 calculations using large basis sets, examining 17 different trimer structures, including all permutations of single/double donor/acceptor quasilinear configurations.[95] In addition to the global minimum structure [$\Delta E^{(mon)} = -5.23$ kcal/mol in MP2/6-311++G(2d,2p) calculations], they found two other ab initio local minima. One was a cyclic structure in which one monomer was a double donor, one a double acceptor, and one a donor + acceptor, with $\Delta E^{(mon)} = -3.4$ kcal/mol. The latter structure collapsed to the equilibrium geometry in HF calculations using the 6-31G* basis. Consistent with the results of Clementi et al.,[6] Mó et al. found a stable quasilinear trimer with the central water acting as a double H-bond donor ($\Delta E^{(mon)} = -3.07$ kcal/mol), but they did not find a minimum corresponding to the double-acceptor structure, which also rapidly relaxed to the equilibrium geometry. All other cyclic structures were transition states or higher-order saddle points on the ab initio IPS. They noted that in all structures except the global minimum, the per-monomer stabilization energy was smaller than the equilibrium water dimer binding energy of −4.07 kcal/mol, calculated at the same level of theory.

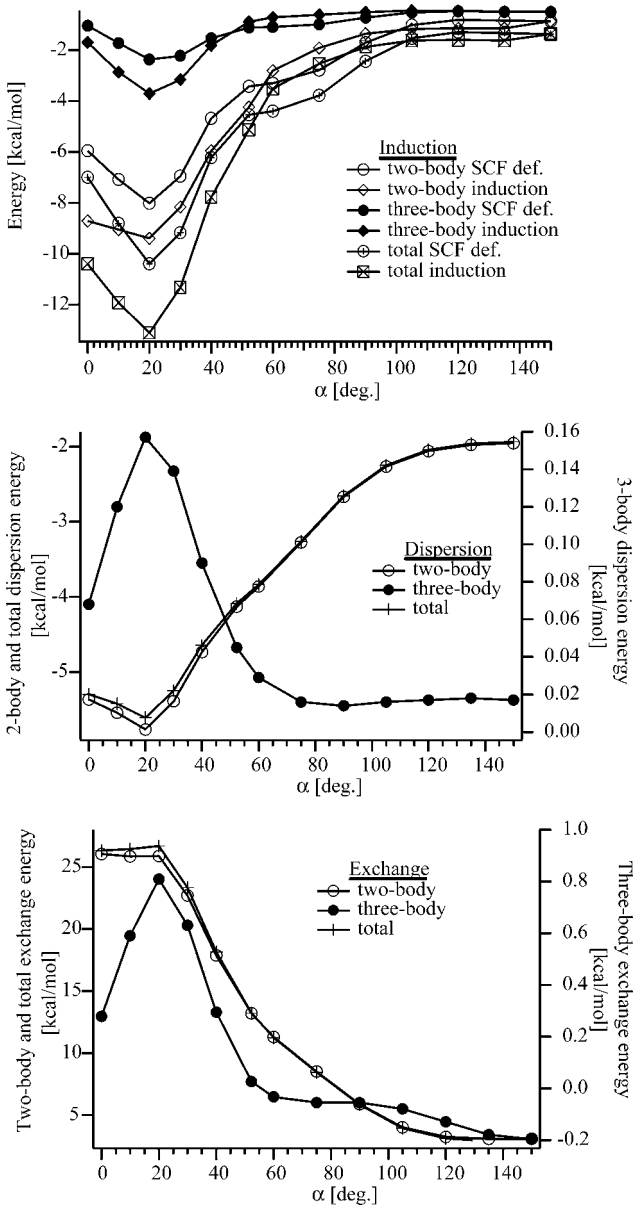

Figure 4. Comparison of the angular anisotropies of the principal two- and three-body components of the induction, dispersion, and exchange intermolecular forces for the cyclic, planar trimer defined in Figure 1b, with R_{OO} fixed at 3.0 Å. (Figure adapted from Chalasinski et al.[150]) At R_{OO} = 3.0 Å, the three-body dispersion and exchange contributions are small, while the three-body induction is about 26% of the total at α = 75°.

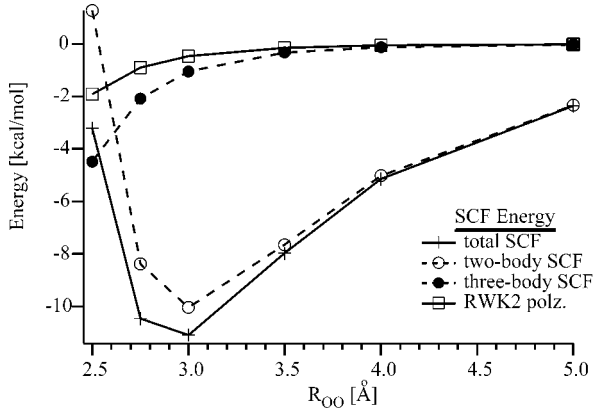

Figure 5. R_{OO} dependence of intermolecular forces calculated by Chalasinski et al.[150] Note that the contribution from three-body forces increases on going from $R_{OO} = 3.0$ to 2.9 Å, the equilibrium structure value.

Pastor and Ortega-Blake[154] studied the effects of relaxation of the monomer geometries on H-bond cooperativity, finding large nonadditive effects at electron-correlated levels of theory. Performing SCF and CI+MP2 calculations (2ζ** and 4ζ** bases), they showed that the dimer r_{OH}^{b} increased by 0.021 Å in the correlated calculations, while the increase was nearly a factor of 10 smaller in their SCF calculations. Upon allowing for intramolecular relaxation, Pastor and Ortega-Blake calculated extremely large three- and four-body nonadditivities for water tetramers — to the extent that a rapidly convergent many-body expansion was no longer appropriate to model the interaction. In a further study of pentameric substructures observed in MD simulations of 20 waters, they found large nonadditivities. They attributed these to intramolecular relaxation and to the asymmetry of the pentameric forms, which are more likely to look like liquid water than the gas-phase cluster structures discussed thus far. Nevertheless, it is difficult to reconcile the large nonadditivities and relaxation contributions observed by Pastor and Ortega-Blake with the results of other calculations using large basis sets at correlated levels of theory. Xantheas,[17] for example, calculated (HF+MP2/aug-cc-pVDZ) relaxation and two-, three-, and four-body energies of the S_4 equilibrium tetramer of +1.00, −18.55, −6.24, and −0.54 kcal/mol, respectively, while Pastor and Ortega-Blakes's calculation (CI+MP2/4ζ**) gave +18.29, −14.89, −10.84, and −0.93 kcal/mol. The exact geometry used in the latter calculation is unclear, but larger polarization contributions would be expected from the r_{OH}^{b} elongations.

Using coupled-cluster methods with a variety of large basis sets, Fowler and Schaeffer[155] fully explored the trimer IPS, finding the relative energies of many stationary points in HBNR pathways. They calculated the H-bond torsion transition state and global minimum energies, as well as the ZPE in a coupled-cluster calculation with single and double excitations (CCSD) and using the TZ2P+diff basis. The flipping barrier and ZPE at that level of theory were both 0.26 kcal/mol, confirming the facility of the flipping motion at a high level of theory. The stationary point energies of Fowler and Schaefer[155] and selected other calculations are collected in Table 2.

Schütz and co-workers[60] addressed the idea of local treatment of electron correlation in ab initio calculations, pointing out the success of such treatments in reducing the BSSE and therefore the need for extensive CP corrections. They noted that BSSE is insignificant at the HF level of theory, regardless of basis set size, because HF calculations are rapidly convergent. Conversely, they pointed out that dispersion correlation converges very slowly. In their local MP2 (LMP2) treatment, they restricted the correlation space of a given electron pair to basis functions in the vicinity of their respective localized orbitals. Using LMP2 and the aug-cc-pVQZ basis set, they calculated $\Delta E^{(mon)} = -5.05$ kcal/mol, while the corresponding dimer energy was −4.80 kcal/mol, for a three-body cohesive energy of 5% of the total. At the equilibrium geometry, the total dispersion energy was −3.56 kcal/mol and the CP correction was small, $\delta_{CP} = +0.03$ kcal/mol.

Recent precise measurements of quantum tunneling splittings in high-resolution water trimer spectra have stimulated several detailed analyses of HBNR pathways on ab initio and empirical IPS's. Schütz and co-workers,[61] Walsh and Wales,[104,156,157] Fowler and Schaeffer,[155] and Klopper et al.[158] studied stationary points and tunneling pathways on ab initio IPS's in an effort to rationalize the observed dynamics. Those efforts have also been extended to studies of the tetramer[74] and pentamer.[159] Schütz et al.[61] characterized five H-bond torsional variants of the cyclic equilibrium trimer. They studied the {*uud*}(6), {*uuu*}(2), {*ppp*}(1), {*upd*}(6), and {*uup*}(3) structures, where the number in parentheses is the number of equivalent versions of the given structure if the monomers are rearranged within the complex. In MP2/6-311++G(d,p), BSSE-corrected calculations, they found the {*uuu*} and {*ppp*} forms to be transition structures lying 0.6 and 0.43 kcal/mol above the global minimum, respectively. The {*upd*} configuration, calculated to lie 0.03 kcal/mol above the global minimum in HF calculations, was found to be a first-order saddle point (one imaginary frequency) in the flipping pathway which interconverts the six global minimum structures, for example, {*uud*} → {*udd*}. Schütz et al. concluded that when the ZPE is taken into consideration, nearly free H-bond torsion must occur in the trimer, and they postulated a pseudorotation model to account for the lowest trimer vibrational eigenstates. That model will be discussed in more detail in a later section.

Wales,[156,157] Walsh and Wales,[104] and Taketsugu and Wales[160] investigated possible structural rearrangement pathways and their manifestations in the VRT spectra in great detail. Walsh and Wales calculated flipping barriers of between 0.04 and 0.3 kcal/mol, and between 0.01 and 0.55 kcal/mol, with a variety of ab initio and empirical potentials, respectively.[104] While the calculations showed the sensitivity of the H-bond torsional subspace of the trimer IPS to the choice of theoretical method, it also confirmed that flipping occurs very near the limit of free internal rotation if ZPE is considered. Walsh and Wales, and Taketsugu and Wales, also explored pathways for bifurcation tunneling (Figure 2b). The

bifurcation motion was shown to be responsible for the quartet tunneling splitting patterns (Figure 7) observed in the trimer VRT data.[156,161] Wales and coworkers proposed six possible bifurcation-tunneling pathways, interconnecting the set of {*uud*} minima, that could lead to those splittings. They calculated the transition state for the most likely bifurcation pathway lying between 720 and 820 cm^{-1} above the global minimum, with different levels of theory. Estimates using the empirical potentials (TIP4P,[55−57] EPEN, and two forms of the ASP potential[162] of Stone et al.) ranged from 248 to 672 cm^{-1} (ASP) above the global minimum, illustrating the disparity between ab initio and at least some modern empirical water cluster potentials.

Recent contributions by Gregory and Clary have been extremely valuable in bridging the gap between theoretical results and experimental data, which necessarily include ZPE vibrational effects.[16,127−129,163−165] Using diffusion quantum Monte Carlo (DQMC) methods in conjunction with the most promising additive and many-body water potentials, those authors explored the ground-state structures of clusters as large as the hexamer and attempted to calculate tunneling splittings due to the large-amplitude H-bond network rearrangements. In particular, they used two forms of the anisotropic site potential (ASP) of Millot and Stone,[162] a pairwise additive form, and one modified to include an iterated many-body induction energy, as well as the Axilrod−Teller triple-dipole energy[103] to approximate the long-range dispersion. Neglecting short-range many-body contributions on the basis that they would not be important at the intermolecular separations sampled in the MC simulations, they found that the three-body IPS (ASP-3B) more faithfully reproduced the experimentally measured moments of inertia (i.e., rotational constants) than the two-body potential (ASP-P). As the following sections will show, the experimental moments of inertia are likely to be significantly contaminated by the large-amplitude dynamics. The calculations of Gregory and Clary were designed to account for these details. By making use of the symmetry imposed by results of the THz-VRT spectra and group theoretical considerations, they were able to construct ground-state wave functions and thereby calculate both flipping and bifurcation-tunneling splittings in qualitative agreement with the VRT data. Gregory and Clary also showed that inclusion of the three-body corrections to the ASP potential decreased the ground-state tunneling splittings by 10% in the flipping coordinate and 30% in the bifurcation coordinate, consistent with the notion of quenching of the rearrangement dynamics with increasing cluster size as a result of cooperativity. In the second of two trimer calculations, they used ab initio (MP2/DZP) calculations to optimize the ASP-3B minimum-energy structure and estimate the destabilizing contribution of monomer relaxation.[16] They found small destabilizations of small clusters, with $\Delta E_{relax} = +0.14$ kcal/mol (1.3% of ΔE_{ABC}) for the trimer, but only 10% of the relaxation energy obtained in Xantheas's ab initio optimized structure. In a study of the water hexamer, they also noted that three-dimensional water cluster structures (e.g., structures containing more H-bonds than a cyclic configuration) are destabilized by many-body interactions, rationalizing the observation that the equilibrium structure of the pentamer, in theory and experiment, is cyclic.

Gonzalez et al. investigated the geometries, vibrational frequencies, and energies of $(H_2O)_n$, $n = 1-3$, with DFT with the B-LYP, B3-LYP, B3-P86, and B3-PW91 functionals.[166] Specifically, the authors investigated how well different density functionals reproduced the many-body interactions. The results showed that both the B-LYP and B3-LYP functionals appear to be good alternatives to ab initio calculations. Increasing the basis set from 6-31+G(d,p) to 6-311++G(3df,2p) decreased the binding energies significantly for all functionals, and similar effects have been observed in ab initio calculations. The three-body contribution varied between 27.7% for the B3-LYP and 22.9% for the B-LYP functional. The intramolecular vibrational frequencies calculated with the B3-LYP functional agreed well with experiment except for the free OH stretch frequencies, which were significantly higher than the experimental ones. This was also observed in vibrational SCF calculations by Jung et al.[167] and most high-level ab initio calculations.

Gregory et al. calculated the dipole moments of $(H_2O)_n$, $n = 2-6$ and 8, at the MP2/aug-cc-pVDZ level of theory using a distributed multipole analysis.[93] The calculated total dipole moment for the (asymmetric equilibrium structure of the) water trimer was 1.071 D, whereas experimentally no dipole moment was observable − a consequence of the facile torsional averaging of the asymmetric equilibrium structure. The authors showed that their results were consistent by comparing the calculated dipole moment of the cage hexamer, $\mu_a = 2.02$ D, with the experimentally observed value of $\mu_a = 1.82-2.07$ D. Gregory et al. also calculated the average monomer dipole moments in these water clusters and demonstrated the increase of monomer dipole moments with cluster size resulting from induction. The average water monomer dipole moments in the water trimer were found to be ca. 2.3 D. Similar results have been reproduced with ab initio methods by Tu and Laaksonen[168] and an empirical potential by Dang and Chang.[92]

Liedl and Kroemer estimated the binding energy of $(HF)_3$ and $(H_2O)_3$ using basis set convergence patterns at the MP2(FC)/aug-cc-pVDZ-aug-cc-pVQZ level of theory.[169] They introduced a scaling factor by investigating the differences between the BSSE-corrected and uncorrected MP2 results. The basis set limit value obtained for the water trimer in this way was $\Delta E^{(mon)} = -5.30$ kcal/mol, and the authors pointed out the importance of using the frozen core method with the aug-cc-pVxZ series of basis sets, which was far more important than reoptimizing the geometry for each basis set.

In the most extensive ab initio study of the water trimer to date, Nielsen et al. studied the complete basis set limit for the water trimer at the MP2 level of theory.[170] The basis sets ranged from aug-cc-pVDZ

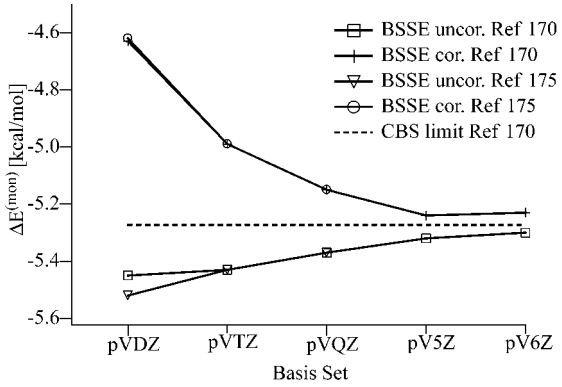

Figure 6. MP2 ab initio trimer binding energies ($\Delta E^{(mon)}$), calculated with and without BSSE correction for basis set sizes from aug-cc-pVDZ−aug-cc-pV6Z, together with the complete basis set limit estimate.[170,175] It should be noted that for small basis sets the BSSE-uncorrected values are closer to the complete basis set limit.

to aug-cc-pV6Z, the latter containing 1329 basis functions. For the infinite basis set frozen core MP2 binding energy, they suggested a value of $\Delta E^{(mon)} = -5.273 \pm 0.066$ kcal/mol (see Figure 6). The energies were computed at the MP2/aug-cc-pVQZ optimized structure. Inclusion of core correlation using the aug-cc-pCV5Z basis set increased the binding energy by 0.08 kcal/mol, and after consideration of core correlation and higher-order effects, the classical binding energy of the water trimer was estimated to be 15.9 ± 0.2 kcal/mol.

Milet et al. studied the importance of pair and many-body interactions in the water trimer through pentamer, including different geometries of the water trimer, e.g., the saddle points for the torsional and bifurcation-tunneling processes.[171] The interactions were calculated directly using symmetry-adapted perturbation theory (SAPT), compared with the results from CCSD(T) calculations (frozen 1s orbitals), and the individual electrostatic, induction, dispersion, and exchange contributions were analyzed. All calculations used the aug-cc-pVDZ basis set. The agreement between the CCSD(T) and SAPT calculations was excellent for both the pair and three-body interactions. The three-body interaction contributed between 14% and 17% of the total binding energy for all of the various trimer structures (and up to 28% for the pentamer). However, it contributed a large amount to the barriers of the bifurcation (ca. 39%) and torsional (ca. 50%)-tunneling motions, which resulted from the fact the three-body interaction was always smaller at the stationary points than at the global minimum. The analysis of the individual contributions to the two-body interaction showed that the pair potential resulted from partial cancellation of the attractive electrostatic, induction, and dispersion contributions with the strongly repulsive exchange term. The three-body term in the water trimer was dominated by the second-order induction nonadditivity, with a still significant (10−30%) contribution from the third-order induction. This is important, as it demonstrates that iteration beyond the first step is required to represent induction correctly. These authors also studied how the relative contribution of the three-body forces in the water trimer structures calculated with DFT methods compared to the SAPT and CCSD(T) results using the most popular (semi)local functions available in Gaussian94: BLYP, BP86, BPW91, B3LYP, B3P86, and B3PW91. Agreement with SAPT and CCSD(T) results was poor, with B3LYP having the smallest errors, which were still as large as 29% for the *ppp* structure and between 6% and 9% for the other structures. The authors noted that the total interactions typically had smaller errors resulting from cancellation of errors in the two- and three-body energies.

Tachikawa[172,173] calculated the structures and nuclear and electronic wave functions of the water dimer through pentamer and hydrogen halide water clusters using a multicomponent molecular orbital approach that includes the coupling effect between nuclei and electrons. The authors noted that substitution of H with D resulted in a shortening of ca. 0.008 Å of R_{OD} compared to R_{OH} but a larger extension of ca. 0.012 Å of $R_{OD\cdots O}$ compared to $R_{OH\cdots O}$, resulting in a distinctly larger R_{OO} for $(D_2O)_3$. Similar effects were observed for the other water clusters.

In the second of a series of three publications appearing in 2002,[117,174,175] Xantheas et al. estimated the complete basis set (CBS) limits for the cluster total association energy at the MP2 level of theory.[175] The augmented correlation-consistent basis sets ranged from the double- through quintuple-zeta quality (aug-cc-pVDZ through aug-cc-pV5Z), allowing for a systematic way of studying the CBS limit. Xantheas et al. noted that it was established early that the CBS limits lie between the uncorrected and BSSE-corrected results. The difference between the uncorrected and BSSE-corrected values diminished with increasing basis set size and allowed the authors to estimate the CBS limit for the binding energy of the water trimer to be $\Delta E^{(mon)} = -5.27$ kcal/mol at the MP2 level of theory, in agreement with the results by Nielsen et al.[170] and Liedl and Kroemer.[169] Furthermore, they showed that although larger basis sets result in more accurate energies, the value of these energies is insensitive to the basis set size at which the geometry optimization was calculated. The trimer cluster geometry appears to be converged by the aug-cc-pVTZ basis set size. The BSSE-uncorrected numbers are closer to the CBS limit, especially for the smaller basis sets.

C. Dynamics

The earliest high-resolution spectra of the gas-phase water dimer showed that its H-bond broke and re-formed many times on a subpicosecond time scale as a result of quantum mechanical tunneling. To date, all of the high-resolution data for water clusters up to the hexamer have exhibited the consequences of similar H-bond network tunneling dynamics. The H-bond bifurcation motion in the water trimer occurs through a relatively high-energy transition state and has been shown to be responsible for the quartet splittings observed in each VRT transition in all THz spectra of homoisotopic ($^1H/^2H$) trimers (Figure 7). Conversely, the H-bond torsional, or flipping motion is virtually a barrierless process and is responsible

Table 3. Symmetry Labels and Nuclear Spin Weights for the G_6 and G_{48} PI Groups of the Water Trimer

$\Gamma_i^{\pm}$ C_1	$(H_2O)_3$	$(D_2O)_3$	$\Gamma_I^{\pm}$ G_6	k	$(H_2O)_3$	$\Gamma_i^{\pm}$ G_{48}	$(H_2O)_3$	$(D_2O)_3$
A	128	1458	A_1^+	0	24	A_{1g}^+	1	76
						T_u^+	3	108
						T_g^+	9	54
						A_{1u}^+	11	11
			A_2^-/A_3^-	±1	20/20	A_{2g}^-/A_{3g}^-	0/0	70/70
						T_u^-/T_u^-	3/3	108/108
						T_g^-/T_g^-	9/9	54/54
						A_{2u}^-/A_{3u}^-	8/8	8/8
			A_2^+/A_3^+	±2	20/20	A_{2g}^+/A_{3g}^+	0/0	70/70
						T_u^+/T_u^+	3/3	108/108
						T_g^+/T_g^+	9/9	54/54
						A_{2u}^+/A_{3u}^+	8/8	8/8
			A_1^-	3	24	A_{1g}^-	1	76
						T_u^-	3	108
						T_g^-	9	54
						A_{1u}^-	11	11

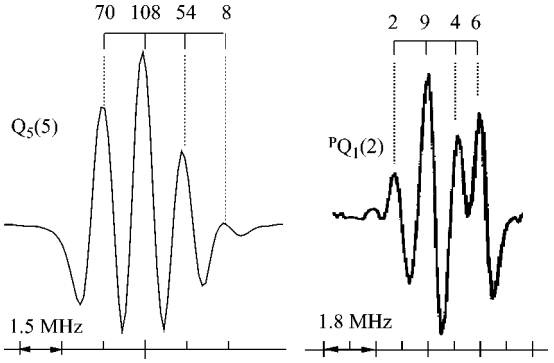

Figure 7. The 1232419.00 MHz $Q_5(5)$ transition of the 41.1 cm^{-1} torsional spectrum of $(D_2O)_3$ first measured by Suzuki et al.[218] and the 841886.5 MHz $^PQ_1(2)$ transition of the 28.0 cm^{-1} $(D_2O)_3$ band. The former is representative for the regular bifurcation-tunneling quartets, and the latter shows an "anomalous" quartet. The spacing of the quartet components in the $Q_5(5)$ rovibrational transition is 1.5 MHz. Each transition in the spectrum is split in a similar manner. The spacing of the $^PQ_1(2)$ transition is ca. 0.9 MHz and slightly unequal. Both splittings are due to rearrangement of the water molecules through a high-barrier bifurcation-tunneling motion (Figure 2b), and the intensity pattern is determined by nuclear spin statistics (see section III.B.1.4). The analogous splittings in $(H_2O)_3$ are 289 and 255 MHz, respectively.

for the high density of low-energy states found in the spectroscopic data.

Although the large-amplitude dynamics characteristic of the water trimer are ultimately manifested in all water cluster or bulk-phase water experimental data, the following discussions will make more frequent reference to the THz-VRT data, where they have profound consequences. The following sections will address theoretical aspects of both the bifurcation and H-bond torsional dynamics, and conclude with discussions of theoretically calculated inter- and intramolecular vibrational frequencies.

1. Group Theory

Structural rearrangements among degenerate IPS minima have profound consequences in the experimental spectra of weakly bound clusters (see Figure 7). Energy-level splittings, shifts, and other perturbations are consequences of the dynamics that directly reflect the topology of the IPS, and thus provide vital information on the intermolecular force field. To connect the rearrangement dynamics with the data, it is essential to develop a group theoretical model that provides a set of state labels and selection rules for spectroscopic (electric dipole) transitions among them. Permutation-inversion (PI) group theory[176] has proven to be indispensable for describing the complicated tunneling dynamics of the water dimer,[177] the ammonia dimer,[178] and other weakly bound systems that exhibit facile structural rearrangement. A thorough group theoretical description of the dynamical symmetry of the homoisotopic trimers, $(H_2O)_3$ and $(D_2O)_3$, was provided by Liu, Loeser, and co-workers,[161] by Wales,[157] and by van der Avoird et al.[28] Liu and Brown[179] also developed similar descriptions of the mixed isotopomers $(H_2O)_l(D_2O)_m(HOD)_n$, $(l + m + n = 3)$.

Liu et al. showed that the PI group C_{3h}(M) (see Table 3) is the smallest group that can rationalize the observed water trimer rearrangement dynamics because the high-resolution trimer THz-VRT spectra arise from a dynamically averaged symmetric top. Van der Avoird and co-workers[28] labeled this group G_6. Their nomenclature will be adopted hereafter. Each PI operation in G_6 corresponds to a C_{3h} point-group operation and some act to flip a non-H-bonded proton from one side of the O−O−O plane to the other. Under G_6, each rotation−vibration energy level of the rigid C_1 trimer is predicted to split into six sublevels, labeled by the irreducible representations (irreps) of G_6: A_1^+, A_1^-, A_2^+, A_2^-, A_3^+, A_3^-. Because two sets of levels are degenerate (A_2^+, A_3^+ and A_2^-, A_3^- correspond to the separably degenerate irreps E' and E'' of C_{3h}, degenerate by time-reversal symmetry), splitting of each level into four sublevels may be expected. The G_6 selection rules predict up to four transitions connecting these levels to yield one possible type of quartet splitting pattern in the THz-VRT spectra.

Two factors arose to show that G_6 is insufficient to account for all of the observed spectral features. First, the careful intensity measurements of Liu et al.[161] showed that the actual quartet intensity ratios of approximately 76:108:54:11 did not match those expected in a G_6 picture, wherein the spin weights

are all nearly equal (Table 3). Second, as suggested by earlier theoretical work, a high-barrier picture is probably inappropriate for describing the torsional motions. Therefore, large energy-level splittings would be expected from the flipping dynamics, although they would not necessarily be manifested in the VRT transitions, which are *differences* between levels. To rationalize the quartet features, it was necessary to incorporate the bifurcation rearrangement (Figure 2b) into the group theoretical description. The PI operation (12) represents bifurcation of molecule A by exchange of the coordinates of the protons labeled "1" and "2" (Figure 1b). The direct product of the set of all of the PI operations which generate the bifurcation motion, {(12),(34),(56)}, and their products, (12)(34), (12)(34)(56), and so on, with the six flipping operations of G_6 yields a group of 48 PI operations, G_{48}. The correlation of the irreps $\Gamma_i^{\pm}$ of C_1, G_6, and G_{48} is given in Table 3.

The electric dipole selection rules under G_6 and G_{48} are $\Gamma_i^+ \leftrightarrow \Gamma_i^-$ and $\Gamma_g^{\pm} \leftrightarrow \Gamma_u^{\mp}$, respectively. By using the group G_{48}, one finds that single transitions under G_6 split into four components, with intensity ratios determined by the relative nuclear spin statistical weights shown in Table 3. Liu and co-workers[161] provided a rigorous confirmation of this analysis in a study of the $(H_2O)_3$ VRT spectrum at 87.1 cm^{-1}, where transitions with zero ground-state nuclear spin statistical weights were indeed missing from the spectrum. All of the VRT spectral features observed to date can be rationalized using G_{48}, reflecting the existence of two low-energy structural rearrangements. A third rearrangement is possible, but no effects of this have ever been observed in the data.

Balasubramanian and Dyke[180] showed that the molecular symmetry (MS) groups of water clusters can be derived as Wreath products (a particular type of semidirect product) of smaller subgroups of PI operations, and they applied their method to the water trimer to derive the state labels and selection rules. The largest possible MS group of the trimer (without breaking covalent bonds) is the Wreath product $S_3[S_2] = G_{96}$, which has 96 operations. S_2 and S_3 are the sets of all possible permutations of two and three identical objects, respectively. The difference between G_{96} and G_{48} is inclusion of the set of operations which exchanges the water monomers within the triangular framework. These operations, called cw $\leftrightarrow$ ccw (clockwise $\leftrightarrow$ counterclockwise) by Pugliano and Saykally,[27] interchange the handedness of the chiral cluster by interchanging the coordinates of any two water monomers. The effects of these additional operations have not yet been observed in the trimer THz-VRT spectra; thus, G_{48} is adequate for describing the dynamics.

Analogous group theoretical descriptions were developed for the mixed ($^1H/^2H$) trimer isotopomers.[179] The principal effect of isotopic substitution on the THz-VRT fine structure is to alter the multiplet patterns which can be observed. For example, triplets rather than quartets were observed for each rovibrational transition of $HOD\cdot(D_2O)_2$, and doublets for $(HOD)_2\cdot D_2O$, reflecting the fact that the number of degenerate bifurcation rearrangements is limited to the number of homoisotopic monomers. The MS groups appropriate for rationalizing the VRT features of mixed trimer isotopomers with a common species in all of the free proton positions were derived by computing the direct product of G_6 with the set of operations describing bifurcation rearrangements of their constituent homoisotopic monomers, H_2O and D_2O. For example, for $HOD\cdot(D_2O)_2$ or $HOD\cdot(H_2O)_2$, having all D atoms or all H atoms in free positions respectively, the MS group is given by the direct product $G_6 \otimes \{(12), (34), (12)(34)\}$, which is called G_{24}. Analogously, the MS group of $(HOD)_2\cdot H_2O$ or $(HOD)_2\cdot H_2O$ is given by $G_6 \otimes \{(12), (34)\}$, which yields a group of 12 elements, G_{12}. For $(HOD)_3$, singlet transitions were observed because all structural degeneracies involving bifurcation tunneling had been removed. In the case of a mixed ($^1H/^2H$) trimer with mixed species in the free positions, H-bond torsional motions interchange nondegenerate structures; i.e., $\{uud\}$ and $\{ddu\}$ cannot necessarily be superimposed. However, these structures are nearly isoenergetic, as shown by Guiang and Wyatt.[83] In contrast, the difference between a deuterium bond and an H-bond in a cyclic trimer is roughly 50 cm^{-1}.[181] Viant et al. argued that THz-VRT spectra of several mixed isotopomers formed in molecular beams supported "freezing" of mixed trimers into one configuration or the other, with reference to bifurcation of an HOD monomer.[182] Karyakin et al. also noted that the preferred $(HOD)_2$ structure is one in which the D atom of the donor monomer is donated in the H-bond.[183]

2. H-Bond Network Rearrangement (HBNR)

The facile H-bond torsional motions of the water trimer have been attributed as the source of the low-energy vibrational states observed in the trimer THz-VRT experiments. The experimental study of Pugliano and Saykally[27] precipitated several theoretical models based on adiabatic separation of H-bond torsion from the remaining nine intermolecular coordinates, in order to rationalize the data. These theories have been based on two principal assumptions: (1) that flipping in the trimer is a low-barrier process, and (2) that it can be described as a simple rotation about an axis containing the bound proton. From a practical viewpoint, the first assumption suggests a separation of the flipping coordinates from those with higher rearrangement barriers, and the second reduces the dimensionality of the problem, i.e., only motion of the free proton is allowed, making it more computationally tractable. The resulting "pseudorotation" model has now been addressed and refined in several articles.

While assumption (1) above is justified by the ab initio results, the validity of assumption (2) is more difficult to gauge. Recent investigations of the water pentamer strongly suggest that oxygen atom motion, as well as H-bond torsion, is involved in averaging that analogous quasiplanar ring structure to the experimentally observed symmetric (C_{5h}) rotor.[73] High-level theoretical calculations have shown that the monomer centers of mass are not coplanar in the equilibrium pentamer. It is therefore reasonable to

Table 4. Comparison of Calculated and Experimental Torsional Energy Levels (cm^{-1})

k^n	exptl	BGLK[188]	DD[220]	BGLK[220]	CKL[83]	SAPT-5st[110]
			$(D_2O)_3$			
0^0	0	0	0	0	0	0
$\pm1^0$	8.53846(1)	4.97	7.68	5.15	1.9	9.4
$\pm2^0$	27.99227(1)	16.60	25.18	17.15	5.1	29.1
3^0	41.09974(1)	23.97	36.62	24.73	7	41.1
3^1	90.38081(1)	87.44	96.15	88.93	82.9	107.7
$\pm2^1$	98.09911(1)	96.9	107.5	98.27	86.9	117.0
			$(H_2O)_3$			
0^0	0	0	0	0	0	0
$\pm1^0$	22.70255(1)	15.93	19.93	13.97	12.3	25.2
$\pm2^0$	65.64441(1)	49.68	59.07	44.15	23.1	69.3
3^0	87.052720(7)	69.56	81.23	62.33	32.4	89.9
3^1		154.42	161.01	143.85	120.8	
$\pm2^1$		165.54	172.02	155.18	128.6	

expect that heavy atom motion, as well as motion of the bridged protons or deuterons, may likewise be coupled with the flipping dynamics in the trimer. The isotopic substitution experiments of Viant and coworkers also provided strong experimental evidence that such couplings are indeed present in the trimer.[182]

Schütz et al.[61] first proposed a pseudorotation model as an approximation to H-bond torsion in the trimer, drawing an analogy to the internal angular momentum generated in ring compounds like cyclopentane via concerted motion of degenerate ring-bending vibrations.[184,185] The first of these efforts presented a model wherein the torsional motion links six degenerate structures by a single flip. A cyclic pathway composed of single flips, $(uud) \rightarrow (udd) \rightarrow (udu) \rightarrow (ddu) \rightarrow (duu) \rightarrow (dud) \rightarrow (uud)$, which visits each of the set of six degenerate $\{uud\}$ torsional variants and returns the original framework, suggested a one-dimensional "particle on a ring" Hamiltonian,

$$H^{\text{pseudo}} = -\frac{h^2}{2\mu_{\text{red}}}\frac{\partial^2}{\partial\phi^2} + \text{V}(\phi) \qquad (5)$$

where μ_{red} is a reduced moment of inertia for the internal rotation, and $V(\phi) = V_6(1 - \cos 6\phi)/2$ is a 6-fold symmetric potential, a one-dimensional cut through the 12-D trimer IPS. V_6, an effective barrier height, is roughly the energy difference between the $\{uud\}$ and $\{upd\}$ structures. Similar treatments of internal-rotation problems are found in Lister's book,[186] which outlines methods for estimating reduced moments of inertia. The Hamiltonian (eq 5) was parametrized by the particle-on-a-ring radial coordinate r. Schütz et al. then solved for the torsional energies using a basis of free rotor functions, $\Psi_{\text{m}} = 1/\sqrt{2\pi}\ \text{e}^{\pm k\phi}$, where the resulting states were quantized by the torsional quantum number k. They calculated the torsional eigenstates as a function of barrier height, V_6. At the time of the study, only one data point, the 89.6 cm^{-1} spectrum of Pugliano and Saykally, was available to calibrate their model ($V_6 = 70$ cm^{-1}, and the effective internal-rotation constants $F = 23.49$ cm^{-1} for $(H_2O)_3$ and 11.75 cm^{-1} for $(D_2O)_3$), but their work set the stage for more detailed studies.

The torsional subspace was investigated in more detail by Bürgi, Klopper, et al., and by van Duijneveldt-van de Rijdt and van Duijneveldt (DD).[75] Using fitting of analytical functions to ab initio points, they obtained a more realistic representation of the subspace spanned by the flipping coordinates, $\{\chi_A, \chi_B, \chi_C\}$. Bürgi, Klopper, and co-workers calculated a grid of 70 ab initio optimized structures by varying χ_i between 0 and ±90°, as measured from the $\{ppp\}$ reference structure.[78] Each point was calculated at the MP2-R12 level of theory (R12 contains terms that depend linearly on interelectron distance; see ref 159 and references therein) using the aug-cc-pVDZ basis set contracted to reproduce water monomer and dimer properties. The EPEN empirical potential of Owicki et al.[69] was fitted to the ab initio points to determine the BGLK torsional potential surface. Similarly, DD calculated 69 points of the χ_i subspace using SCF+MP2 and the ESPB basis set that they had developed earlier.[75] A sixth-degree polynomial was fit to the ab initio grid to determine the DD torsional potential.

Using the BGLK potential, Klopper and Schütz extended their 1-D pseudorotation model to two dimensions, allowing for a limited degree of coupling between the flipping coordinates.[187] Forming three symmetry-adapted linear combinations of the flipping coordinates, they transformed the Hamiltonian,

$$H = -F\left[\frac{\partial^2}{\partial\chi_A^2} + \frac{\partial^2}{\partial\chi_B^2} + \frac{\partial^2}{\partial\chi_C^2}\right] + V(\Omega) \qquad (6)$$

into one using the abstract spherical polar coordinates, R, θ, and ϕ. By parametrizing the R coordinate and the reduced internal-rotation constant F, which is inversely proportional to the flipping moment of inertia, the problem was reduced to a two-dimensional one and was solved variationally using a basis of spherical harmonics. The authors were able to adjust F and R to match the calculated transition frequencies to the observed spectra. At that time, four $(D_2O)_3$ THz-VRT bands had been measured, although one spectrum, lying near 81.8 cm^{-1}, had yet to be fully analyzed. The results of the calculation of Klopper and Schütz are collected in Table 4. Later, using a similar coordinate transformation strategy and a pointwise discrete variable representation (DVR), Sabo et al. performed three-dimensional calculations for $(H_2O)_3$ and $(D_2O)_3$,[188] wherein eq 6 was solved in a basis set containing R, θ, and ϕ

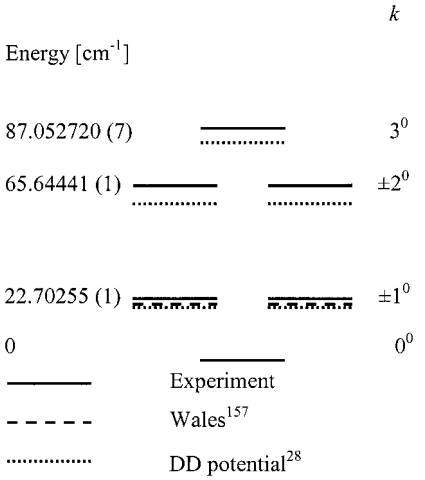

Figure 8. Comparison of the experimental torsional levels with those calculated with the DD potential and eq 7[28] or calculated using eq 12,[157] with the splitting parameter β adjusted to reproduce the energy difference between the $k = 0^0$ and 3^0 levels. Clearly, the simple Hückel approach reproduces the energy level structure within a torsional manifold well. The experimentally determined values are shown on the left.

explicitly, thereby including coupling of all three flipping motions. For the mixed isotopomers $(H_2O)_2$-(D_2O) and $(H_2O)(D_2O)_2$, they modified the Hamiltonian to include distinct reduced internal-rotation constants for the free OD or OH groups.[189] The resulting energy level structure of these calculations consist of sets of six (with $k = 0, \pm1, \pm2$, and 3) which will be referred to as manifolds (see Figures 7−9). Agreement with the VRT data was much worse for this three-dimensional model. A principal criticism of these early models, notably by the authors themselves,[187,188] was that they lacked terms in the Hamiltonian coupling the internal rotations with the overall rotation of the cluster, and therefore angular momentum was not conserved.

In an extension of this work, Sabo et al. extended this model to a (3 + 1)-dimensional model that took into account the coupling between the symmetric H-bond stretch with the torsional motion.[114] They calculated the rotational constants for all water trimer isotopomers for $k = 0^0$, 3^0, and 3^1,[113] and all torsional states up to $k = 0^1$ of $(D_2O)_3$[112] and $k = 3^1$ of $(H_2O)_3$. In the first of these the authors noted that a purely torsional three-dimensional model predicts an increase of the A and B rotational constants for excitation to $k = 3^0$, whereas experimentally a decrease has been observed. This motivated the inclusion of the symmetric H-bond stretch by calculating the potential along this coordinate for four stationary points on the BGLK torsional surface. The H-bond length was found to increase on increasing the torsional angles away from planarity, and the torsional barrier was found to decrease for deviations from the equilibrium H-bond length. The result is a decrease of the torsional barrier and an increase of the torsional splitting on inclusion of the H-bond stretch, even for the ground state due to zero-point motion. For the first torsional manifold, the (3 + 1)-D model correctly predicted the decrease of the vibrationally averaged A and B rotational constants

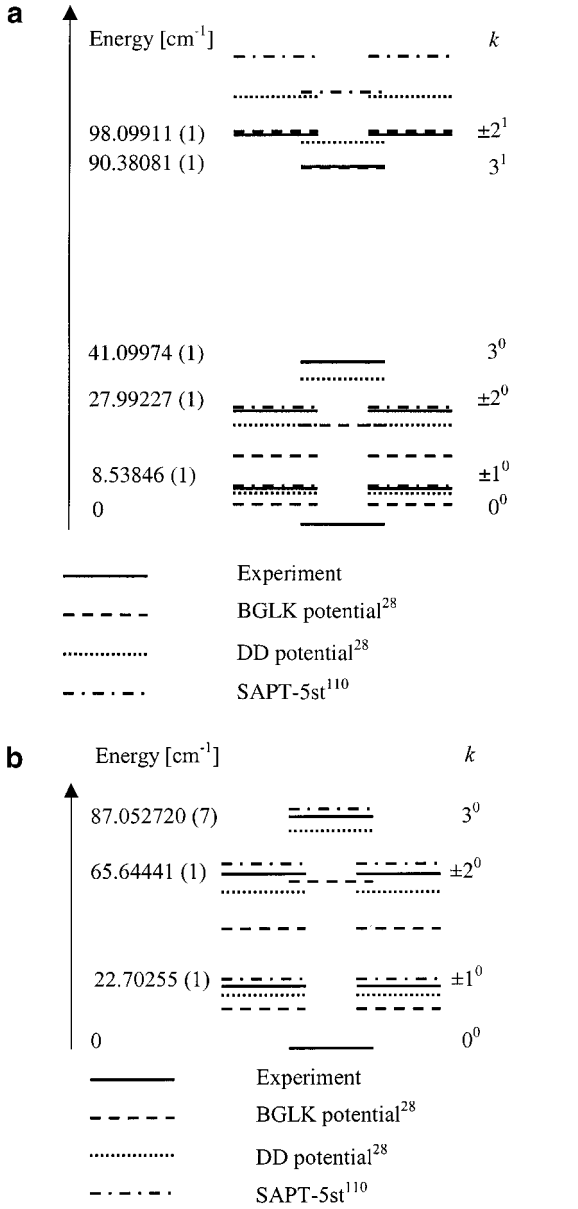

Figure 9. Comparison of the experimental[191] and calculated torsional levels, using the DD,[28] BGLK,[28] and SAPT-5st[110] potentials and eq 7, for $(D_2O)_3$ (a) and $(H_2O)_3$ (b). For the lower torsional manifold ($k = \pm n^0$) of $(D_2O)_3$, the agreement between experiment and the SAPT-5st potential is excellent. The calculated values using the DD and especially the BGLK potential are significantly too small. For the excited torsional manifold, the values calculated using the BGLK potential and, to a lesser degree, the DD potential agree well with experiment, whereas the SAPT-5st values are too large. All calculations ignore coupling with translational (and librational) degrees of freedom, which has been shown to be important for the excited torsional manifold. Inclusion of these degrees of freedom is expected to improve agreement between the experimental values and those calculated using the SAPT-5st results and worsen agreement for the BGLK potential. For $(H_2O)_3$, agreement between the experimental values and those calculated with SAPT-5st is very good, whereas the values calculated with the DD and especially the BGLK potential are significantly too small.

as well as the increase of the C rotational constant. The change of the rotation constants results from changes of both torsional angle and H-bond length. Subsequent work on $(D_2O)_3$ showed that the experi-

mentally observed nearly linear decrease of the A and B rotational constants with torsional energy, which continues in the second torsional manifold, was not reproduced with the (3 + 1)-D model, possibly because of the exclusion of the asymmetric H-bond stretch vibration, which could couple strongly to the torsional motion. However, the experimentally observed discontinuous behavior of the experimental ΔC values between the first and second torsional manifolds was predicted by both the 3-D and the (3 + 1)-D models, and reflects the changes of the averaged torsional angles, and not the torsional energy.

Gregory and Clary have used diffusion quantum Monte Carlo (DQMC) methods to calculate the splittings arising from tunneling in the water dimer through pentamer.[163,165] For the trimer they calculated a torsional splitting of 22 ± 3 cm^{-1} for $(H_2O)_3$ and 9 ± 3 cm^{-1} for $(D_2O)_3$ using the ASP potential with Szczesniak's dispersion energies.[163]

Blume and Whaley calculated the torsional splitting levels of $(H_2O)_3$ using Monte Carlo methods with the projection operator imaginary time spectral evolution method.[190] This method has the advantage that no nodes have to be defined for excited states, but rather the choice of a projector allows determination of the difference between an excited state and the ground state directly. Their calculations with the BGLK potential and projectors chosen on a group theoretical basis were in reasonably good agreement with DVR results reported by van der Avoird et al.

In developing a more physically realistic Hamiltonian, van der Avoird and co-workers considered the fact that H-bond torsion must be affected by the rotation of the complex, and therefore must be described within a rotating framework.[28] That correction yielded adjustments to the torsional energies of 5% on average from the model of Sabo et al.,[188] bringing them more into agreement with experiment. Additionally, in considering the coupling of bifurcation dynamics with torsion−rotation, they provided satisfying explanations for many of the more subtle perturbations that have been observed in the VRT data. Their internal-rotation Hamiltonian is

$$H = H^{\mathrm{rot}} + H^{\mathrm{Cor}} + H^{\mathrm{int}} \tag{7}$$

where the first term is the oblate symmetric rotor Hamiltonian,

$$H^{\mathrm{rot}} = B(J_x^2 + J_y^2) + CJ_z^2 \tag{8}$$

$A = B$ and C are the rotational constants of $(H_2O)_3$ and $(D_2O)_3$, and the operators J_x, J_y, and J_z are the body-fixed components of the total angular momentum operator $\boldsymbol{J}$, depending on the Euler angles with respect to a space-fixed axis.

$$H^{\mathrm{Cor}} = -\frac{B}{2}[(j_+ + j_-^\dagger)J_+ + (j_- + j_+^\dagger)J_-] - C(j_z + j_z^\dagger)J_z \tag{9}$$

describes the Coriolis coupling between the overall angular momentum $\boldsymbol{J}$ ($J_\pm = J_x \mp J_y$) and the internal (torsional) angular momentum $\boldsymbol{j}$ ($j_\pm = j_x \pm ij_y$), and explicit expressions can be found in refs 28 and 191. The third term,

$$H^{\mathrm{int}} = -\frac{h^2}{2\Lambda}\sum_{A,B,C}\frac{\partial^2}{\partial\chi_i^2} + \frac{B}{2}(j_+^\dagger j_+ + j_-^\dagger j_-) + Cj_z^\dagger j_z + V(\chi_A, \chi_B, \chi_C) \tag{10}$$

where Λ is the flipping moment of inertia, B and C are the unique rotational constants of an oblate symmetric rotor, and V describes the torsional potential energy surface. The coordinate system of van der Avoird et al. (Figure 1b) differed from previous models in that the flipping axes were defined to lie between the monomer centers of mass and the bound H atoms, rather than along the H-bonded O−H axes, which pass near but not through the monomer mass centers. Their choice of coordinates greatly facilitated their calculation of the coupling terms. While their Hamiltonian was still an approximation to the full dynamics, it was rigorously calculated in terms of angular momentum conservation. They computed the Coriolis-coupled rotation−pseudorotation energy levels using the Hamiltonian from eq 7 in a product basis of rotation and internal-rotation functions, $|\phi_k\rangle\,|JKM\rangle$, using both the BGLK and DD potentials, and compared the results to the experimental data using the transition assignments of Klopper and coworkers. In general, better agreement with the experimental results was obtained using the DD potential, although the overall agreement both between the two potentials and between the calculated and experimental results was not good. Many of these results will appear in the VRT analyses that follow.

The $J = 0$ internal-rotation levels of van der Avoird et al. were calculated in a basis of flipping wave functions as

$$E_k = \frac{\langle\phi_k|\,H^{\mathrm{int}}\,|\phi_k\rangle}{\langle\phi_k|\phi_k\rangle} \tag{11}$$

where $|\phi_k\rangle$ are the eigenstates of H^{int}. Whereas the full internal Hamiltonian matrix would include terms involving more than one flip per operation, multiple flips have been omitted from all of the theoretical treatments thus far, except for the recent treatment by Keutsch et al.[192] Wales[157] insightfully pointed out the similarities between the trimer system under these assumptions with a 6-fold cyclic system neglecting non-nearest-neighbor interactions, e.g., a simple Hückel molecular orbital treatment of benzene. The energies of such a system are approximated by

$$E_k = \frac{E^{(0)} + 2\cos(k\pi/3)\beta_1}{1 + 2\cos(k\pi/3)S} \tag{12}$$

where $\beta_1 = \langle uud|\,H^{\mathrm{int}}\,|udd\rangle$ and $S = \langle uud|udd\rangle$ are single flip and overlap matrix elements, respectively. In Figure 8, the lowest energy levels of van der Avoird, calculated using the BGLK potential, can be compared to the pattern predicted by eq 12 for the lowest four pseudorotation levels. The agreement between Wales's simple model and the more sophis-

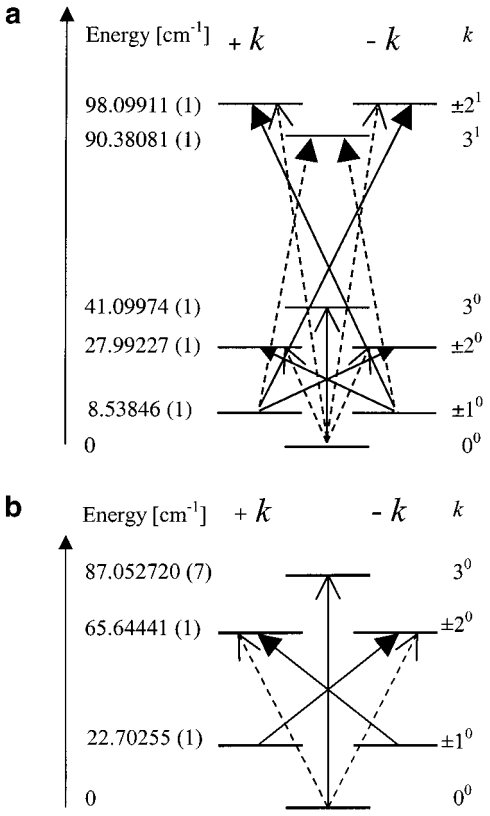

Figure 10. Experimentally determined torsional energy level manifolds for $(D_2O)_3$[191] (a) and $(H_2O)_3$[220] (b) with the k quantum number and all observed transitions. The dashed arrows correspond to perpendicular bands ($\Delta K = \pm 1$) and the solid arrows to parallel bands ($\Delta K = 0$). The open arrowheads correspond to transitions from the vibrational ground state and the closed ones to hotband transitions from the $k = \pm 1^0$ level. All transitions involving degenerate $k = \pm n$ levels are severely perturbed by a Coriolis interaction resulting from coupling of the torsional motion of the free deuterium atoms with the overall rotation of the cluster, which can be seen in the example of the P(8)-branch of the 19.5 cm^{-1} band (see Figure 12).

ticated calculation of van der Avoird et al. for the first four levels is remarkable and allows for convenient first-order calculations to be made in the analysis of the THz-VRT data set to follow. The 6 observed $(D_2O)_3$ torsional transitions (11 when counting the degenerate states separately) are drawn in Figure 10a, and the 3 observed $(H_2O)_3$ torsional transitions (5 when counting the degenerate states separately) are drawn in Figure 10b. Because the pseudorotation model and the assignment of the data to it predict three instances of common states between the transitions, establishment of those shared states with experimental evidence is a crucial component of the analyses to follow. In a study of water trimer isotopomers, Geleijns and van der Avoird were able to demonstrate that agreement with experimental results required that the axis of the torsional motion not extend from the bonded hydrogen through the center of mass of the monomer, but rather closer to the oxygen−oxygen line. Similarly, it appeared that motion of the bonded hydrogens was incorporated in the torsional motion if they are not in the plane defined by the oxygens.[193]

In addition to calculating the pseudorotation levels, van der Avoird and co-workers also determined the effects of coupling of the internal dynamics (flipping and bifurcation) with the overall rotation, finding splittings and/or shifts of the pseudorotation levels. These predictions have proven very helpful in understanding the $(D_2O)_3$ and $(H_2O)_3$ data, much of which exhibit perturbations. Many of the details of that work will be discussed in the analysis of the THz-VRT data to follow.

Bifurcation tunneling represents the second important hydrogen bond network rearrangement mechanism and is of special importance as it represents the lowest-energy pathway for breaking and making H-bonds in water clusters. Wales and co-workers,[104,156,157,160] Fowler and Schaeffer,[155] and Milet et al.[171] have calculated the barrier for the bifurcation-tunneling motion at different ab initio levels, as well as with the TIP4P, EPEN, ASP-W2, and ASP-W4 potentials. The barrier for bifurcation tunneling does not vary much for different levels of ab initio theory and was calculated by Fowler and Schaeffer to lie between 1.52 (TZ2P SCF)[155] and 2.04 kcal/mol (TZ2P+diff/DZP+diff CCSD),[155] by Wales and co-workers between 1.65 (DZP/SCF and 6-31G**/SCF)[157] and 2.34 (MP2/aug-cc-pVTZ)[160] or 2.45 kcal/mol (DZP+diff/MP2), and by Milet et al. at 1.84 kcal/mol (CCSD(T)).[171] Taking zero-point energy into account lowers the barriers by ~0.5−0.6 kcal/mol,[155,157] and the "effective" tunneling barriers thus vary between ~1.1 and 1.9 kcal/mol (385−665 cm^{-1}), which is close to the energy of the librational vibrations. Walsh and Wales also calculated the bifurcation-tunneling barriers for a number of empirical potentials, which were found to be in the same range as for the ab initio calculations with 1.92 (TIP4P),[157] 1.91 (ASP-W4),[104] and 2.57 kcal/mol (ASP-W2),[104] except for the EPEN potential, with a very low value of 0.71 kcal/mol (EPEN).[104]

The magnitudes of the experimental tunneling splittings depend not just on the barrier height, but, of course, on the details of the tunneling path, such as the length and the masses involved. Wales and co-workers[104,156,157,160] have examined the bifurcation-tunneling path in detail, exploring several possible tunneling pathways on different ab initio IPS and empirical potentials. The authors found that although the mechanism for the torsional flipping tunneling is stable with respect to basis set, this is not true for the bifurcation-tunneling pathway. Specifically, whereas the motion of the bifurcating water molecule is fairly consistent, the number of torsional flips of neighboring water molecules accompanying the bifurcation motion varies with the level of ab initio theory or empirical potential employed, resulting from the facile nature of the flip, and the most recent calculations of Taketsugu and Wales suggest that the pathways pass close to a transition state for a single flip.[160] The authors showed that there are six different bifurcation-tunneling pathways and that two different splitting patterns can result from this, which will be referred to as patterns A and B, with three possible tunneling pathways each. Table 5 shows that four of the six tunneling pathways were found in studies using various levels of ab initio theory and empirical potentials. It should be noted

Table 5. Bifurcation-Tunneling Pathways in the Water Trimer

number	description	generator	level of theory
A1	min + maj acceptor flip	(ACB)(164253)	EPEN
	maj donor + min flip	(ABC)(135246)	DZP/SCF
			DZP/BLYP
			aug-cc-pVDZ/MP2
			aug-cc-pVTZ/MP2
A2	min + maj donor flip	(ABC)(136245)	not found
	maj acceptor + min flip	(ACB)(154263)	
A3	maj acceptor + no flips	(ABC)(143625)*	ASP-W2
	maj donor + no flips	(ACB)(152634)*	ASP-W4
			DZP+diff/BLYP
			DZP/MP2
			6-31G**/SCF
			4-31G**/SCF
B1	min + double flip	(56)*	DZP+diff/SCF
			4-31G/SCF
B2	maj donor + double flip	(12)*	not found
B3	maj acceptor + double flip	(34)*	TIP4P

that the motion of the bifurcating water molecule resembles a rotation perpendicular to its C_2 symmetry axis more closely than about this axis. For the pathway depicted in Figure 2b, the bifurcation motion is accompanied by the flipping of both neighboring water molecules. The transition state contains a bifurcated hydrogen bond in which the bifurcating water molecule acts as a double H-bond donor and one of the neighboring water molecules acts as a double H-bond acceptor. The free hydrogen of the latter water is rotated into the plane, aligning the two free orbitals of the oxygen with the two free hydrogens of the bifurcating water molecule. Whereas all the studies mentioned above treated bifurcation tunneling in the high barrier and torsional tunneling in the low barrier approximation, Keutsch et al. recently investigated the effects of the breakdown of the high barrier limit on the bifurcation-tunneling splittings.[192] The results of this study will be discussed in the analysis of the experimental THz-VRT spectra.

It should be noted that, in addition to the torsional and bifurcation-tunneling pathways, a third tunneling pathway corresponding to a concerted proton transfer of the three bonded hydrogens in the ring, that interchanges the handedness of the trimer, was investigated by Liedl and co-workers.[194,195] They calculated a tunneling splitting of ca. 0.5 MHz for $(H_2O)_3$ using an ab initio and DFT-derived potential energy surface, ca. 3 orders of magnitude smaller than the smallest experimentally observed splitting. This tunneling pathway involves the breaking of covalent bonds and thus would not result in the G_{96} group.

3. Intramolecular Vibrations

Shifts of intramolecular vibrational frequencies from gas-phase monomer values, in both gas-phase cluster spectra (red shifts) and matrix IR spectra (blue shifts), have shown that the chemical environments of H-bonded and nonbonded protons are nonequivalent. These shifts, particularly in the bound O−H stretching local modes, are indicative of coupling between the mismatched intra- and intermolecular vibrational motions. Because one effect of many-body forces in water clusters is polarization along and contraction of the donor O−H bond, the vibrational red shifts provide valuable information on the shape of the potential functions of interest. Hermansson and co-workers,[196] for example, performed MP2/DZP ab initio calculations on a so-called "star pentamer", a single water monomer tetrahedrally coordinated by four other monomers. They dissected the vibrational frequency shifts of the central monomer into pairwise and three-body components, finding that the shift arising from two-body interactions accounted for up to 84% of the total red shift of two different star pentamers, where three-body corrections accounted for most of the balance.

Xantheas and Dunning showed a 1:1 correlation between elongation of r_{OH}^{b}, the H-bonded O−H bond length, and the large vibrational shifts of the modes associated with stretching of that bond.[26] Their MP2 results predicted a monotonic red shift as a function of cluster size (for cyclic clusters) continuing past the tetramer, while HF results predicted only small further shifts for clusters larger than the tetramer. The recent measurements of Huisken et al.[197] support the MP2 results, showing bound OH frequency shifts continuing up to the hexamer. The gas-phase free OH vibrational (blue) shifts are predicted to be much smaller, consistent with theoretical predictions that r_{OH}^{f} changes very little (<1%) as a function of H-bonding. Xantheas and Dunning[26] predicted (MP2) free OH vibrational shifts in the trimer as large as +26 cm^{-1} from the free monomer value, while the measured shift[197] of the bound OH stretch is more than 300 cm^{-1}. In HF and MP2 results, they also showed an increase in the monomer HOH angle up to the trimer, followed by a slow decrease, as a function of cluster size, to very near the gas-phase value by (cyclic) $n = 6$.

Van Duijneveldt-van de Rijdt and van Duijneveldt performed SCF+MP2 calculations to study the influence of structure and three-body forces on the intramolecular vibrational shifts of the trimer.[198] They found that the bound OH stretching frequency in the trimer is red shifted by more than twice the dimer shift (the calculated shifts are −135 and −230 cm^{-1}, respectively, for H_2O dimer and trimer), mainly due to nonadditive induction. Because of that induction dependence, they argued, the calculated trimer shift

is very sensitive to R_{OO} in geometry optimizations. They also demonstrated a significant sensitivity of the calculated frequencies to the torsional coordinates, noting that optimized values of those angles should probably be scaled to account for the anharmonicity in the flipping coordinate, which tends to decrease the expectation value of the torsional angle as measured from the planar free proton positions.

Masella and Flament[199] added an intermolecular potential term derived from experimental water cluster results to their TCPE model to estimate the water cluster OH stretch frequencies. They introduced a fifth-order term instead of the quartic terms more commonly used in this type of approach. Although some discrepancies with ab initio results remained, these results typically also have to be scaled to achieve agreement with experimental values, and calculations with the modified TCPE potential are computationally feasible even for larger systems.

Selected calculated water trimer intramolecular vibrational frequencies are compared with measured values in Table 6. From the table, it is clear that the frequencies are quite dependent upon both level of ab initio theory and the choice of basis set, or the choice of empirical IPS in dynamics calculations. Because of coupling of the intramolecular vibrations to the anharmonic intermolecular potential, calculations resorting to normal-mode methods are likely to fail when accuracy approaching the uncertainty in the experimental measurements is required. Recent applications of DQMC methods show promise for calculation of intermolecular vibrations of systems wherein the inherent symmetries allow for reasonably reliable construction of excited-state wave functions, but DQMC is relatively untested for calculation of intramolecular frequencies in clusters.[127−129,163]

Two groups have used novel methods for calculating the intramolecular frequencies. Coker and Watts used the RWK2 pair potential with a combination of local-mode variational theory and quantum Monte Carlo simulation to calculate very accurate intramolecular frequencies for the water dimer.[200] Jung and Gerber calculated intramolecular vibrational spectra for water clusters up to the pentamer using vibrational mode correlation-corrected variational SCF calculations.[167] In their method, correlations between the vibrational modes were corrected using a perturbation theory that considered each vibrational mode to move in the average field of the others, thus effectively coupling the high-frequency modes. The intermolecular vibrational frequencies were significantly increased when coupling was taken into account, indicating that the coupling to the intramolecular modes is more important than the intrinsic (diagonal) anharmonicity for the low-lying vibrational modes.

Low and Kjaergaard calculated the fundamental and overtone OH stretching frequencies and band intensities for the water $(H_2O)_2$ and $(H_2O)_3$, using a simple harmonically coupled anharmonic local-mode model and ab initio dipole moment functions.[201] The authors investigated both the effect of basis set size and the difference between HF and quadratic configuration interactions including single and double excitations on the vibrational frequencies and dipole moment function and, thus, intensities. The frequency and anharmonicity of the various local modes were derived from scaled (by comparison with water monomer vibrational frequencies) results of ab initio calculations. The $(H_2O)_3$ vibrational frequencies and oscillator strengths were calculated at the HF/6-311++G(2d,2p) level of theory, and a comparison was made between various scaled and unscaled local-mode parameters. The calculated OH stretch frequencies with the scaled local-mode parameters are in excellent agreement with experimental results, for both the free and bound O−H bonds. The authors note that the decrease in oscillator strength for the overtone transitions of the water dimer and trimer is similar to that of the water monomer.

4. Intermolecular Vibrations

Normal-mode calculations of intermolecular vibrational frequencies of water clusters suffer even more from the effects of the large anharmonicity in the IPS. Moreover, the fact that many of the internal motions correspond to internal rotations, not to vibrations, implies different boundary conditions and large deviations from harmonic oscillator predictions. Experiments have clearly shown that the dimer and trimer fully explore their respective intermolecular coordinate spaces, ruling out virtually any effectiveness of the harmonic approximation. The ammonia dimer study of Loeser et al.,[178] wherein the ammonia monomer umbrella inversion motion was observed to occur even in $(NH_3)_2$, makes this point emphatically.

Althorpe and Clary applied a five-dimensional coupled dynamics calculation to the water dimer, adiabatically separating only the radial (intermonomer stretching) coordinate from the remaining five angular coordinates.[202] In this manner, they were able to obtain intermolecular vibrational frequencies that not only were close to the observations, but also helped in assigning the lowest two intermolecular THz-VRT bands of $(D_2O)_2$. LeForestier and co-workers recently computed the intermolecular frequencies in a fully coupled 6-D dynamics calculation using a variety of pair potentials. This treatment has now been enhanced to include the intermolecular degrees of freedom in an adiabatic fashion. To date, no such computations have been performed for the trimer. Many of the methods of vibrational frequency estimation discussed in the previous section have also been applied to the intermolecular vibrations. Selected results are collected in Table 7, which makes it clear that the observed frequencies are not yet accounted for by the calculations. Only a realistic quantum dynamics simulation is capable of reproducing those frequencies, which are now widely regarded as arising from large-amplitude internal motions. This underscores the necessity of pursuing realistic dynamics approaches to systems larger than the dimer.

III. Experimental Data

The cyclic water trimer has now been observed in many different spectroscopic studies and different

Table 6. Calculated and Experimental Water Trimer Intramolecular Frequencies (cm^{-1})

method	SCF	HF	HF	HF	MP2	MP2	MP2	CCSD	DFT/ PP	DFT/ BLYP 6-31+ G(d,p)	DFT/ BLYP aug-cc- pVDZ	DFT /B3LYP 6-31+ G(d,p)	DFT/ B3LYP 6-311++ G**	VSCF[a]	TCPE	RWK-2
basis set	6-31G*	6-311++ G(2d,2p)	HCAO	aug-cc- pVDZ	aug-cc- pVDZ	aug-cc- pVDZ	aug-cc- pVTZ	DZP+diff								normal modes
ref	142	95	201	26	170	26	170	155	149	166	25	166	267	167	199	265
ν_1	4071	4148.2		4134	3803	3807	3822	3864		3780	3650	3808	3816		3831	
ν_2	1827	1761.4		1742	1622	1623	1628	1644		1569	1583	1608	1603			
ν_3	4189	4248.7		4236	3938	3936	3948	3985		3780	3759	3930	3921		3939	
	−130	−108	3571	−108	−228	−234	−244	−172	−328	−300	−317	−268	−257	3355	−166	3473
$\Delta\nu_1$	−86	−79	3573	−81	−171	−175	−181	−102	−252	−243	−247	−207	−198	3370	−138	3532
	−82	−75	3580	−77	−162	−166	−172	−95	−246	−217	−234	−192	−188	3440	−136	3626
	15	14		11	9	9	11	23	10	21	4	23	21	1610		1625
$\Delta\nu_2$	24	17		14	12	12	14	27	12	25	7	28	26	1635		1649
	37	36		34	36	37	39	76	31	43	8	53	49	1675		1681
	−42	−32	3721	27	−48	−44	−46	−34	−32	−37	−41	−38	−33	3725	−52	3841
$\Delta\nu_3$	−39	−28	3723	23	−44	−40	−43	−32	−25	−32	−38	−32	−29	3731	−52	3846
	−37	−27	3724	21	−42	−38	−42	−28	−25	−30	−35	−31	−27	3770	−46	3859
gas-phase H_2O	size-selected $(H_2O)_3$	CRDS $(H_2O)_3$	CRDS $(D_2O)_3$	liquid He $(H_2O)_3$	liquid He $(H_2O)_3$	Ne matrix $(H_2O)_3$	Ar matrix $(H_2O)_3$	Ar matrix $(H_2O)_3$	Ar matrix $(H_2O)_3$	Ar matrix $(D_2O)_3$	Ar matrix $(D_2O)_3$	Kr matrix $(H_2O)_3$	N_2 matrix $(H_2O)_3$	N_2 matrix $(H_2O)_3$	N_2 matrix $(D_2O)_3$	para-H_2 matrix $(H_2O)_3$
	197	233, 235	234	216	217	268	212	209	207	212	209	213	209	203	209	214
ν_1	3533	3532	2588	3532	∼3528	3529	3516	3516	3517	2578.5	2580	3514	3510	3385	2599	3518
3652			2592	3545	∼3544		3527	3528	3525		2615			3510	2575	3531
ss[b]								3612								
ν_2		1609					1602.3	1602		1183.4	1183		1614		1200	
1595		1638						1620			1196		1630		1190	
b[b]								1632								
ν_3	3726		2756	3719			3707.2	3695		2737.8	2733		3688		2724	
3756								3700			2738					
as[b]																

[a] Estimated (±10 cm^{-1}) from Figure 9 of ref 167. [b] Gas-phase monomer normal-mode frequencies from Herzberg, ref 269.

Table 7. Comparison of Calculated Intermolecular Frequencies (cm^{-1})

method	HF	HF	MP2	MP2	MP2	MP2	CCSD	DFT/ BLYP	DFT/ BLYP	DFT/ B3-LYP	NEMO	MCY	VSCF[a]	TIP4P	EPEN	ASP-W2	ASP-W4
basis set	6-311++ G(2d,2p)	aug-cc-pVDZ	6-311++ G(d,p)	aug-cc-pVDZ	aug-cc-pVDZ	aug-cc-pVTZ	DZP+ diff	aug-cc-pVDZ	6-31+ G(d,p)	6-31+ G(d,p)							
ref	95	26	158	26	170	170	155	25	166	166	91	77	167	104	104	104	104
	134	101	177.4	158	157	175	170	178	185	183	106	131	250	56	131	160	154
	146	135	184.7	173	184	184	177	179	192	195	161	135	290	111	135	170	163
	149	146	197.8	185	193	189	186	199	214	200	127	164	490	134	161	179	181
	167	151	214.8	193	172	205	195	210	225	223	169	170	530	180	166	185	193
	182	178	218.4	218	217	219	208	214	232	232	186	192	565	193	190	204	205
	212	192	265.5	235	233	241	264	246	278	273	205	207	600	265	205	214	216
	298	294	346.9	343	340	347	331	357	369	366	271	331	600	369	326	306	290
	307	302	358.1	351	349	360	356	387	385	381	288	345	610	391	339	327	313
	387	379	443.2	444	441	447	443	459	475	473	338	362	630	450	355	401	401
	485	473	559.8	571	568	576	536	600	610	603	409	438	750	533	422	524	502
	594	586	697.1	667	664	669	664	676	718	723		556	800	686	530	589	598
	752	730	827.9	863	858	864	941	896	920	911		720	1050	832	699	805	786

[a] Estimated (± 10 cm^{-1}) from Figure 9 of ref 167.

chemical environments — from the gas phase to cryogenic matrices and even stabilized in inorganic host complexes. Although the water trimer was first detected in cryogenic matrices (1957),[203] the more recent THz-VRT studies of the gas-phase water trimer have been the main contributor to the understanding of the structure, vibrational, and HBNR dynamics of this water cluster as well as the role of three-body interactions. The experimental water trimer THz-VRT data set is the most extensive existing for any weakly bound cluster with four, seven, and six extensive vibrational bands observed for $(H_2O)_3$, $(D_2O)_3$, and mixed isotopomers, respectively. Furthermore, the water trimer is presently the only water cluster for which all three different types of intermolecular vibrations — free hydrogen torsions, translations (H-bond stretch), and librations (hindered rotations) — have been observed by high-resolution spectroscopy. Moreover, studies of substituted water trimers or water trimers coordinated to organic chromophores promise to extend the study of the water−water interactions to water−solute interactions.

A. Condensed-Phase Environments

1. Matrix-Isolation Spectroscopy

The first experimental observations of small water clusters were those of Pimentel and co-workers in 1957.[203] They recorded the IR absorption bands of water trapped in 20 K N_2 matrices corresponding to the asymmetric stretching and bending intramolecular (covalent) vibrations of gas-phase water. Using a variety of N_2/H_2O ratios ($N_2/H_2O = 39-1012$), a series of sequentially shifted bands correlating with the water concentration were observed and assigned to monomers, dimers, and larger clusters. By examining patterns in frequency shifts, this group tentatively assigned asymmetric stretching bands at 3510 and 3385 cm^{-1} (Table 6) to the bound and free OH stretches of the trimer. Several subsequent studies have also measured vibrational frequencies and estimated structures for the dimer and larger clusters.[204−214] Tursi and Nixon[204] and Fredin et al.[208] found four distinct IR peaks which helped to confirm that the equilibrium form of the dimer was a singly H-bonded isomer. Two of the IR frequencies were close to the monomer values and were (incorrectly) assigned as arising from the symmetric and asymmetric stretches of the proton-acceptor monomer, while the remaining modes were assigned to the bound and free OH stretch local modes of the donor. Using a similar analysis, Bentwood and co-workers performed IR and FIR Ar matrix studies and concluded (incorrectly) that the dominant trimer structure in their matrices was an open form.[209] More recently, however, Engdahl and Nelander[212] performed matrix studies using Ar and Kr matrices and a higher-resolution (0.5 cm^{-1}) FTIR instrument. By examining IR spectra of several isotopomers of the trimer, they were able to correctly infer that the vibrationally averaged structure consisted of three equivalent monomers and was thus most consistent with a cyclic structure. In a recent study of the cyclic water hexamer isolated in a para-hydrogen matrix,

Fajardo and Tam also observed cyclic water trimer vibrational bands, with frequencies close to those observed in an Ar matrix.[214]

2. Inorganic Host Complexes

Macgillivray et al. have established the existence of a water trimer with a structure resembling that found in the gas phase in a cobalt-containing alkylammonium complex.[215] The average O−O separation of 2.91(3) Å is slightly larger than the experimentally established value of ca. 2.85 Å for the gas-phase structure. The difference between the O−O distances results from the environment (e.g., H-bonding to groups outside of the water cluster and steric effects) as well as the significantly higher temperature of the inorganic complex compared to the molecular beam conditions of the gas-phase cluster experiment.

3. Water Trimer in Liquid Helium Droplets

Fröchtenicht and co-workers were able to form small water clusters trapped in cold (as low as 0.4 K) helium droplets.[216] They observed a narrowing of both the bound and free OH stretching signals over their gas-phase work and were able to resolve the IR-active bound OH stretching modes. Their frequencies are shown in Table 6. A second recent study of water clusters in liquid helium droplets has demonstrated the existence of the linear water dimer, as well as cyclic forms of the water trimer through hexamer.[217]

B. Gas-Phase Spectroscopy of the Free Water Trimer

Water trimer vibrational bands have now been observed in the gas phase from the FIR (or THz) region (10−550 cm^{-1}) to the mid-infrared (1500−3700 cm^{-1}). Additionally, water trimers coordinated to organic chromophores, or substituted water trimers, have been observed in mid-infrared, resonant ion-dip, infrared−ultraviolet double-resonance, and microwave studies. The high-resolution THz vibration−rotation−tunneling (VRT) spectra demonstrate that the uncoordinated water trimer has an oblate symmetric rotor spectrum, which results from vibrational averaging of the asymmetric equilibrium structure via large-amplitude torsional motions of the unbound protons/deuterons on the experimental time scale. In contrast to the equilibrium structure, the vibrationally averaged structure has no dipole moment, which explains the fact that, unlike the water dimer, no pure rotational spectra have been obtained. Thus, the lowest-frequency transitions that are observed are those among the torsional states, as discussed in detail below. The G_6 dipole selection rules for the water trimer were derived in section II.C.1 and can be expressed in terms of k and K as $\Delta(k - K) = 3$ (modulo 6). Parallel transitions correspond to $\Delta K = 0$ and $\Delta k = \pm 3$, and perpendicular transitions, which are usually split by Coriolis interactions, can be separated into two sub-bands, $\Delta K = +1$, $\Delta k = -2$ and $\Delta K = -1$, $\Delta k = +2$. The extension to the G_{48} selection rules, and thus inclusion of the bifurcation-tunneling components, is achieved by taking into account that only transitions with the same irrep Γ (see Table 3) but opposite parity are allowed ($\Gamma_g^{\pm} \leftrightarrow \Gamma_u^{\mp}$).

1. Far-Infrared Vibration–Rotation–Tunneling (VRT) Spectroscopy

The far-infrared region (10−550 cm^{-1}) includes all three types of water cluster intermolecular vibrations: free hydrogen torsional, translational (H-bond stretch), and librational (hindered rotations of water monomers) vibrations. The torsional manifold of energy levels described in section II.C.2, resulting from the facile torsional motion of the free protons/deuterons, dominates the low-frequency (<100 cm^{-1}) part of the spectrum, and all of the experimental THz-VRT spectra of water trimer except for the recently reported 142.8 cm^{-1} translational band of $(D_2O)_3$ and 520 cm^{-1} librational band of $(H_2O)_3$ have been obtained in this region.

Intricate tunneling splitting patterns of each rovibrational transition are present in all THz-VRT spectra, and these tunneling splittings provide a more sensitive test of a model IPS than do the equilibrium structure or vibrational frequencies, as they sample much larger regions of the IPS. Except in the librational vibrations of $(H_2O)_3$, the bifurcation-tunneling motion manifests itself in a small [<1−10 MHz for $(D_2O)_3$ and 40−300 MHz for $(H_2O)_3$] splitting of each rovibrational transition. In contrast, the splittings of the torsional manifold are on the order of many cm^{-1} — larger than the entire rotational envelope of a typical trimer vibrational band. This, and the fact that similar torsional energy level structures are observed for mixed-isotope trimers, wherein the symmetry of the pure trimer is broken, suggests addressing the torsional energy levels as vibrational rather than tunneling levels. Water trimer spectra also frequently show splittings and perturbations arising from the extensive Coriolis interactions, for which detailed theoretical descriptions have been developed (see section II.C.2) and which are presently well understood, and their manifestation in the spectra will be discussed below. The effects of these tunneling motions and Coriolis interactions are obscured in the mid-IR spectra due to the strong vibrational predissociation broadening, thus revealing much less detail than do the THz spectra.

Pugliano and Saykally reported the first detection of a gas-phase water trimer band in 1992 with the 89.5 cm^{-1} $(D_2O)_3$ band, which also was the first observation of a gas-phase vibrational band of any water cluster.[27] The spectrum exhibited a strongly perturbed oblate symmetric top pattern, and every line was split into a characteristic quartet, which the authors suggested could occur from either bifurcation tunneling or a tunneling motion connecting a clockwise (cw) and counterclockwise (ccw) handedness of the trimer. Liu et al. followed with the observation of a parallel 87.1 cm^{-1} $(H_2O)_3$ band and a perpendicular 98.1 cm^{-1} $(D_2O)_3$ band, both of which appeared largely unperturbed.[161] From careful intensity measurements of the 98.1 cm^{-1} $(D_2O)_3$ band, the authors concluded that the quartets correspond to

Table 8. Summary of the Water Trimer Intermolecular Vibrational Bands

assignment $k'' \leftarrow k'$	ν (cm^{-1})	relative intensity obsd	relative intensity calcd[i]	regular quartet splitting (MHz)	anomalous splitting transitions	anomalous splitting intensities
			$(D_2O)_3$			
$\pm 2^0 \leftarrow \mp 1^0$ [a]	19.5			<1	$K = 2 \leftarrow 2$, $J(J+1)$	2.5:1:1:2.5
					$K = 0 \leftarrow 0$, 2 MHz	1:2
$\pm 2^0 \leftarrow 0^0$ [b]	28.0	5	11	−0.9	$K = 0 \leftarrow 1$, 0.9 MHz	2:9:4:6
$3^0 \leftarrow 0^0$ [b]	41.1	125	125	−1.5[e]	not observed	
$3^1 \leftarrow \pm 1^0$ [b]	81.8			2.7[b]	$K = 1 \leftarrow 0$, ~2.7 MHz	5:3:5:2
				5[f]		
$\pm 2^1 \leftarrow \mp 1^0$ [b]	89.6			6[g]	unknown	
$\pm 2^1 \leftarrow 0^0$ [b]	98.0	5	35	5[f]	$K = 0 \leftarrow 1$, ~5 MHz[h]	8:2:4:3
$\pm 2^{trans} \leftarrow 0^0$ [c]	142.8	0.6		<1	$K = 0 \leftarrow 1$, ~10 MHz[h]	1:1:1
			$(H_2O)_3$			
$\pm 2^0 \leftarrow \mp 1^0$ [d]	42.9			39	shift of T states	
$\pm 2^0 \leftarrow 0^0$ [d]	65.6			−255	shift of T states	
$3^0 \leftarrow 0^0$ [d]	87.1			−289[f]	T states $K = 1 \leftarrow 1$, $J(J+1)$	1:1
libration[j]	~520			>40 000	T states of 532.9 cm^{-1} band $K = 1 \leftarrow 1$, $J(J+1)$	1:1

[a] Reference 191. [b] Reference 221. [c] Reference 223. [d] Reference 220. [e] Reference 218. [f] Reference 219. [g] Reference 27. [h] Reference 29. [i] Reference 193. [j] Reference 222.

bifurcation tunneling and not the cw−ccw tunneling path. As a result of the large mass difference, the tunneling splitting in $(H_2O)_3$ was found to be nearly 2 orders of magnitude larger than that in $(D_2O)_3$. Liu et al. also determined that the 89.5 and 98.1 cm^{-1} $(D_2O)_3$ bands did not arise from the same lower state. Suzuki and Blake followed with the observation of the very intense 41.1 cm^{-1} $(D_2O)_3$ vibrational band, which also showed a characteristic quartet pattern, albeit with a smaller splitting of the quartet components (see Table 8).[218] This band was determined to have the same lower state as the 98.1 cm^{-1} $(D_2O)_3$ band. Liu et al. measured another parallel band of $(D_2O)_3$ centered at 81.8 cm^{-1} (initially referred to as the 82.5 cm^{-1} band), which was severely perturbed and could not be fitted accurately.[219] Measurements of a total of six torsional bands of different water trimer isotopomers by Liu et al. and Viant et al. followed.[179,182] The observation of a strongly perturbed $(D_2O)_3$ band at 28 cm^{-1} and additional measurements of the 81.8 cm^{-1} $(D_2O)_3$ band by Viant et al. prompted a further investigation, and a collaboration between the groups in Berkeley and Nijmegen produced an excellent simultaneous fit of all five observed $(D_2O)_3$ bands within the torsional manifold. The measurement of two additional $(H_2O)_3$ bands at 42.9 and 65.6 cm^{-1} by Brown et al. prompted a similar analysis for $(H_2O)_3$.[220] The observation of the 19.5 cm^{-1} torsional hot band of $(D_2O)_3$ by Keutsch et al. verified the assignment and effective Hamiltonian developed by Viant et al., which predicted nearly all transitions of this band to within spectral accuracy.[221] At the same time, Keutsch et al. reported the first observations of both a translational band of $(D_2O)_3$ centered at 142.8 cm^{-1} and a librational band of $(H_2O)_3$ at ca. 520 cm^{-1}.[222,223]

1. Torsional Vibrations (15−100 cm^{-1}). The torsional energy levels of the water trimer are now well understood and have been characterized in great detail. Fitting of $(H_2O)_3$ and $(D_2O)_3$ torsional bands requires the use of a Hamiltonian which takes the effects of Coriolis coupling explicitly into account. Viant et al. derived such an effective Hamiltonian with the help of Van Vleck perturbation theory and the Hamiltonian in eq 7. The effective Hamiltonian for a torsional eigenstate of eq 10 with torsional quantum number k is given by

$$H_{\mathrm{eff}}^{\mathrm{rot}(k',k)} = \delta_{k',k}[B^{|k|}J^2 + (C^{|k|} - B^{|k|})J_z^2 \pm (\mu_{+-}^{|k|} - \mu_{-+}^{|k|})J_z] + \delta_{k',k-2(\mathrm{mod}\,6)}\mu_{--}^{(k)}J_-J_- + \delta_{k',k+2(\mathrm{mod}\,6)}\mu_{++}^{(k)}J_+J_+ \quad (13)$$

The definitions of $\mu_{+-}^{|k|}$, $\mu_{-+}^{|k|}$, $\mu_{--}^{(k)}$, and $\mu_{++}^{(k)}$ can be found in ref 191, and these matrix elements include coupling to levels with $k' = k + 1$ or $k' = k - 1$. This effective Hamiltonian includes Coriolis perturbations up to second order from the H^{Cor} (eq 9); effects of bifurcation tunneling are not shown and will be discussed later. For the nondegenerate levels with $k = 0$ and $k = 3$, $\mu_{--}^{(k)}$ and $\mu_{++}^{(k)}$ vanish and $\mu_{+-}^{|k|} = \mu_{-+}^{|k|}$, and thus $H_{\mathrm{eff}}^{\mathrm{rot}(k',k)}$ reduces to a standard symmetric rotor Hamiltonian. However, it is important to note that using this Hamiltonian to fit the experimental data gives effective rotational constants that are slightly Coriolis-contaminated, and $B^{|k|} = B + 2\mu_{+-}^{k}$, and $C^{|k|} = C + \mu_{zz}^{k}$. The simple symmetric rotor Hamiltonian reveals that for transitions involving only $k = 0$ and $k = 3$, no Coriolis perturbations are expected.

For the degenerate levels with $k = 1$ and $k = 2$, all terms in eq 13 are effective, and the resulting splittings can make assignment of individual transitions quite challenging. As for the nondegenerate levels, the rotational constants are also contaminated, and $B^{|k|} = B + \mu_{+-}^{k} + \mu_{-+}^{k}$, and $C^{|k|} = C + \mu_{zz}^{k}$. Most remarkable is the existence of the $\pm\delta_{k',k}(\mu_{+-}^{|k|} - \mu_{-+}^{|k|})J_z$ term, which corresponds to a linear Coriolis interaction. Typically, such terms are associated with nonzero vibrational angular momentum; however, for the water trimer the expectation value for the torsional angular momentum vanishes, and the linear Coriolis term originates from second-order effects. Viant et al. have pointed out that for a molecule with large-amplitude internal motion, the usual definition of a body-fixed frame by the Eckart conditions, which minimizes the Coriolis coupling, does not make sense.[191] Usually linear Coriolis terms

Table 9. Molecular Constants of the Intermolecular Vibrational Levels of $(D_2O)_3$[a]

k^n	0^0	$+1^0$	-1^0	$+2^0$	-2^0	3^0	3^1	$+2^1$	-2^1	translation[b]
E_0	0.0*	255976.7(4)		839187.0(3)		1232139.3(4)	2709548.5(6)	2940937.2(4)		4284781.9(3)
$B(=A)$	5796.32(2)	5795.95(2)		5794.63(3)		5792.85(4)	5788.66(3)	5786.26(2)		5782.33(5)
ΔC	0	2.75(3)		8.11(2)		11.83(2)	2.12(4)	0.89(3)		−5.03(6)
D_J	0.029(3)	0.0279(3)	0.0279(4)	0.0273(2)	0.0273(3)	0.0265(5)	0.027(3)	0.0266(5)	0.0265(3)	0.0274(8) 0.0280(7)
D_{JK}	−0.042(1)	−0.0472(8)	−0.0449(8)	−0.041(1)	−0.0436(9)	−0.045(1)	−0.0393(9)	−0.043(1)	−0.040(1)	−0.045(3) −0.038(4)
D_K	0.0179(17)	0.024(3)	0.024(3)	0.020(3)	0.021(2)	0.023(2)	0.017(2)	0.023(3)	0.016(2)	0.011(3) 0.011(6)
ζ^c	0.0	−0.04384(1)		−0.04820(2)		0.0	0.0	0.00031(2)		−0.02708(2)
$\lvert\mu_{++}\rvert^c$	0.0	26.69(1)		13.74(2)		0.0	0.0	3.61(1)		12.81(2)
$\Delta\Delta$	0	−5.87		−17.91		−27.13	−11.9	−11.84		−3.93

[a] RMS: 1.5 MHz for global fit of all torsional states; 0.86 MHz for fit of the translational band. 1σ uncertainties of fitted constants are given in parentheses. *, fixed. [b] Differences between the ground-state constants determined from the fit of the translational and torsional band are insignificant. [c] As defined by Viant et al.[191]

Table 10. Molecular Constants of the Intermolecular Vibrational Levels of $(H_2O)_3$[a]

k^n	0^0	$+1^0$	-1^0	$+2^0$	-2^0	3^0	517.2 cm^{-1}	523.9 cm^{-1}	525.3 cm^{-1}
E_0	0.0*	680605.3(4)		1967970.0(3)		2609774.9(2)	15503814(6)	15706153(5)	15748986(4)
$B(=A)$	6646.91(2)	6641.73(4)		6632.11(2)		6626.10(2)	6567.9(7)	6537.8(8)	6525.3(4)
ΔC	0	2.37(2)		4.09(2)		0.79(1)	−29.84(3)	−60.44(7)	−110.64(8)
D_J	0.0417(2)	0.041(1)	0.0413(9)	0.0410(5)	0.0404(4)	0.0405(3)	.292(12)	−0.074(29)	0.087(7)
D_{JK}	−0.0631(6)	−0.064(3)	−0.064(2)	−0.063(2)	−0.062(1)	−0.0627(8)	−0.305(13)	0.202(37)	−0.111(20)
D_K	0.027(2)	0.030(3)	0.028(3)	0.028(3)	0.027(2)	0.027(2)	0*	0*	0*
ζ^b	0.0	−0.05302(2)		−0.03950(2)		0.0		$\gamma = 16.81(4)^c$	
$\lvert\mu_{++}\rvert^b$	0.0	15.344(2)		17.47(1)		0.0			
$\Delta\Delta$	0	−9.98		−22.98		−22.39	−19.33	11.77	99.67

[a] 1σ uncertainties of fitted constants are given in parentheses. *, fixed. [b] As defined by Viant et al.[191] [c] Constant, γ, introduced to take the $K = 1$ splitting into account. For all other states $\gamma = 0$.

are represented as $\mp 2\zeta C J_z$ in the rotational Hamiltonian, and ref 191 shows that the linear Coriolis term in eq 13 can be expressed in this way, $-2\zeta^{|k|}C^{|k|} = (\mu_{+-}^{|k|} - \mu_{-+}^{|k|})$. The last two terms in eq 13, containing $J_- J_-$, and $J_+ J_+$, normally apply for asymmetric rotors ($A \neq B \neq C$), but for the water trimer they result from second-order Coriolis coupling and do not appear for $k = 0$ and $k = 3$. These terms occur only in the off-diagonal blocks of the effective rotational Hamiltonian and couple degenerate substates with both $k = -k'$ and $k = k' \pm 2$, and the shift operators couple states with $K = K' + 2$ and $K = K' - 2$, thus conserving the symmetry rule that $k - K = k' - K'$. The Hamiltonian matrix is easily diagonalized, allowing the Coriolis terms $\zeta^{|k|}$ and $\mu_{++}^{|k|} = \mu_{--}^{|k|*}$ to be used as fitting parameters. It should be noted that the Coriolis coupling for the degenerate levels does not always allow unambiguous assignment of a K quantum number to a transition, as only $k - K$ is a good quantum number.

Tables 9 and 10 show the results of a global fit of all torsional $(D_2O)_3$ bands (including 659 transitions) and all torsional $(H_2O)_3$ bands (including 361 lines) performed with the use of the effective Hamiltonian of eq 13. The quality of the fit is evidenced by the root-mean-square deviation of the frequency of the residuals of 1.5 and 0.93 MHz for $(D_2O)_3$ and $(H_2O)_3$, respectively, less than the average experimental uncertainty of ca. 2 MHz. Typically, perpendicular bands of oblate symmetric rotors allow determination of the C rotational constant. However, for the water trimer, the ground-state C rotational constant had to be fixed to avoid correlations. Figure 9 shows a comparison of the experimentally determined torsional energy level diagrams for $(H_2O)_3$, $(D_2O)_3$, and some water trimer isotopomers with results from theoretical calculations using the full Hamiltonian (eq 7) in a DVR calculation with the DD potential.[191] Table 4 shows a comparison of the experimental torsional energies with various calculations. The torsional energies calculated by Sabo et al. using the BGLK potential and the 3D model (eq 6) are significantly too low for the first torsional manifold for both $(D_2O)_3$ and $(H_2O)_3$.[188] However, the energy level structure is predicted correctly and is close enough to aid in assignment of the observed vibrational bands. Interestingly, inclusion of the Coriolis interaction (eq 7) slightly improves agreement with experimental values for $(D_2O)_3$ but makes it worse for $(H_2O)_3$.[220] Agreement using both eqs 6 and 7 with the BGLK potential is much better for the second torsional manifold of $(D_2O)_3$, with slightly better agreement for calculations including the Coriolis coupling. Calculations with the DD potential and eq 7 show better agreement with experiment than those with the BGLK potential for the first torsional manifold, but the opposite is true for the second torsional manifold. The calculations with the SAPT-5st potential show excellent agreement with experimental results for the first torsional manifolds of both $(D_2O)_3$ and $(H_2O)_3$. However, agreement for the second torsional manifold is worse than for either the DD or the BGLK potential.[110] Groenenboom et al. argue that the poor agreement for the second torsional manifold results from exclusion of the coupling of the hydrogen-bond-stretching vibrations with the torsional states, which is more important at the higher torsional energy levels. This seems likely, as the better agreement of calculations with the DD and especially the BGLK potentials, which also do not include coupling to hydrogen bond stretches for the second torsional manifold, may result from the fact that these potentials, especially the BGLK potential, always give energy levels that are too low, and thus

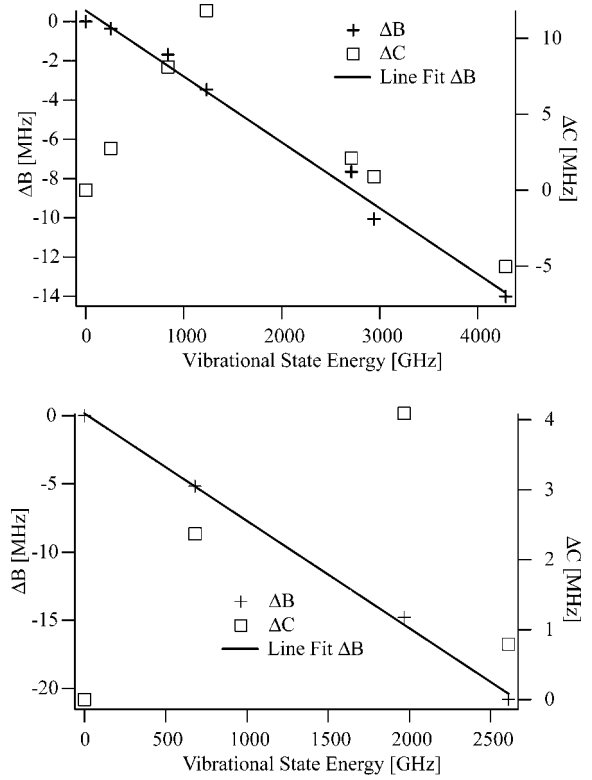

Figure 11. Experimentally determined values of ΔB and ΔC as a function of vibrational energy. The crosses and open squares correspond to the ΔB and ΔC values, respectively. The C rotational constants of both $(H_2O)_3$ and $(D_2O)_3$ change discontinuously with vibrational energy, whereas the B rotational constants decrease linearly with vibrational energy, as shown by the close agreement to a linear fit. ΔC is positive for all trimer torsional bands, leading to a more negative inertial defect, indicative of an out-of-plane torsional vibration. The B rotational constant of the translational 142.8 cm^{-1} $(D_2O)_3$ band lies close to this linear fit, but this band is the only $(D_2O)_3$ band that shows a negative change of the C rotational constant.

for the second torsional manifold are apparently more accurate, but only because of the exclusion of this coupling.

Besides the torsional energy levels, the rotational constants provide a valuable comparison between results from theoretical calculations and experiment. The rotational constants offer the best choice for an analysis of the structural properties of water trimer, as other structural parameters — like the oxygen−oxygen distance, or O−H bond lengths and torsional angles — cannot be determined directly from the experimental data. The rotational constants of the water trimer show an interesting trend with torsional energy (see Figure 11). The B rotational constant decreases linearly for both $(D_2O)_3$ and $(H_2O)_3$, whereas the trend of the C rotational constant is discontinuous (Figure 11). For $(D_2O)_3$, ΔC increases linearly with torsional energy within the first manifold to $\Delta C = +11.83$ MHz for $k = 3^0$ and shows a sudden drop to $\Delta C = +2.26$ MHz for $k = 3^1$. As explained in an earlier section (section II.C.2), Sabo et al. showed that this discontinuous behavior results from coupling to the symmetric hydrogen bond stretch. In contrast, the continuous, linear trend of the experimental B rotational constants most likely requires inclusion of coupling to the asymmetric hydrogen-bond-stretching vibration. Below is a detailed description the appearance of the experimental THz-VRT spectra of the water trimer.

$k = 3 \leftarrow 0$ Parallel ($\Delta K = 0$) Bands. Only nondegenerate torsional levels are involved in these $\Delta K = 0$ (parallel) transitions, and strong Coriolis perturbations are thus absent; hence, the spectra are typical for an oblate symmetric rotor. Table 8 shows a summary of all observed water trimer vibrational bands, of which the 41.1 cm^{-1} $(D_2O)_3$ and 87.1 cm^{-1} $(H_2O)_3$ bands are the most intense torsional bands. Both bands show splittings of each rovibrational line into an equally spaced quartet that result from bifurcation tunneling, and these will be explained later. The 87.1 cm^{-1} $(H_2O)_3$ band shows an additional small Coriolis-induced bifurcation splitting of all P- and R-branch T-state transitions with $K = 1$. The splitting, which is proportional to J^2, arises from Coriolis coupling of, e.g., the $k = 0, K = 1$ levels with the $k = 1$, $K = 0$ levels, which have split T-states (see section III.B.1.4).

$k = 2 \leftarrow 0$ and $3 \leftarrow 1$ Perpendicular ($\Delta K = \pm 1$) Bands. The 28, 81.8, and 98.1 cm^{-1} $(D_2O)_3$ and 42.9 cm^{-1} $(H_2O)_3$ perpendicular ($\Delta K = \pm 1$) bands involve one nondegenerate and one degenerate torsional level. The bands are split into two sub-bands by the linear Coriolis term of the degenerate torsional level. Furthermore, those transitions involving $|K| = 1$ that are lowered in frequency by the Coriolis perturbation are split into doublets for all bifurcation-tunneling components; this splitting is J- and K-dependent and can be quite large. Further Coriolis effects in the example of a $k = 2 \leftarrow 0$ transition are that the $^RQ_0$-branch ($\Delta J = 0$, $\Delta K = +1$, $K = 1 \leftarrow 0$) is expanded and the $^PQ_1$-branch ($\Delta J = 0$, $\Delta K = -1$, $K = 0 \leftarrow 1$) is compressed compared to other Q-branches. For $(D_2O)_3$, all transitions are again split into equally spaced quartets by bifurcation tunneling. The only exceptions are transitions involving $K = 0$ of the degenerate states (see Table 8) which show bifurcation-tunneling splittings with unequal spacing and unusual intensity patterns, and they will be referred to as "anomalous" quartets. For $(H_2O)_3$, the spectra are further complicated by the fact that the splittings arising from the Coriolis interaction and bifurcation tunneling are similar to each other in magnitude, as well as to the spacing of rotational transitions. The effective Hamiltonian of eq 13 requires addition of a term $\delta_{k',-k}\,\delta_{\Gamma,T}\,\delta$ for the degenerate torsional levels to account for this. The first two Kronecker δ terms ensure that the splitting by the δ related to the bifurcation-tunneling matrix elements (detailed later) only occurs for T-states of the same symmetry and $k' = -k$. Thus, for $(H_2O)_3$, the distinction between "anomalous" and the regular bifurcation-tunneling quartets is not as clear. Finally, the 65.6 cm^{-1} $(H_2O)_3$ band showed an unexplained shift of the T-state bifurcation-tunneling components with respect to the A-states.

$k = 2 \leftarrow 1$ Parallel ($\Delta K = 0$) Bands. These vibrational bands, which include the 19.5 and 89.6 cm^{-1} $(D_2O)_3$ and 42.9 cm^{-1} $(H_2O)_3$ bands, correspond to transitions between degenerate torsional levels. Therefore, they are severely perturbed, as all effects

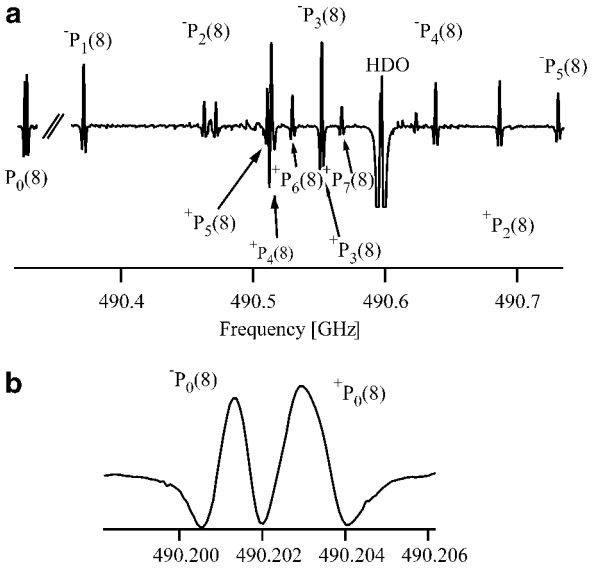

Figure 12. (a) The P(8) transition of the 19.5 cm^{-1} band (shown in inset a) demonstrates the effects of the Coriolis perturbation on the spectrum. The transitions corresponding to the $k = +2^0 \leftarrow -1^0$ sub-band are labeled $^{-}P_K(8)$, and the transitions corresponding to the $k = -2^0 \leftarrow +1^0$ sub-band are labeled $^{+}P_K(8)$. The purely second- and higher-order Coriolis interaction splits the degenerate vibrational levels $\sim K$ (usually arising from first-order effects) with additional higher-order effects. The $^{+}P_K(8)$-branch shows severe perturbations, evidenced by an atypical rotational progression. The $^{+}P_0(8)$ transitions is observed at lower frequency, the $^{+}P_1(8)$ transitions is split into a doublet by a large amount and was not observed, and the $^{+}P_2(8)-{}^{+}P_7(8)$ transitions form a progression starting at higher frequency with a bandhead at $^{+}P_5(8)$. The $^{-}P_2(8)$ transition is split into a quartet (see Figure 13). (b) The $^{\pm}P_0(8)$ transitions separated by ca. 2 MHz.

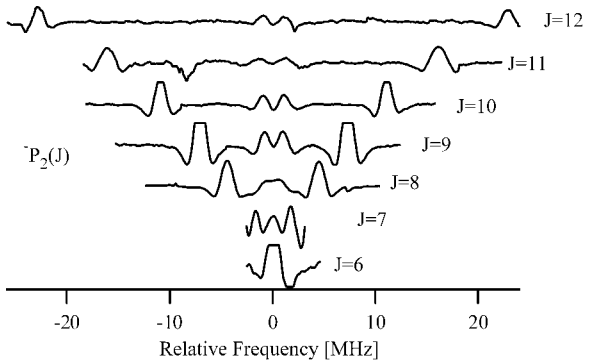

Figure 13. The $K = 2$ transitions of the $k = +2^0 \leftarrow -1^0$ sub-band are split into quartets. The splitting is symmetrical about the position predicted for an unperturbed transition. The splitting is observable only for $J > 7$ and increases with J (ca. as $J(J + 1)$). The broadening of the $^{-}P_2(6)$ transition is probably due to convolution with the $^{+}P_2(6)$ transition. The two higher-intensity components are split by a large amount and the two lower-intensity components by a very small amount (<2.5 MHz). This has not been observed for any of the other $(D_2O)_3$ bands, probably as no high-J, low-K transitions have been observed due to low intensities.

on the spectra described above now appear in both the lower and upper torsional levels (see Figure 12). However, the effective Hamiltonian of eq 13 allows analysis and fitting of even these severely perturbed bands. The only feature that has not been fully explained is the J-dependent splitting of the $K = 2$ transitions of one sub-band of the 19.5 cm^{-1} $(D_2O)_3$ band (see Figure 13) into a symmetrical quartet consisting of one closely spaced, low-intensity doublet and one widely spaced, higher-intensity doublet. Keutsch et al. argue that the splitting could arise from Coriolis coupling similar to the large J-dependent splitting of the $|K| = 1$ transitions described above, with the splitting for the T-states being different from the A-states, resulting in a quartet rather than a doublet.[221] However, in this case it arises from effects higher than second-order and is thus not included in the effective rotational Hamiltonian of eq 13. The reason that no such splitting has been observed for other bands is that, in the case of the 19.5 cm^{-1} band, much higher J values (up to $J'' = 11$ for $K = 2$) were observed than for other bands.

Mixed-Isotope Water Trimers (see Table 11). In a detailed study of the torsional bands of water trimers, starting with $(D_2O)_3$, in which the bound deuterons were sequentially substituted with protons, Viant et al. showed that motion of the bound protons/deuterons has to accompany the torsional motion of the free deuterons.[182] The theoretical models treating the torsional motion did not consider such participation of the bound protons/hydrogens, and as mentioned above, Geleijns and van der Avoird[193] confirmed that agreement with experiment required a choice of the axis of the torsional motion that did not extend from the bonded hydrogen through the center of mass of the monomer, but closer to the oxygen−oxygen line. In this work, Geleijns and van der Avoird[193] also confirmed the assignment of all experimentally observed mixed-isotope torsional bands, except for the 97.3 cm^{-1} $(D_2O)_2DOH$ band, which they reassigned on the basis of experimentally calculated intensities (see Figure 14).

2. Translational Vibrations. The translational (hydrogen bond stretch) band region of water, centered at ca. 180 cm^{-1}, was investigated only after technological advances extended the frequency range of the FIR spectrometers to ca. 150 cm^{-1}.[224] Recently, Keutsch et al. measured a perpendicular ($k = \pm 2 \leftarrow 0$) vibrational band of $(D_2O)_3$ centered at 142.8 cm^{-1} (see Figure 15), which they assigned to transitions from the vibrational ground state to the excited state of the degenerate translational state (degenerate asymmetric H-bond stretch).[223] The band constitutes the only published translational vibration for a water cluster. The spectrum exhibited perturbations analogous to those observed in the torsional $k = \pm 2^n \leftarrow 0^0$ bands, and thus was fitted with the effective Hamiltonian developed by Viant et al.[191] for the torsional states (see above), and the results are shown in Table 9. The spectrum was unusual for $(D_2O)_3$ in a number of respects: The bifurcation-tunneling splitting of this band was determined to be smaller than 1 MHz — less than the experimental resolution. All $K = 0 \leftarrow 1$ transitions of this band are split into roughly equal intensity triplets; however, no conclusive explanation for this splitting has been found to date. Furthermore, the spectrum is one of the weakest water cluster absorptions detected to date and was the first water trimer band to show a negative value of ΔC. The change in inertial defect is also the

Table 11. Molecular Constants of the Intermolecular Vibrational Levels of Mixed-Isotope Trimer Bands[a]

	d_5a	d_4a	d_3a	d_4b	d_3b	d_5b	h_5
ν	1283478.64(25)	1329895.03(23)	1372214.54(34)	1392426.06(25)	1375644.45(25)	2917820.44(87)	~2580000
A''	5907.99(10)	5955.72(4)	5940.98(4)	6426.23(8)	6478.67(7)	6195.69(29)	
B''	5783.11(10)	5832.12(4)	$=A''$	6047.48(8)	6099.85(7)	5833.90(25)	
D_J''	0.0283(29)	0.0338(5)	0.0323(7)	0.0363*	0.0363(15)		
D_{JK}''	−0.0464(51)	−0.0484(13)	−0.0497(16)	−0.0505*	−0.0505(40)	0.1350*	
A'	5902.04(7)	5948.53(5)	5934.16(4)	6422.81(8)	6463.54(7)	6192.48(28)	
B'	5799.49(7)	5827.33(5)	$=A'$	6031.71(8)	6095.05(7)	5811.80(29)	
D_J'	0.0257(17)	0.0276(5)	0.0278(8)	0.0379(3)	0.0384(16)		
D_{JK}'	−0.0441(40)	−0.0421(13)	−0.0451(18)	−0.0520(3)	−0.0526(41)	0.1358(3)	
ΔC	11.75(2)	11.84(1)	12.01(2)	−4.42(1)	−4.03(2)	−7.871(51)	

[a] 1σ uncertainties of fitted constants are given in parentheses. *, fixed.

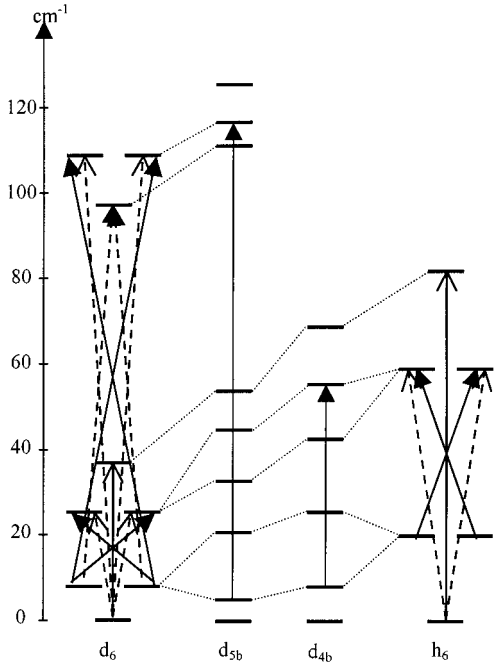

Figure 14. Torsional energy level diagram for water trimers with substitution of the free protons/deuterons with the DD potential.[193] Generally, the spacing of the torsional energy levels increases from the d_6 trimer to the h_6 trimer. However, the breaking of the G_6 torsional symmetry results in splitting of the degenerate levels of the pure trimers. The fact that the same general energy level structure is observed for all trimers suggests addressing the torsional levels as vibrational rather than tunneling levels.

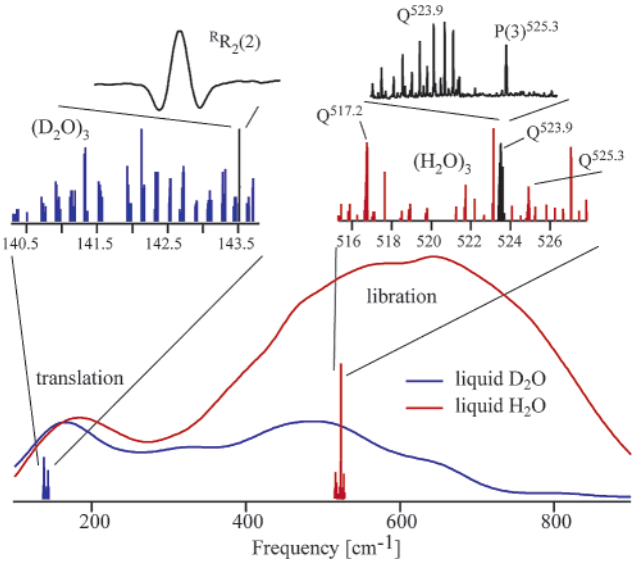

Figure 15. Overview of the translational and librational band region of liquid H_2O and D_2O, together with the observed D_2O transitions of the 142.8 cm^{-1} $(D_2O)_3$ and ~ 520 cm^{-1} $(H_2O)_3$ bands. The water trimer bands lie well within the corresponding bands of the liquid. The left-hand insets show a stick spectrum representation of the 142.8 cm^{-1} $(D_2O)_3$ band and a scan of the $^RR_2(2)$ transition, representative of the strongest observed rovibrational transitions of this trimer band. A stick spectrum representation of the three VRT bands of $(H_2O)_3$, together with a scan of the Q-branch of the 523.9 cm^{-1} band and the P(3) clump of the 525.3 cm^{-1} band, are shown in the right-hand insets.

smallest observed to date, indicating a predominantly in-plane vibration, and the Coriolis constants are closer to those of the first torsional manifold than to the second one. All of these facts strongly indicate an excitation of a novel type of vibration. Theoretical calculations suggested four possible vibrational states with the correct symmetry and energy. The first was the lowest previously unobserved purely torsional energy level $k = \pm 2^2$, which was calculated at 166.95 and 165.92 cm^{-1} by Olthof et al. with the DD and BGLK potentials, respectively.[29] The second vibrational state considered was the degenerate translational vibration (degenerate asymmetric H-bond stretch), the third one was a combination band of symmetric translation and a torsional vibration, and the fourth one was a mixed translational/torsional state. Theoretical calculations, which typically use the asymmetric equilibrium structure, generally give three translational frequencies, and not one symmetric (A_1^+, $k = 0$, in G_6) and one degenerate asymmetric translation (A_2^+/A_3^+, $k = \pm 2$, in G_6). However, the latter is expected as a result of the symmetry of the ground-state wave function being equivalent to that of an oblate symmetric rotor. Xantheas et al. calculated the ab initio harmonic frequency of the symmetric translation at 235 cm^{-1}, and the average of the asymmetric translations at 179 cm^{-1}.[26] Klopper and Schütz calculated harmonic frequencies that were a bit smaller, 207.5 and 169.9 cm^{-1}.[158] Keutsch et al. concluded from the unusual properties of the vibrational band and fitted constants that the observed vibration most likely was the degenerate translation, and further argued that the Coriolis perturbation resembling those of the degenerate torsional levels did not necessarily imply excitation of a torsional vibration and could arise from the ground-state torsional motion — even in an excited degenerate state. However, they note that the asymmetric translation could itself form a manifold of pseudorotational states that could then couple

strongly to the torsional levels, thus lowering the calculated vibrational frequencies considerably and, perhaps, making a distinction between the two types of motion impossible at these energies. A full analysis and verification of the assignment of this band requires further theoretical studies, especially calculations taking into account coupling between torsional and translational degrees of freedom.

3. Librational Vibrations. The librational band region of water (300−1000 cm^{-1}) has been studied with tunable diode laser spectrometers, as theoretical calculations predicted that the librational vibrations of water clusters should occur in the same region. Librations correspond to hindered rotational motions of water molecules and are of interest as they are predicted to be the dominant motion for the initial breaking of hydrogen bonds in liquid water.[225,226] Recently, Keutsch et al. observed at least four parallel bands of $(H_2O)_3$ between 515 and 528 cm^{-1}, which represent the only water cluster librational bands reported to date.[222] The bands at 517.2, 523.9, and 525.3 cm^{-1} were assigned and fit (see Table 10) individually to transitions from the A_1^+ ground state to excited vibrational states with A_1^- symmetry ($k = 3 \leftarrow 0$ transitions). The band centered at 517.5 cm^{-1} showed perturbations and was tentatively assigned to a hot band but not fit. All other bands were fitted using a simple oblate symmetric rotor Hamiltonian, except for the 523.9 cm^{-1} band, which had a *J*-dependent doublet splitting of all $K = 0$ transitions similar to the 81.8 cm^{-1} $(H_2O)_3$ torsional band. For these $K = 0$ states, an additional term taking the splitting into account was added. In contrast to the 81.8 cm^{-1} band, in which this splitting was observed only for the P- and R-branches, the P-, Q-, and R-branches of the 523.9 cm^{-1} band are split into doublets. This results from the fact that the splitting is dominated by the excited state.[192] The individual $k = 3 \leftarrow 0$ bands showed no signs of bifurcation-tunneling splittings, and calculations predict only one A_1^- vibrational state corresponding to a fundamental vibrational transition. The three distinct vibrational bands were instead assigned to three of the four bifurcation-tunneling symmetries of the same vibrational state — the nondegenerate out-of-plane libration at ca. 520 cm^{-1}. Klopper and Schütz calculated the A_1^- out-of-plane vibration at 697.1 cm^{-1} (see Table 7).[158] Xantheas et al. calculated the A_1^- out-of-plane vibration at 668 cm^{-1}[1227] (see Table 7), and his calculations also showed that it is the most intense librational band of the water trimer.[26] The dramatic increase of the bifurcation splitting was attributed to the fact that the nuclear displacements of the librational motion resemble those of the initial part of the bifurcation-tunneling pathway. The change in the rotational constants (see Table 10) for these bands is the largest observed for any water trimer vibrational band, which is expected, as the excitation energies are much larger and a new large-amplitude motion has been excited (bifurcation tunneling). However, it is interesting to note that the rotational constants of the three excited states are quite different, typically indicating excitation of different vibrational motions. Two explanations were offered for this: It has been shown that structural interpretations derived from rotational constants have to be viewed with care, as the rotational constants can be contaminated by perturbations and, in fact, this is the case for the water trimer, as explained in the torsional case. Second, for facile motions, excitations of higher energies do not necessarily result in larger vibrational amplitudes. The torsional motions are again such a case. In $(H_2O)_3$, the free hydrogens are delocalized over the entire torsional subspace, even for the ground state. Sabo et al. have shown that a higher torsional excitation does not result in a larger amplitude of the torsional motion of the hydrogens but rather that the highest probability of the location of the hydrogens depends sensitively on the details of the torsional wave functions.[112] The energy of the librational states is close to the barrier for bifurcation tunneling, and thus might be sampling the whole bifurcation subspace, possibly resulting in a nontrivial dependence of the rotational constants on vibrational excitation and bifurcation tunneling.

4. Bifurcation Tunneling and H-Bond Lifetime in the Water Trimer. Bifurcation tunneling was observed in the first water trimer spectrum measured by Pugliano et al. and manifests itself as a characteristic quartet splitting in most of the trimer spectra.[27] The bifurcation splittings in $(D_2O)_3$ are closely spaced (<10 MHz), and thus act as a fingerprint and aid in identification and assignment of $(D_2O)_3$ spectra. In contrast, the splittings in $(H_2O)_3$ are hundreds of megahertz and can seriously complicate the spectra, as they are similar to the splittings between different rotational transitions.

Experimental Bifurcation-Tunneling Splittings. The bifurcation-tunneling splittings of $(D_2O)_3$ can be divided into "regular" (see Figure 7a) and "anomalous" (see Figure 7b) quartets, which are observed exclusively for all transitions involving $K = 0$ levels of degenerate torsional states ($k = \pm 1, \pm 2$). The regular quartets appear as equally spaced quartets with an intensity pattern, determined by the nuclear spin statistics, of ~7:11:5:1 in $(D_2O)_3$ and 1:3:9:11 for $K = 3m$ and 0:3:9:8 for $K \neq 3m$ in $(H_2O)_3$ (see Figure 16), but the ordering of the experimental splittings can be reversed for different vibrational transitions. For the degenerate levels of $(H_2O)_3$, no clear distinction between anomalous and regular quartets is possible, and the resulting patterns can be quite complicated. A further anomaly was observed in that the T-states of the 65.6 cm^{-1} band of $(H_2O)_3$ are shifted with respect to the A-states. Last, there is a splitting of the T-state bifurcation-tunneling components of $K = 1$ of the $k = 0$ and 3 levels of $(H_2O)_3$.

Analysis. Inspection of Table 12, which shows the A and B patterns determined by Wales,[157] shows that for transitions involving only nondegenerate torsional levels, the experimentally observed tunneling splittings are indeed expected to consist of equally spaced quartets. The experimentally observed bifurcation splittings correspond to the difference of the bifurcation-tunneling splitting in the lower and upper levels, and for the case of a $k = 3 \leftarrow 0$ transition, the splitting is $\delta = {}^4/_3\Delta\beta_A - \beta_B(3) - \beta_B(0)$, with A and B referring to the splitting pattern and $\beta_i(3)$ and $\beta_i(0)$

Table 12. Torsional and Bifurcation-Tunneling Levels for $K = 0$ and $K = 1$

	$K = 0$		$K = 1$			
	$k - K = 0$		$k - K = \pm 1$			
$k = 0$	A_{1g}^+	$2\beta_A + \beta_B$	A_{2g}^-/A_{3g}^-	$2\beta_A + \beta_B$		
	T_u^+	$^2/_3\beta_A + {}^1/_3\beta_B$	$2T_u^-$	$^2/_3\beta_A + {}^1/_3\beta_B$		
	T_g^+	$-^2/_3\beta_A - {}^1/_3\beta_B$	$2T_g^-$	$-^2/_3\beta_A - {}^1/_3\beta_B$		
	A_{1u}^+	$-2\beta_A - \beta_B$	A_{2u}^-/A_{3u}^-	$-2\beta_A - \beta_B$		
	$k - K = \pm 1$		$k - K = 0$		$k - K = \pm 2$	
$k = \pm 1$	A_{2g}^-/A_{3g}^-	$-\beta_A - \beta_B$	$2A_{1g}^+$	$-\beta_A - \beta_B$	A_{2g}^+/A_{3g}^+	$-\beta_A - \beta_B$
	T_u^-	$\beta_A - \beta_B$	$2T_u^+$	$-^1/_3\beta_A - {}^1/_3\beta_B$	$2T_u^+$	$-^1/_3\beta_A - {}^1/_3\beta_B$
	T_u^-	$-^5/_3\beta_A + {}^1/_3\beta_B$				
	T_g^-	$^5/_3\beta_A - {}^1/_3\beta_B$	$2T_g^+$	$^1/_3\beta_A + {}^1/_3\beta_B$	$2T_g^+$	$^1/_3\beta_A + {}^1/_3\beta_B$
	T_g^-	$-\beta_A + \beta_B$				
	A_{2u}^-/A_{3u}^-	$\beta_A + \beta_B$	$2A_{1u}^+$	$\beta_A + \beta_B$	A_{2u}^+/A_{3u}^+	$\beta_A + \beta_B$
	$k - K = \pm 2$		$k - K = \pm 1$		$k - K = 3$	
$k = \pm 2$	A_{2g}^+/A_{3g}^+	$-\beta_A + \beta_B$	A_{2g}^-/A_{3g}^-	$-\beta_A + \beta_B$	$2A_{1g}^-$	$-\beta_A + \beta_B$
	T_u^+	$\beta_A + \beta_B$	$2T_u^-$	$-^1/_3\beta_A + {}^1/_3\beta_B$	$2T_u^-$	$-^1/_3\beta_A + {}^1/_3\beta_B$
	T_u^+	$-^5/_3\beta_A - {}^1/_3\beta_B$				
	T_g^+	$^5/_3\beta_A + {}^1/_3b_B$	$2T_g^-$	$^1/_3\beta_A - {}^1/_3\beta_B$	$2T_g^-$	$^1/_3\beta_A - {}^1/_3\beta_B$
	T_g^+	$-\beta_A - \beta_B$				
	A_{2u}^+/A_{3u}^+	$\beta_A - \beta_B$	A_{2u}^-/A_{3u}^-	$\beta_A - \beta_B$	$2A_{1u}^-$	$\beta_A - \beta_B$
	$k - K = 3$		$k - K = \pm 2$			
$k = 3$	A_{1g}^-	$2\beta_A - \beta_B$	A_{2g}^+/A_{3g}^+	$2\beta_A - \beta_B$		
	T_u^-	$^2/_3\beta_A - {}^1/_3\beta_B$	$2T_u^+$	$^2/_3\beta_A - {}^1/_3\beta_B$		
	T_g^-	$-^2/_3\beta_A + {}^1/_3\beta_B$	$2T_g^+$	$-^2/_3\beta_A + {}^1/_3\beta_B$		
	A_{1u}^-	$-2\beta_A + \beta_B$	A_{2u}^+/A_{3u}^+	$-2\beta_A + \beta_B$		

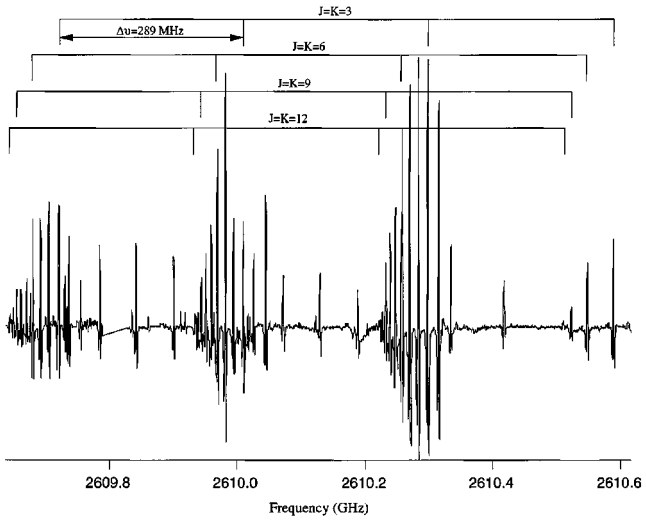

Figure 16. Part of the Q-branch region of the 87.1 cm^{-1} torsional band of $(H_2O)_3$. The spectrum is typical for a parallel band of an oblate symmetric top, and each rovibrational transition is split by ca. 289 MHz by bifurcation tunneling. The relative intensities of the bifurcation-tunneling components are determined by the nuclear spin weights, and from the figure it is evident that one of the components has nonzero nuclear spin weight only for $K = 3m$. (Reprinted with permission from ref 18. Copyright 2000 American Chemical Society.)

referring to the splitting in the $k = 3$ and 0 levels, respectively. The ordering of the tunneling components thus depends on the sign of the δ. There are six allowed (bifurcation-tunneling) transitions between $K = 1$ states of nondegenerate levels and $K = 0$ states of degenerate levels, as there are four T-state energies in the degenerate levels. Overlapping signals as well as weak intensities for some of the transitions produce a complex pattern, which results in observation of anomalous quartets. For transitions between degenerate torsional states, there are 10 transitions that are allowed by symmetry for a given K level. Experimentally, however, only some of these are observed and also result in anomalous quartets. It is interesting that without the Coriolis interaction, these "anomalous" quartets should, in fact, be observed for all trimer transitions involving degenerate torsional states, and not just for those with $K = 0$. For larger K values, the experimental splitting pattern resembles that for the nondegenerate torsional levels, as the Coriolis interaction lifts the degeneracy and thus eliminates (in $(D_2O)_3$) or reduces (in $(H_2O)_3$) the "splitting" of the T-states. For $(H_2O)_3$, the bifurcation splittings are comparable to the shifts and splittings caused by the Coriolis perturbation and the spacing of the rotational levels. The "stronger" bifurcation interaction can thus affect T-states even for levels which are already split by the Coriolis interaction.

Van der Avoird and co-workers[28,29] used the splitting patterns derived by Wales (Table 12) to demonstrate that the experimental splitting patterns of the vibrational bands observed at the time corresponded to a tunneling path producing a B pattern (see Figure 17). The limited data set required the use of fixed tunneling matrix elements within each torsional manifold. The presently existing data set (see Table 8) proves that this assumption is incorrect, but in an extensive analysis including contributions from various tunneling pathways, Keutsch et al. recently showed that the experimental splitting patterns indeed result from a B-pattern pathway. These authors also showed that, although the pathway corresponding to either (12)*, (34)*, or (56)* permutation-inversion operators was the primary tunneling pathway, other pathways could contribute as well. The authors quantified the bifurcation-tunneling

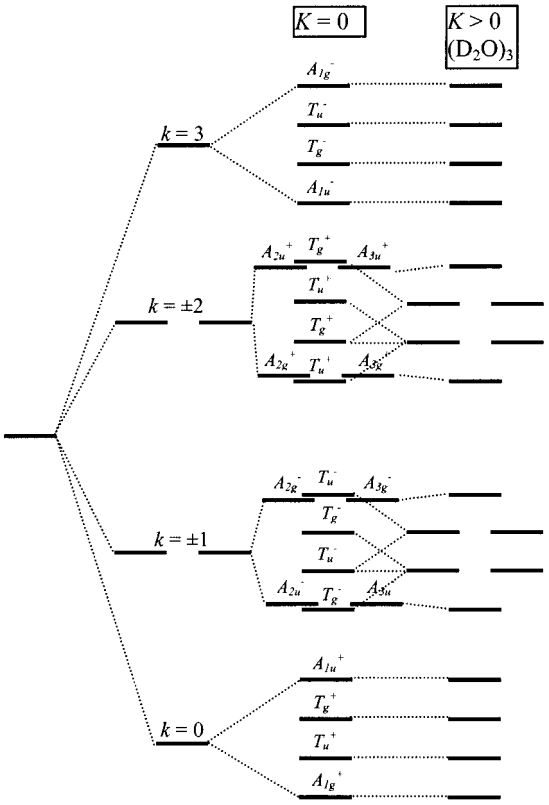

Figure 17. Energy level diagram of the bifurcation-tunneling states for the lowest torsional manifold for $K = 0$. For $k = 0$ and $k = 3$, each rovibrational level is split into an equally spaced quartet of states, which is also the case for $K > 0$. For $K = 0$ and $k = \pm 1$ or $k = \pm 2$, each rovibrational level is also split into an equally spaced quartet, albeit with accidental degeneracies. The ordering of the symmetry components is distinct from the nondegenerate torsional levels. If the splitting of the T-states with identical symmetries is removed, the pattern is reduced to the same one as in the nondegenerate states [as indicated for the $K > 0$ $(D_2O)_3$ case]. Transitions involving these levels can give rise to complicated patterns with unequal spacing, and are referred to as "anomalous" quartets. For $K > 0$ in $(D_2O)_3$, the pattern is reduced to that of the nondegenerate states due to the Coriolis interaction. In $(H_2O)_3$, the bifurcation-tunneling matrix elements are much larger, and thus the Coriolis interaction reduces the "splitting" of the T-states with identical symmetry significantly, but does not eliminate it altogether.

Table 13. Bifurcation-Tunneling Matrix Elements of the Water Trimer

k	β $(D_2O)_3$	β $(H_2O)_3$
0^0	−0.55 MHz	$\beta_b{}^0$
$\pm 1^0$	−0.35 MHz	−441 MHz − $\beta_b{}^0$
$\pm 2^0$	0.8 MHz	382.5 MHz + $\beta_b{}^0$
3^0	−1.7 MHz	−433.5 MHz − $\beta_b{}^0$
3^1	3.7 MHz	
$\pm 2^1$	−8.05 MHz	
$\pm 2^{trans}$	unknown (<1 MHz)	
libration		−2.3 or +4.6 cm^{-1}

matrix elements for all torsional $(D_2O)_3$ levels in an analysis using all regular quartets and adjusted the matrix element for $k = 0^0$ to best reproduce the anomalous quartets of the 28 and 98 cm^{-1} $(D_2O)_3$ (see Table 13). The matrix element β varies between $\beta = -1.7$ and 0.8 MHz for the first torsional manifold and increases to $\beta = -8.05$ MHz for $k = \pm 2^1$. The only features of $(D_2O)_3$ which presently are not fully characterized and quantified, and which probably result form bifurcation tunneling, are the J-dependent $K = 2$ splitting of the 19.5 cm^{-1} band and the J-independent $K = 0 \leftarrow 1$ splitting of the 142.8 cm^{-1} translational band. The former forms a quartet (see Figure 13) consisting of two doublets, one of low intensity which is split by a very small amount (<3 MHz), and one of high-intensity which is split by a large, J-dependent amount.[221] As mentioned earlier, Coriolis effects higher than second-order will result in a splitting of the $K = 2$ states, and it is possible that the magnitude of the splitting is different for the (high-intensity) T-states and the (low-intensity) A-states. The splitting of all $K = 0 \leftarrow 1$ transitions of the 142.8 cm^{-1} translational band into a nearly equally spaced equal intensity triplet probably represents an "anomalous quartet" which has collapsed to a triplet.[223] However, no detailed explanation for this has been given. For $(H_2O)_3$, Keutsch et al.[192] attempted a similar quantification of the bifurcation matrix elements as for $(D_2O)_3$ and investigated whether the shifts of the T-states of the 65.6 cm^{-1} band and asymmetric splitting of the librational band result from the breakdown of the high barrier limit for bifurcation tunneling. The authors were only able to estimate the bifurcation-tunneling matrix elements for the torsional states (see Table 13), and showed that the shifts of the T-states of the 65.6 cm^{-1} band with respect the A-states do not result from the breakdown of the high barrier limit. However, an extension of the earlier treatments by Wales[157] to low barrier treatment of torsional flipping and bifurcation tunneling explains the observed spacing of the 520 cm^{-1} torsional band and allows quantification of the flipping and bifurcation matrix elements within this framework.[192] The values determined for the torsional (β_f) and bifurcation (β_b) matrix elements were either $\beta_f = -3.1$ cm^{-1} and $\beta_b = -2.3$ cm^{-1} or $\beta_f = 1.6$ cm^{-1} and $\beta_b = 4.6$ cm^{-1}. The magnitude of both matrix elements is comparable, representing a dramatic increase of the bifurcation-tunneling matrix elements and a small decrease of the torsional matrix element. This may seem surprising, but it should be noted that the torsional motion is already delocalized over the entire torsional subspace in the vibrational ground state. Further investigation of the librational band region and observation of the missing $A_g^{\pm}$ tunneling component would be helpful for verification of these results.

Liu et al.[179] developed the group theory for the water trimer isotopomers and explained the observed bifurcation-tunneling splittings. Only the pure isotope water monomers show splittings due bifurcation tunneling, and the magnitude of the splittings generally is very close to those for the same monomers in the pure water trimers. In the $(D_2O)_2(HDO)$ trimer, the two D_2O monomers experience slightly different environments, as evidenced by the observation of a quartet rather than a triplet splitting. Similar results are observed for $(H_2O)_2(HDO)$, only with much larger splittings.

Hydrogen Bond Lifetime. Keutsch et al. have investigated the effect of excitation of the three distinct classes of intermolecular vibrations on the

H-bond lifetime of the trimer.[228] The H-bond lifetime was defined as the time for breaking and making a H-bond via bifurcation tunneling. The H-bond lifetime of 1−2 ns for the vibrational ground state of $(H_2O)_3$ changed insignificantly on torsional and translational excitation, but decreased to 1−6 ps on librational excitation. This is remarkable, as it shows that the same motions that have been proposed to be responsible for the initial H-bond breaking in liquid water also facilitate H-bond breaking in the water trimer. It is also worth noting that bifurcation tunneling has been observed for all water clusters except the water tetramer, and thus bifurcation represents the lowest-energy pathway for breaking and making hydrogen bonds in water clusters in general.

2. IR Spectroscopy of the Free Water Trimer

In two gas-phase cluster studies, Vernon et al.[229] and Page et al.[230] were the first to study the intramolecular vibrational frequency shifts and predissociation dynamics of water clusters in the gas phase. In the first study, Vernon and co-workers crossed a molecular beam containing water clusters with an IR laser beam. The IR beam was of sufficient intensity to induce predissociation of the clusters, the fragments of which were detected as a function of angle from the unperturbed beam trajectory using a mass spectrometer. In this manner, different absorption spectra were assigned to $(H_2O)_n$, $n = 1-5$. They recorded a narrow (15 cm^{-1}) transition near 3715 cm^{-1} in all of the spectra, which they attributed to the free OH stretch in cyclic water clusters. A much broader (200 cm^{-1}) feature, peaking at a lower frequency, was more difficult to fully rationalize, but was attributed to the bound OH stretch. Page and co-workers concentrated on the water dimer in a later contribution, finding four IR peaks due to the gas-phase dimer, including a broad transition at 3545 cm^{-1}, red-shifted from the free monomer asymmetric stretch, that was assigned to the bound OH stretch. Although care was taken to compensate for such effects, those experiments were plagued by unpredictable fragmentation due to the electron impact ionization scheme used to detect the products. In a more recent study, Huisken and co-workers[197] found an elegant method to circumvent that problem and measured reliable IR frequencies for several gas-phase water clusters. The introduction to that paper is a good review of IR water cluster spectroscopy.

Coker and co-workers[231] reprised the molecular beam study of Vernon et al. [229] using a different laser system operating between 3000 and 3800 cm^{-1}, and bolometer detection to circumvent the fragmentation problem. They found four dimer IR frequencies identical to those of Page et al.[230] and were able to spectroscopically monitor the evolution of larger clusters in supersonic expansions carrying increasing concentrations of water. Coker et al. assigned absorptions near 3400 and 3357 cm^{-1} to the H-bonded and free trimer OH stretches. Wuelfert and co-workers observed a set of three distinct vibrational Raman transitions which increased in strength upon increasing the water concentration in a supersonic expansion.[232] They tentatively attributed all of these features, centered near 3350 cm^{-1}, to the bound OH stretch of the trimer. However, Xantheas showed that only one of the modes was Raman active.[26] It seems more likely that Wuelfert et al. were observing bound OH stretching signals from different clusters.

In more recent IR experiments, Huisken and co-workers employed a size selection technique in which a He beam is used to eject clusters from a molecular beam as a function of their size.[197] Because clusters of a given size will scatter into different solid angles upon collision with He atoms, they can be selectively mass detected at those angles by a rotating mass spectrometer. In this manner, Huisken et al. were able to measure free and bound OH stretching frequencies for the clusters up to the pentamer. Each cluster yielded two peaks characteristic of cyclic structures, consistent with vibrational averaging over the flipping coordinates. Their trimer results are shown in Table 6 and compared to theoretical calculations. Paul et al.[233−235] were able to measure IR spectra of a wide range of cluster sizes in direct absorption, using the cavity ringdown laser spectroscopy technique.[236] With the use of theoretical integrated band intensities, these cavity ringdown measurements permitted the first determination of the absolute water cluster concentrations in a supersonic beam.[235] Interestingly, the trimer dominates the cluster distribution for both H_2O and D_2O. This is probably due to the discontinuous increase in the per-monomer binding energy, which jumps from $^1/_2D_0$ to D_0 from dimer to trimer, while increasing much more slowly for larger clusters. While the OH stretching vibrations of gaseous H_2O clusters had been studied previously, mostly with indirect methods, cavity ringdown spectroscopy permitted the first detailed studies of both the covalent bending vibrations of H_2O clusters, which occur near 1600 cm^{-1},[233] and the stretching vibrations of D_2O clusters, which fall near 2700 cm^{-1}.[234] All of the observed clusters except the dimer exhibit strong vibrational predissociation broadening of their O−D stretch spectra that obscures rotation−tunneling features. All bands observed for the cluster HOH bending vibrations are severely broadened, implying a stronger coupling with the dissociation coordinate.[233]

C. Gas-Phase Spectroscopy of Coordinated Water Trimers and Water Trimer Derivatives

There has been much interest in studies of $X{\cdot}W_n$ clusters [which can be regarded as water clusters that are coordinated to other molecules, e.g., benzene·$(H_2O)_3$] and W_nX clusters [which can be regarded as water clusters in which one water is substituted by some other molecule, e.g., $(H_2O)_2$phenole]. These systems extend the study from solvent−solvent to solvent−solute interactions and promise new insight into solvation phenomena. These clusters will not be discussed in detail, as this is beyond the scope of this article, but an overview of such clusters as they pertain to the water trimer will follow. The two most interesting aspects of these systems with respect to the water trimer are those of the above-mentioned solvent−solute interaction and the perturbing effects

on the hydrogen bond rearrangement dynamics, which can result from lowering of the symmetry of the water trimer, similar to those resulting from isotopic substitution. Similarly, it is interesting that, depending on the complex, a particular one of the six torsional {*uud*} structures of the free trimer is more stable, a different torsional structure, e.g., {*ddd*}, or even the open-chain structure, which, in a slightly different conformation, is predicted to be the most stable structure of the pure water trimer only at very high electric fields.[237]

1. X·W$_3$: Coordinated Water Trimers

The Ar·W$_3$ complex was one of the first complexes of this type to be studied in detail, using a pulsed nozzle Fourier transform microwave spectrometer.[238] This study also comprises one of the few high-resolution spectroscopic studies of a X·W$_3$ system, and, from the analysis of the spectrum, the authors determined that the structure of Ar·W$_3$ is that of a prolate-symmetric top with the Ar positioned on the symmetry axis of the water trimer. The Ar suppresses the hydrogen bond network rearrangement dynamics dramatically, but still appears to allow the water trimer to retain the same minimum energy structure. The bifurcation-tunneling splittings are reduced to 40 kHz in Ar·(H$_2$O)$_3$ compared to 200−300 MHz in (H$_2$O)$_3$ and were not observed in Ar·(D$_2$O)$_3$.

Zwier and co-workers have measured the spectra of benzene water clusters up to B·W$_9$ with resonant ion-dip IR spectroscopy.[239−243] The structural evolution of these complexed water clusters, in which a free OH forms a π H-bond with benzene, shows a remarkable similarity to that of the pure water clusters. The B·W$_3$ spectra showed three OH stretch categories:[239] the free OH at 3716 cm^{-1}, the π H-bonded OH at 3657 cm^{-1}, and three single donor OH's at 3550, 3508, and 3423 cm^{-1}. The sixth OH stretch was either unresolved or had negligible intensity. The structure of B·W$_3$ corresponds to a cyclic water trimer, in which one free OH group is π H-bonding to benzene. Fredericks *et* al.[240] showed that benzene stabilizes the *uuD* torsional minimum. The benzene thus lowers the symmetry of the free trimer and effects a localization of the normal modes, and through the π H-bond and geometrical changes shifts the vibrational OH stretch frequencies. The two free O−H bonds pointing away from the benzene are largely unaffected and have frequencies very close to those of the free trimer, whereas the π H-bonded OH is red shifted from the free OH stretch frequency. The most dramatic effect is observed in the bonded ring OH bands. Whereas the free trimer has one ring OH normal mode with nearly zero intensity and another broad ring OH feature, the B·W$_3$ spectrum shows three nearly equally intense bands that are split by 192 cm^{-1}, which the authors argued results mainly from geometrical changes rather than coupling between the localized OH stretch modes.

Barth et al.[244] studied the effect of substitution of benzene hydrogens on the H-bonding of B·W$_n$ ($n \leq 4$) clusters using infrared ion-depletion spectroscopy. The shift of the π H-bonding OH stretch from that of the free water trimer of all studied B·W$_3$ clusters (B = *p*-difluorbenzene, fluorobenzene, benzene, toluene, *p*-xylene, anisole), except for anisole·W$_3$, correlated nearly linearly with the calculated electron density (or charge) of the aromatic ring. The π H-bonding OH stretch of *p*-xylene·W$_3$, which was the complex with the largest π electron density, was 65 cm^{-1} lower in frequency than that of *p*-difluorbenzene·W$_3$. Tarakeshwar et al.[245] calculated the energies of the water trimer complexes with *p*-difluorbenzene, fluorobenzene, benzene, and toluene for different trimer torsional minima. In agreement with Barth et al.'s experimental results[244] and Federicks et al.'s calculations for benzene·W$_3$,[240] the fluorobenzene complexes prefer the *udD* minimum, whereas the *uuD* minimum is most stable for toluene·W$_3$ and benzene·W$_3$. In the fluorobenzene complexes, a σ H-bond to the fluorine is formed by a free OH in addition to the π H-bond to the aromatic ring. This is in agreement with the experimentally observed OH stretch vibrational frequencies. Although the fluorobenzene complexes contain an additional H-bond, the binding energies are close to those of the benzene and toluene complexes, as the sum of σ and π H-bonds is comparable for them. Thus, the main effect of substituted benzenes, like for benzene itself, is energetic stabilization of one of the torsional minima and lowering of the symmetry of the free water trimer, which results in localization of normal modes, as demonstrated by OH stretch vibrational spectra. However, substitution on the benzene ring can stabilize different torsional minima.

Palmer et al.[246] observed two perylene·(H$_2$O)$_3$ conformers in a study of jet-cooled perylene·W$_n$ ($n < 9$) clusters using infrared-optical double-resonance spectroscopy. However, they were unable to investigate one of the conformers due to its low signal-to-noise ratio. In contrast to benzene·(H$_2$O)$_3$, the other perylene·(H$_2$O)$_3$ conformer showed at least three closely spaced vibrational bands between the free OH and the π H-bonded OH of benzene·(H$_2$O)$_3$. Similarly, this perylene·(H$_2$O)$_3$ conformer showed only two closely spaced vibrational bands in the bonded ring OH region. The authors argued that this was indicative of a water trimer with three weak π H-bonded OH's, unlike benzene·(H$_2$O)$_3$, with its two free OH's and one π H-bonded OH. This would result in a structure with a trimer that retains much of its symmetry, which explains the observation of only two bonded OH bands, except for the free OHs, which are all significantly perturbed but remain nearly equivalent.

Maxton et al.[247] studied intermolecular vibrations of benzene·W$_n$ using mass-selective, ionization-loss stimulated Raman spectroscopy. They measured bands in the 35−65 cm^{-1} region for all water clusters and an additional feature below 10 cm^{-1} for the n = 1 and 3 species. On the basis of isotopic substitution experiments, they attributed the majority of the former bands to vibrations corresponding to motions of the W$_n$ species with respect to benzene. However, high-resolution spectroscopic experiments would greatly aid in analysis and assignment of the origin of these bands.

Gruenloh et al.[248] studied ternary benzene·(methanol)$_m$W$_n$ clusters to study preferential solvation. These clusters contain substituted (with methanol) water clusters π H-bonding to the benzene. For B·MW$_2$ and B·W$_3$ the cyclic structure of the free water trimer was observed. Two conformers for B·MW$_2$ were observed, in both of which water is π H-bonding and which differ in the position of the methanol within the ring. For the methanol-rich members B·M$_2$W and B·M$_3$, the authors were able to determine that a chain structure dominated, and comparison with the CH stretch spectrum of B·M$_3$ showed that in B·M$_2$W the water acts as the OH donor at the other end of the chain starting with the π H-bonding methanol.

Carney and Zwier[249] observed two isomers for 1-methylindole·W$_3$ using a combination of resonant two-photon ionization, resonant ion-dip infrared spectroscopy, and infrared−ultraviolet hole-burning spectroscopy. The authors showed that coordination of the water trimer to 1-methylindole effectively quenches the torsional flipping and freezes out the chiral (in the complex diastereomeric) clockwise and anticlockwise *uDD* structures. Although such a suppression of the torsional flipping in, e.g., benzene·W$_3$ certainly seems likely, no confirmation of the existence of two energetically different isomers has been reported. Analysis of the 1-methylindole·W$_3$ OH stretch spectra and comparison with DFT calculations further revealed that the π H-bond to the pyrrole ring is stronger than that to the phenyl ring.

From an analysis of the OH stretch frequencies of X$^-$·(H$_2$O)$_3$ (X = Cl, Br, I), obtained using predissociation spectroscopy and comparison with ab initio results, Ayotte et al.[270] determined that these clusters adopt a similar structure to Ar·(H$_2$O)$_3$. However the binding energy to the ion is much stronger and does not only suppress the hydrogen bond dynamics of the free trimer but forces it into the crown *uuu* structure, with all free hydrogens forming H-bonds with the ion.

2. W$_2$X: Chemically Substituted Water Trimers

A number of W$_2$X clusters in which X corresponds to an aromatic alcohol, such as phenol,[250−252] *p*-cyanophenol,[250] 1-naphthol,[250,253,254] and 2-naphthol,[250,255] have been investigated. These clusters all share a similar basic structural principle in that they consist of a water trimer in which one hydrogen is substituted by the aromatic ring. The energetically most stable torsional isomer of W$_2$·phenol was calculated to be the *Dud* conformer, 156 cm^{-1} more stable than the *Ddu* conformer, and 192 cm^{-1} more stable than the *Duu* conformer.[250] This structural scheme has been generally verified by the experimental studies. From resonant two-photon ionization spectroscopic results, Leutwyler suggested that either there are two isomers for phenol·W$_2$, whose electronic origins are spaced by only 3 cm^{-1}, or there exist two vibrations with frequencies of ca. 3 and 6.5 cm^{-1}. Watanabe et al.[252] confirmed the cyclic structure of phenol·W$_2$ using IR−UV double-resonance spectroscopy, and Roth et al.[251] subsequently measured and assigned the intermolecular vibrations of the excited electronic state and found the lowest six intermolecular vibration to lie between ca. 37 and 186 cm^{-1}. The authors also argued that their hole-burning experiments ruled out the existence of two different conformers.

Connell et al.[253] suggested that the structure of 1-naphthol·W$_2$ corresponded to either a *Dud* or *Duu* on the basis of results from rotational coherence spectroscopy and ab initio calculations. Yoshino et al.[254] measured the OH stretch spectrum of 1-naphthol·W$_2$ using IR dip spectroscopy and confirmed the cyclic *Dud* structure by comparing the experimental results with ab initio molecular orbital calculations. In contrast to 1-naphthol·W$_2$, Leutwyler et al.[250] reported observation of three conformers of the 2-naphthol·W$_2$ cluster. They assigned them to cyclic *cis*-2-naphthol·W$_2$, *trans*-2-naphthol·W$_2$, and an open water chain cluster. The latter was not observed for deuterated 2-naphthol·W$_2$. Matsumoto et al.[255] measured the OH stretching vibrations of 2-naphthol·W$_2$ by infrared−ultraviolet double-resonance spectroscopy and determined the spectra of *cis*-2-naphthol·W$_2$ and *trans*-2-naphthol·W$_2$.

Kisiel et al.[256] observed the (H$_2$O)$_2$HCl cluster using Fourier transform microwave spectroscopy and determined a cyclic structure in which one of the water molecules of the water trimer is substituted by HCl. The rotational spectrum is that of an asymmetric near-prolate rotor, and the authors determined detailed molecular properties, such as dipole moments and bond lengths. The cluster has a lower symmetry, G_8, than the water trimer, and both torsional and bifurcation tunneling are important. In this cluster, only a double flip, E^*, will result in tunneling between degenerate torsional minima, splitting each level into a doublet, A$^+$/A$^-$. Struniewicz et al.[257] calculated the ground-state splitting, taking the flipping and overall rotation into account, to be 19.33 cm^{-1}, whereas Wormer et al.[258] calculated a value of 8.94 cm^{-1} (and 1.39 cm^{-1} for the fully deuterated isotopomer). Interestingly, the Coriolis interaction appears to be very small compared to that of the trimer.[258] The water−water interoxygen distance was determined to be $r_{(OH\cdots O)}$ = 2.8151(8) Å and $r_{(OH\cdots Cl)}$ = 3.0840(11) Å, considerably shorter than in the corresponding dimers. The distance of the third bond, $r_{(ClH\cdots O)}$ = 3.4152(13) Å, is close the sum of the van der Waals radii, and the authors stated that this bond should be addressed as a van der Waals bond rather than a H-bond. This is in accordance with the fact that the calculated ab initio (aug-cc-pVDZ/MP2) binding energy is about 2 kcal/mol lower than that of (H$_2$O)$_3$, whereas the pair interactions are very similar.[259] The lower symmetry and simplified molecular dynamics allow this very high level of detail — compared with the free water trimer — to be extracted.

3. Water Trimer Chains

Some weakly bound clusters do not adopt structures resembling those of the free water clusters and will only be mentioned very briefly. In the 2-pyridone·W and 2-hydroxypyridine·W clusters, the water molecule is part of a cyclic H-bonded ring reminiscent of a severely distorted water trimer.[260] Interestingly, for 2-hydroxypyridine·W, splitting of the free OH

stretch was tentatively assigned to result from the torsional flipping motion. The structures of 7-hydroxyquinoline·W_n clusters do not resemble those of the free water clusters but rather form linear chains[261] as a result of the nitrogen in the second aromatic ring, and similar water chains have been observed in tryptamine·W_n clusters.[262] Zwier has pointed out that in the latter case the clusters' solvent effects are quite important as the tryptamine adopts a conformation which requires substantial reconfiguration away from its free minimum energy conformation.[262] In tryptamine·W_3, three H-bonds are formed with tryptamine. The water molecule at one end of the water chain forms a H-bond with the indole nitrogen, and the water molecule at the other end of the chain forms a H-bond with the amine nitrogen and a π H-bond with the indole ring. Sakai et al.[271] measured the OH stretch spectra of carbazole·W_2 using IR dip spectroscopy and found a structure reminiscent of a distorted cyclic structure, in which the H-bonded ring is perpendicular to the plane of the carbazole and involves a π H-bond to either the nitrogen atom or a neighboring carbon atom. This structure can also be viewed as a coordinated open-chain water cluster similar to the indole·W_2 cluster.[249]

IV. Conclusions

It is clear from this review that the study of water clusters is currently an area of much activity. Recently, a complete (12-dimensional) dynamical model of the dimer has been developed that includes flexibility of the monomers, and this is being used to extract a rigorous model for the potential surface through fitting of the dimer VRT spectra.[263] Interestingly, the spectroscopic data set is actually more complete for the trimer than for the dimer, as the librational motions in the trimer have been at least partially characterized.[192] Hence, one of the most important future directions will be to develop a similarly detailed theoretical description of the trimer VRT dynamics, explicitly including all nine Euler angles and the three center of mass lengths, and perhaps even the nine monomer coordinates required to incorporate flexibility. This would then permit the explicit determination of the three-body exchange interactions via direct fitting of the trimer VRT spectra and comparison to the pairwise IPS constructed from the dimer potential.

From an experimental perspective, the most important task remaining in the characterization of the trimer is the further study of the librational and translational vibrations. This requires further developments of the requisite laser technology in the terahertz and FIR regions. We hope that this review will motivate both the theoretical and experimental efforts required for a truly complete understanding of the water trimer — this important prototype of aqueous hydrogen bonding.

V. Abbreviations

r_{OH}^{f}	free O−H bond length
r_{OH}^{b}	H-bonding O−H bond length
BLYP	Becke-Lee−Yang−Parr (density functional)
BSSE	basis set superposition error
CC	coupled cluster (CCSD(T): coupled cluster, single, double, and triple excitations)
CI	configuration interaction
CP	counterpoise (BSSE correction)
DFT	density functional theory
DQMC	diffusion quantum Monte Carlo
FIR−VRT	terahertz vibration−rotation-tunneling
HBNR	H-bond network rearrangement
HF	Hartree−Fock
IMPPT	intermolecular Møller−Plesset perturbation theory
IPS	intermolecular potential energy surface
LJ	Lennard-Jones
MPn	nth-order Møller−Plesset perturbation theory
PI	permutation-inversion
R_{OO}	interoxygen separation
SCF	self-consistent field
ZPE	zero-point energy

VI. Acknowledgments

This work was supported by the Experimental Physical Chemistry Program of the National Science Foundation.

VII. Appendix: Summary of Tables

Table 1. Calculated Water Trimer Average Bond Lengths, Angles, and Energies. Results from several ab initio calculations and calculations with empirical potentials of averaged bond lengths (Å), averaged bond angles (degrees), and energies (kcal/mol) of the equilibrium water trimer are given. The structural parameters are defined in Figure 1. Slightly different results for calculations at the same level of theory and basis set result from small differences in the computational details, e.g., with which basis set the geometry was optimized.

Table 2. Energies of Important Stationary Points on the Trimer IPS. The energies (kcal/mol) of important stationary points on the trimer IPS, calculated with ab initio methods and empirical potentials, are shown relative to the equilibrium structure. Slightly different results for calculations using the same potential or the some level of theory and basis set result from small differences in the computational details, e.g., geometry optimization.

Table 3. Symmetry Labels and Nuclear Spin Weights for the G_6 and G_{48} PI Groups of the Water Trimer. A summary of important group theoretical results for the homoisotopic water trimers $(H_2O)_3$ and $(D_2O)_3$ is shown. The nuclear spin statistical weights of the states labeled by their respective irreps are shown. The point group of the rigid, equilibrium water trimer is C_1; that structure is therefore chiral. The PI group G_6 describes a trimer vibrationally averaged over the H-bond torsional coordinates into a symmetric rotor. Inclusion of the PI operations that allow bifurcation tunneling gives the group G_{48}. The correlation between the irreps of C_1, G_6, and G_{48} is shown. Similar tables for mixed trimers can be found in ref 179.

Table 4. Comparison of Calculated and Experimental Torsional Energy Levels. A comparison of experimental and calculated torsional energy levels is shown. The agreement between the SAPT-

5st calculated and experimental values for the first torsional manifold is excellent. For the second torsional manifold, calculations using the BGLK potential and including Coriolis interactions yield the best results.

Table 5. Bifurcation-Tunneling Pathways in the Water Trimer. The details of the six different bifurcation-tunneling pathways are shown together with the generators and the levels of theory at which they were found. The nomenclature follows Wales and co-workers,[104,157] with the minority monomer being the water molecule that has the free hydrogen on one side of the oxygen plane and majority monomers having the free hydrogens on the other side.

Table 6. Calculated and Experimental Water Trimer Intramolecular Frequencies. A comparison of intramolecular vibrational frequency shifts (cm^{-1}) of the water trimer calculated by a variety of theoretical methods with respect to the monomer values at the same level of theory is shown. If no monomer values (HF/HCAO, VSCF, and RWK-2) were available, the absolute frequencies are given. Also shown are the experimentally determined frequencies from matrix and gas-phase studies. The band at 3385 cm^{-1} reported by van Thiel et al., which is included in the table, does not arise from the trimer.

Table 7. Comparison of Calculated Intermolecular Frequencies. The intermolecular vibrational frequencies (cm^{-1}) calculated by a variety of theoretical methods are shown.

Table 8. Summary of the Water Trimer Intermolecular Vibrational Bands. All observed $(D_2O)_3$ and $(H_2O)_3$ vibrational transitions are shown with the torsional k assignment, vibrational band origin, ν (cm^{-1}), and the approximate intensity pattern of the anomalous bifurcation splittings. The regular quartets are equally spaced, and the splittings listed are for the order A_g, T_u, T_g, A_u; thus, a negative value indicates that the A_g is the highest-frequency component of the quartet. The K values for which "anomalous" bifurcation splittings are observed are shown, and J-dependent splittings proportional to $J(J+1)$ are indicated.

Table 9. Molecular Constants of the Intermolecular Vibrational Levels of $(D_2O)_3$. The results of a global fit of all torsional bands (659 rovibrational transitions) are shown together with an independent fit of the 142.8 cm^{-1} translational band. All values are in MHz, except for ζ, which is dimensionless. Only ΔC has been determined, as it is not possible to fit C' and C'' without correlation. $\Delta\Delta = \Delta B - 2\Delta C$ is related to the difference in inertial defect, Δ ($\Delta = I_c - I_a - I_b$), between the excited state and ground state. Like the inertial defect, it is a measure of the planarity of a molecule, with a planar molecule having $B - 2C = 0$, and $\Delta = 0$, and a negative sign indicates nonplanarity. ζ is the linear Coriolis term and $|\mu_{++}|$ the second-order term developed by Viant and Geleijns.[191] The excited state of the 142.8 cm^{-1} band is the first $(D_2O)_3$ vibrational level with a negative ΔC and has the smallest increase of the inertial defect for any band.

Table 10. Molecular Constants of the Intermolecular Vibrational Levels of $(H_2O)_3$. The results of a global fit of all torsional $(H_2O)_3$ bands and independent fits of the 500 cm^{-1} librational bands are shown. For the fits of the librational band, the values of the ground-state constants were fixed to the values determined by Brown et al.;[220] D_K' was fixed as it could not be fit without correlation. All values are in MHz, and all parameters are defined as in Table 9. γ is a constant introduced to take account of the $K = 1$ splittings in the 523.9 cm^{-1} band. The dramatic decrease of the rotational constants is remarkable and is indicative of significant structural rearrangement or a strong perturbation

Table 11. Molecular Constants of the Intermolecular Vibrational Levels of Mixed-Isotope Trimer Bands. The results of the fits of independent isotopically substituted torsional trimer bands are shown. All values are in MHz. All trimers except for the d_3a trimer correspond to asymmetric rotors and have $A \neq B \neq C$. In the d_na trimers, deuterons occupy all non-H-bonding positions and some of the hydrogen-bonded ones. In the d_3b and d_4b trimers, two and three of the deuterons participate in H-bonding, respectively, and in the d_5b trimer the sole hydrogen is in a non-H-bonding position. The h_5 trimer band has not been fit. The vibrational assignments can be given in analogy to the homoisotopic trimers (disregarding splitting of the degenerate torsional $k = \pm 2^n$ and $\pm 1^n$ states resulting from most isotopic substitutions). The d_na trimer vibrations correspond to a $k = 3^0 \leftarrow 0^0$ vibration, the d_3b and d_4b vibrations to a $k = 2^1 \leftarrow 1^1$, and the d_5b vibration to a $k = 2^1 \leftarrow 1^0$ vibration.

Table 12. Torsional and Bifurcation-Tunneling Levels for $K = 0$ and $K = 1$. The torsional and bifurcation-tunneling levels for $K = 0$ and $K = 1$ are shown together with the A and B pattern contributions from bifurcation tunneling. β_A and β_B refer to the bifurcation matrix elements for the A and B patterns, respectively. For $K = 0$ there are no Coriolis effects, but for $K > 0$, $k - K$ labels cannot be rigorously assigned for T-states if Coriolis effects are included. The $K = 1$ T-states of $k = 0$ and 3 are split via Coriolis coupling with the $K = 0$ T-states of $k = \pm 1$, as well as the $k - K = 3$ states of $k = \pm 2$. However, the T-states of $k - K = \pm 2$, $k = \pm 1$ and $k - K = \pm 1$, $k = \pm 2$ would not be split by Coriolis coupling as they are not degenerate. Therefore, anomalous quartets can be observed only for transitions involving $K = 0$ and the $k = \pm 1$, $k = \pm 2$ torsional levels. The notation $2A_1^+$ indicates that two levels of A_1^+ symmetry exist, which would be split by Coriolis interactions.

Table 13. Bifurcation-Tunneling Matrix Elements of the Water Trimer. The fitted bifurcation-tunneling matrix elements of $(D_2O)_3$ and $(H_2O)_3$ from ref 192 are shown.

VIII. References

(1) Ojamae, L.; Hermansson, K. *J. Phys. Chem.* **1994**, *98*, 4271.
(2) Keutsch, F. N.; Saykally, R. J. *Proc. Natl. Acad. Sci. U.S.A.* **2001**, *98*, 10533.
(3) Frank, H. S.; Wen, W. Y. *Discuss. Faraday Soc.* **1957**, *24*, 133.

(4) Popkie, H.; Kistenmacher, H.; Clementi, E. *J. Chem. Phys.* **1973**, *59*, 1325.
(5) Lie, G. C.; Clementi, E.; Yoshimine, M. *J. Chem. Phys.* **1976**, *64*, 2314.
(6) Clementi, E.; Kolos, W.; Lie, G. C.; Ranghino, G. *Int. J. Quantum Chem.* **1980**, *17*, 377.
(7) Habitz, P.; Bagus, P.; Siegbahn, P.; Clementi, E. *Int. J. Quantum Chem.* **1983**, *23*, 1803.
(8) Detrich, J.; Corongiu, G.; Clementi, E. *Chem. Phys. Lett.* **1984**, *112*, 426.
(9) Wojcik, M.; Clementi, E. *J. Chem. Phys.* **1986**, *84*, 5970.
(10) Niesar, U.; Corongiu, G.; Clementi, E.; Kneller, G. R.; Bhattacharya, D. K. *J. Phys. Chem.* **1990**, *94*, 7949.
(11) Corongiu, G.; Clementi, E. *J. Chem. Phys.* **1992**, *97*, 2030.
(12) Corongiu, G.; Clementi, E. *J. Chem. Phys.* **1993**, *98*, 2241.
(13) Barnes, P.; Finney, J. L.; Nicholas, J. D.; Quinn, J. E. *Nature* **1979**, *282*, 459.
(14) Caldwell, J.; Dang, L. X.; Kollman, P. A. *J. Am. Chem. Soc.* **1990**, *112*, 9144.
(15) Gil-Adalid, L.; Ortega-Blake, I. *J. Chem. Phys.* **1991**, *94*, 3748.
(16) Gregory, J. K.; Clary, D. C. *J. Phys. Chem.* **1996**, *100*, 18014.
(17) Xantheas, S. S. *J. Chem. Phys.* **1994**, *100*, 7523.
(18) Wormer, P. E. S.; van der Avoird, A. *Chem. Rev.* **2000**, *100*, 4109.
(19) Cohen, R. C. Ph.D. Thesis, University of California, Berkeley, 1991.
(20) Cohen, R. C.; Saykally, R. J. *J. Phys. Chem.* **1992**, *96*, 1024.
(21) Elrod, M. J.; Saykally, R. J. *J. Chem. Phys.* **1995**, *103*, 933.
(22) Schmuttenmaer, C. A.; Cohen, R. C.; Saykally, R. J. *J. Chem. Phys.* **1994**, *101*, 146.
(23) Saykally, R. J.; Blake, G. A. *Science* **1993**, *259*, 1570.
(24) Liu, K.; Cruzan, J. D.; Saykally, R. J. *Science* **1996**, *271*, 929.
(25) Xantheas, S. S. *J. Chem. Phys.* **1995**, *102*, 4505.
(26) Xantheas, S. S.; Dunning, T. H., Jr. *J. Chem. Phys.* **1993**, *99*, 8774.
(27) Pugliano, N.; Saykally, R. J. *Science* **1992**, *257*, 1937.
(28) van der Avoird, A.; Olthof, E. H. T.; Wormer, P. E. S. *J. Chem. Phys.* **1996**, *105*, 8034.
(29) Olthof, E. H. T.; van der Avoird, A.; Wormer, P. E. S.; Liu, K.; Saykally, R. J. *J. Chem. Phys.* **1996**, *105*, 8051.
(30) Perram, J. W.; Levine, S. *Mol. Phys.* **1971**, *21*, 701.
(31) Stillinger, F. H. *J. Phys. Chem.* **1970**, *74*, 3677.
(32) Stillinger, F. H. *J. Chem. Phys.* **1972**, *57*, 1780.
(33) Rahman, A.; Stillinger, F. *J. Am. Chem. Soc.* **1973**, *95*, 7943.
(34) Nemethy, G.; Scheraga, H. A. *J. Phys. Chem.* **1962**, *66*, 1773.
(35) Hagler, A. T.; Scheraga, H. A.; Nemethy, G. *J. Phys. Chem.* **1972**, *76*, 3229.
(36) Lentz, B. R.; Hagler, A. T.; Scheraga, H. A. *J. Phys. Chem.* **1974**, *78*, 1531.
(37) Owicki, J. C.; Lentz, B. R.; Hagler, A. T.; Scheraga, H. A. *J. Phys. Chem.* **1975**, *79*, 2352.
(38) Owicki, J. C.; Scheraga, H. A. *J. Am. Chem. Soc.* **1977**, *99*, 7403.
(39) Owicki, J. C.; Scheraga, H. A. *J. Am. Chem. Soc.* **1977**, *99*, 7413.
(40) Sasai, M.; Ohmine, I.; Ramaswamy, R. *J. Chem. Phys.* **1992**, *96*, 3045.
(41) Ohmine, I.; Tanaka, H. *Chem. Rev.* **1993**, *93*, 2545.
(42) Saito, S.; Ohmine, I. *J. Chem. Phys.* **1995**, *102*, 3566.
(43) Saito, S.; Ohmine, I. *J. Chem. Phys.* **1994**, *101*, 6063.
(44) Ohmine, I. *J. Phys. Chem.* **1995**, *99*, 6767.
(45) Wales, D. J.; Ohmine, I. *J. Chem. Phys.* **1993**, *98*, 7257.
(46) Wales, D. J.; Ohmine, I. *J. Chem. Phys.* **1993**, *98*, 7245.
(47) Sceats, M. G.; Stavola, M.; Rice, S. A. *J. Chem. Phys.* **1979**, *70*, 3927.
(48) Sceats, M. G.; Rice, S. A. *J. Chem. Phys.* **1979**, *71*, 973.
(49) Sceats, M. G.; Rice, S. A. *J. Chem. Phys.* **1980**, *72*, 6183.
(50) Sceats, M. G.; Rice, S. A. *J. Chem. Phys.* **1980**, *72*, 3236.
(51) Sceats, M. G.; Rice, S. A. *J. Chem. Phys.* **1980**, *72*, 3248.
(52) Sceats, M. G.; Rice, S. A. *J. Chem. Phys.* **1980**, *72*, 3260.
(53) Speedy, R. J. *J. Phys. Chem.* **1984**, *88*, 3364.
(54) Speedy, R. J.; Mezei, M. *J. Phys. Chem.* **1985**, *89*, 171.
(55) Jorgensen, W. L.; Chandrasekhar, J.; Madura, J. D.; Impey, R. W.; Klein, M. L. *J. Chem. Phys.* **1983**, *79*, 926.
(56) Jorgensen, W. L. *J. Chem. Phys.* **1982**, *77*, 4156.
(57) Jorgensen, W. L. *J. Am. Chem. Soc.* **1981**, *103*, 335.
(58) Berendsen, H. J. C.; Grigera, J. R.; Straatsma, T. P. *J. Phys. Chem.* **1987**, *91*, 6269.
(59) Mahoney, M. L.; Jorgensen, W. L. *J. Chem. Phys.* **2000**, *112*, 8910.
(60) Schütz, M.; Rauhut, G.; Werner, H.-J. *J. Phys. Chem. A* **1998**, *102*, 5997.
(61) Schütz, M.; Bürgi, T.; Leutwyler, S.; Bürgi, H. B. *J. Chem. Phys.* **1993**, *99*, 5228.
(62) Car, R.; Parrinello, M. *Phys. Rev. Lett.* **1985**, *55*, 2471.
(63) Wesolowski, T. A.; Tran, F. *J. Chem. Phys.* **2003**, *118*, 2072.
(64) Tsuzuki, S.; Lüthi, H. P. *J. Chem. Phys.* **2001**, *114*, 3949.
(65) Berendsen, H. J. C.; Postma, J. P. M.; Gunsteren, W. F. v.; Hermans, J. *Intermolecular Forces*; Reidel Publishing Co.: Dordrecht, 1981.
(66) Berweger, C. D.; Gunsteren, W. F. v.; Muller-Plathe, F. *Chem. Phys. Lett.* **1995**, *232*, 429.
(67) Ferguson, D. *J. Comput. Chem.* **1995**, *16*, 501.
(68) Torres, F. M.; Agichtein, E.; Grinberg, L.; Yu, G.; Topper, R. Q. *J. Mol. Struct.: THEOCHEM* **1997**, *419*, 85.
(69) Owicki, J. C.; Shipman, L. L.; Scheraga, H. A. *J. Phys. Chem.* **1975**, *79*, 1794.
(70) Schröder, K. P. *Chem. Phys.* **1988**, *123*, 91.
(71) Cruzan, J. D.; Brown, M. G.; Liu, K.; Braly, L. B.; Saykally, R. J. *J. Chem. Phys.* **1996**, *105*, 6634.
(72) Cruzan, J. D.; Braly, L. B.; Liu, K.; Brown, M. G.; Loeser, J. G.; Saykally, R. J. *Science* **1996**, *271*, 59.
(73) Liu, K.; Brown, M. G.; Cruzan, J. D.; Saykally, R. J. *Science* **1996**, *271*, 62.
(74) Schütz, M.; Klopper, W.; Luthi, H. P.; Leutwyler, S. *J. Chem. Phys.* **1995**, *103*, 6114.
(75) van Duijneveldt-van de Rijdt, J. G. C. M.; van Duijneveldt, F. B. *Chem. Phys. Lett.* **1995**, *237*, 560.
(76) Matsuoka, O.; Clementi, E.; Yoshimine, M. *J. Chem. Phys.* **1976**, *64*, 1351.
(77) Wawak, R. J.; Wimmer, M. M.; Scheraga, H. A. *J. Phys. Chem.* **1992**, *96*, 5138.
(78) Bürgi, T.; Graf, S.; Leutwyler, S.; Klopper, W. *J. Chem. Phys.* **1995**, *103*, 1077.
(79) Watts, R. O. *Chem. Phys.* **1977**, *26*, 367.
(80) Reimers, J. R.; Watts, R. O.; Klein, M. L. *Chem. Phys.* **1982**, *64*, 95.
(81) Douketis, C.; Scoles, G.; Marchetti, S.; Zen, M.; Thakkar, A. J. *Chem. Phys.* **1982**, *76*, 3057.
(82) Cieplak, P.; Kollman, P.; Lybrand, T. *J. Chem. Phys.* **1990**, *92*, 6755.
(83) Guiang, C. S.; Wyatt, R. E. *Int. J. Quantum Chem.* **1998**, *68*, 233.
(84) Whalley, E. *Chem. Phys. Lett.* **1978**, *53*, 449.
(85) Stone, A. J. *Chem. Phys. Lett.* **1989**, *155*, 102.
(86) Del Bene, J.; Pople, J. A. *J. Chem. Phys.* **1970**, *52*, 4858.
(87) Dykstra, C. E. *J. Chem. Phys.* **1989**, *91*, 6472.
(88) Belford, D.; Campbell, E. S. *J. Chem. Phys.* **1987**, *86*, 7013.
(89) Campbell, E. S.; Mezei, M. *J. Chem. Phys.* **1977**, *67*, 2338.
(90) Wallqvist, A.; Ahlstrom, P.; Karlstrom, G. *J. Phys. Chem.* **1990**, *94*, 1649.
(91) Wallqvist, A.; Karlstrom, G. *Chem. Scr. A* **1989**, *29*, 131.
(92) Dang, L. X.; Chang, T. M. *J. Chem. Phys.* **1997**, *106*, 8149.
(93) Gregory, J. K.; Glary, D. C.; Liu, K.; Brown, M. G.; Saykally, R. J. *Science* **1997**, *275*, 814.
(94) Masella, M.; Flament, J. P. *J. Chem. Phys.* **1997**, *107*, 9105.
(95) Mó, O.; Yanez, M.; Elguero, J. *J. Chem. Phys.* **1992**, *97*, 6628.
(96) Hayes, I. C.; Stone, A. J. *Mol. Phys.* **1984**, *53*, 69.
(97) Stone, A. J.; Alderton, M. *Mol. Phys.* **1985**, *56*, 1047.
(98) Stone, A. J. *Chem. Phys. Lett.* **1981**, *83*, 233.
(99) Rijks, W.; Wormer, P. E. S. *J. Chem. Phys.* **1988**, *88*, 5704.
(100) Tang, K. T.; Toennies, J. P. *J. Chem. Phys.* **1984**, *80*, 3726.
(101) Szczesniak, M. M.; Scheiner, S. *J. Chem. Phys.* **1986**, *84*, 6328.
(102) Stone, A. J. *Mol. Phys.* **1985**, *56*, 1065.
(103) Axilrod, B. M.; Teller, E. *J. Chem. Phys.* **1943**, *11*, 299.
(104) Walsh, T. R.; Wales, D. J. *J. Chem. Soc., Faraday Trans.* **1996**, *92*, 2505.
(105) Hodges, M. P.; Stone, A. J.; Xantheas, S. S. *J. Phys. Chem. A* **1997**, *101*, 9163.
(106) Xantheas, S. S. *Chem. Phys.* **2000**, *258*, 225.
(107) Millot, C.; Soetens, J.-C.; Martins Costa, M. T. C.; Hodges, M. P.; Stone, A. J. *J. Phys. Chem.* **1998**, *102*, 754.
(108) Fellers, R. S.; Braly, L. B.; Saykally, R. J.; Leforestier, C. *J. Chem. Phys.* **1999**, *110*, 6306.
(109) Leforestier, C.; Braly, L. B.; Liu, K.; Elrod, M. J.; Saykally, R. J. *J. Chem. Phys.* **1997**, *106*, 8527.
(110) Groenenboom, G. C.; Mas, E. M.; Bukowski, R.; Szalewicz, K.; Wormer, P. E. S.; van der Avoird, A. *Phys. Rev. Lett.* **2000**, *84*, 4072.
(111) Lotrich, V. F.; Szalewicz, K. *J. Chem. Phys.* **1997**, *106*, 9668.
(112) Sabo, D.; Bacic, Z.; Graf, S.; Leutwyler, S. *J. Chem. Phys.* **1999**, *111*, 5331.
(113) Sabo, D.; Bacic, Z.; Graf, S.; Leutwyler, S. *J. Chem. Phys.* **1999**, *110*, 5745.
(114) Sabo, D.; Bacic, Z.; Graf, S.; Leutwyler, S. *J. Chem. Phys.* **1999**, *111*, 10727.
(115) Thole, B. T. *Chem. Phys.* **1981**, *59*, 341.
(116) Burnham, C. J.; Li, J. C.; Xantheas, S. S.; Leslie, M. *J. Chem. Phys.* **1999**, *110*, 4566.
(117) Burnham, C. J.; Xantheas, S. S. *J. Chem. Phys.* **2002**, *116*, 1500.
(118) Mas, E. M.; Bukowski, R.; Szalewicz, K.; Groenenboom, G. C.; Wormer, P. E. S.; van der Avoird, A. *J. Chem. Phys.* **2000**, *113*, 6687.
(119) Burnham, C. J.; Xantheas, S. S. *J. Chem. Phys.* **2002**, *116*, 5115.
(120) Long, X. P.; Nicholas, J. B.; Guest, M. F.; Ornstein, R. L. *J. Mol. Struct.* **1997**, *412*, 121.
(121) Merrill, G. N.; Gordon, M. S. *J. Phys. Chem. A* **1998**, *102*, 2650.
(122) Kitaura, K.; Sawai, T.; Asada, T.; Nakano, T.; Uebayasi, M. *Chem. Phys. Lett.* **1999**, *312*, 319.
(123) Grigorenko, B. L.; Nemukhin, A. V.; Topol, I. A.; Burt, S. K. *J. Chem. Phys.* **2000**, *113*, 2638.

(124) Aida, M.; Yamataka, H.; Dupuis, M. *Int. J. Quantum Chem.* **2000**, *77*, 199.
(125) Dang, L. X. *J. Chem. Phys.* **1992**, *97*, 2659.
(126) Scheiner, S. *Annu. Rev. Phys. Chem.* **1994**, *45*, 23.
(127) Gregory, J. K.; Clary, D. C. *Chem. Phys. Lett.* **1994**, *228*, 547.
(128) Gregory, J. K.; Wales, D. J.; Clary, D. C. *J. Chem. Phys.* **1994**, *102*, 1592.
(129) Gregory, J. K.; Clary, D. C. *J. Chem. Phys.* **1995**, *103*, 8924.
(130) Hehre, W. J.; Stewart, R. F.; Pople, J. A. *J. Chem. Phys.* **1969**, *51*, 2657.
(131) Del Bene, J.; Pople, J. A. *Chem. Phys. Lett.* **1969**, *4*, 426.
(132) van Duijneveldt, F. B.; van Duijneveldt-van de Rijdt, J. G. C. M.; van Lenthe, J. H. *Chem. Rev.* **1994**, *94*, 1873.
(133) Del Bene, J. E.; Pople, J. A. *J. Chem. Phys.* **1973**, *58*, 3605.
(134) Ditchfield, R.; Hehre, W. J.; Pople, J. A. *Chem. Phys.* **1970**, *52*, 5001.
(135) Hankins, D.; Moskowitz, J. W.; Stillinger, F. H. *Chem. Phys. Lett.* **1970**, *4*, 527.
(136) Hankins, D.; Moskowitz, J. W.; Stillinger, F. H. *J. Chem. Phys.* **1970**, *53*, 4544.
(137) Lobban, C.; Finney, J. L.; Kuhs, W. F. *Nature* **1998**, *391*, 268.
(138) Lentz, B. R.; Scheraga, H. A. *J. Chem. Phys.* **1973**, *58*, 5296.
(139) Kistenmacher, H.; Lie, G. C.; Popkie, H.; Clementi, E. *J. Chem. Phys.* **1974**, *61*, 546.
(140) Mhin, B. J.; Kim, J. S.; Lee, S.; Lee, J. Y.; Kim, K. S. *J. Chem. Phys.* **1994**, *100*, 4484.
(141) Elrod, M. J.; Saykally, R. J. *Chem. Rev.* **1994**, *94*, 1975.
(142) Honegger, E.; Leutwyler, S. *J. Chem. Phys.* **1988**, *88*, 2582.
(143) Laasonen, K.; Parrinello, M.; Car, R.; Lee, C. Y.; Vanderbilt, D. *Chem. Phys. Lett.* **1993**, *207*, 208.
(144) Lee, C. T.; Chen, H.; Fitzgerald, G. *J. Chem. Phys.* **1995**, *102*, 1266.
(145) Lee, C. T.; Yang, W. T.; Parr, R. G. *Phys. Rev. B* **1988**, *37*, 785.
(146) Belch, A. C.; Rice, S. A. *J. Chem. Phys.* **1987**, *86*, 5676.
(147) Benson, S. W.; Siebert, E. D. *J. Am. Chem. Soc.* **1992**, *114*, 4269.
(148) Perdew, J. P. *Phys. Rev. B* **1986**, *33*, 8822.
(149) Estrin, D. A.; Paglieri, L.; Corungiu, G.; Clementi, E. *J. Phys. Chem.* **1996**, *100*, 8701.
(150) Chalasinski, G.; Szczesniak, M. M.; Cieplak, P.; Scheiner, S. *J. Chem. Phys.* **1991**, *94*, 2873.
(151) Szczesniak, M. M.; Chalasinski, G. *J. Mol. Struct.: THEOCHEM* **1992**, *93*, 37.
(152) Chalasinski, G.; Szczesniak, M. M. *Chem. Rev.* **1994**, *94*, 1723.
(153) Xantheas, S. S.; Dunning, T. H. *J. Chem. Phys.* **1993**, *98*, 8037.
(154) Pastor, N.; Ortega-Blake, I. *J. Chem. Phys.* **1993**, *99*, 7899.
(155) Fowler, J. E.; Schaefer, H. F. *J. Am. Chem. Soc.* **1995**, *117*, 446.
(156) Wales, D. J. *J. Am. Chem. Soc.* **1993**, *115*, 11191.
(157) Wales, D. J. *J. Am. Chem. Soc.* **1993**, *115*, 11180.
(158) Klopper, W.; Schütz, M.; Lüthi, H. P.; Leutwyler, S. *J. Chem. Phys.* **1995**, *103*, 1085.
(159) Wales, D. J.; Walsh, T. R. *J. Chem. Phys.* **1996**, *105*, 6957.
(160) Taketsugu, T.; Wales, D. J. *Mol. Phys.* **2002**, *100*, 2793.
(161) Liu, K.; Loeser, J. G.; Elrod, M. J.; Host, B. C.; Rzepiela, J. A.; Pugliano, N.; Saykally, R. J. *J. Am. Chem. Soc.* **1994**, *116*, 3507.
(162) Millot, C.; Stone, A. J. *Mol. Phys.* **1992**, *77*, 439.
(163) Gregory, J. K.; Clary, D. C. *J. Chem. Phys.* **1995**, *102*, 7817.
(164) Gregory, J. K.; Clary, D. C. *Chem. Phys. Lett.* **1995**, *237*, 39.
(165) Gregory, J. K.; Clary, D. C. *J. Chem. Phys.* **1996**, *105*, 6626.
(166) Gonzalez, L.; Mó, O.; Yanez, M.; Elguero, J. *J. Mol. Struct.: THEOCHEM* **1996**, *371*, 1.
(167) Jung, J. O.; Gerber, R. B. *J. Chem. Phys.* **1996**, *105*, 10332.
(168) Tu, Y. Q.; Laaksonen, A. *Chem. Phys. Lett.* **2000**, *329*, 283.
(169) Liedl, K. R.; Kroemer, R. T. *J. Phys. Chem. A* **1998**, *102*, 1832.
(170) Nielsen, I. M. B.; Seidl, E. T.; Janssen, C. L. *J. Chem. Phys.* **1999**, *110*, 9435.
(171) Milet, A.; Moszynski, R.; Wormer, P. E. S.; van der Avoird, A. *J. Phys. Chem. A* **1999**, *103*, 6811.
(172) Tachikawa, M.; Iguchi, K. *J. Chem. Phys.* **1994**, *101*, 3062.
(173) Tachikawa, M. *Mol. Phys.* **2002**, *100*, 881.
(174) Burnham, C. J.; Xantheas, S. S. *J. Chem. Phys.* **2002**, *116*, 1479.
(175) Xantheas, S. S.; Burnham, C. J.; Harrison, R. J. *J. Chem. Phys.* **2002**, *116*, 1493.
(176) Bunker, P. R.; Jensen, P. *Molecular Symmetry and Spectroscopy*, 2nd ed.; NRC Research Press: Ottawa, 1998.
(177) Dyke, T. R. *J. Chem. Phys.* **1977**, *66*, 492.
(178) Loeser, J. G.; Schmuttenmaer, C. A.; Cohen, R. C.; Elrod, M. J.; Steyert, D. W.; Saykally, R. J.; Bumgarner, R. E.; Blake, G. A. *J. Chem. Phys.* **1992**, *97*, 4727.
(179) Liu, K.; Brown, M. G.; Viant, M. R.; Cruzan, J. D.; Saykally, R. J. *Mol. Phys.* **1996**, *89*, 1373.
(180) Balasubramanian, K.; Dyke, T. R. *J. Phys. Chem.* **1984**, *88*, 4688.
(181) Sorenson, J. M.; Gregory, J. K.; Clary, D. C. *Chem. Phys. Lett.* **1996**, *263*, 680.
(182) Viant, M. R.; Cruzan, J. D.; Lucas, D. D.; Brown, M. G.; Liu, K.; Saykally, R. J. *J. Phys. Chem. A* **1997**, *101*, 9032.
(183) Karyakin, E. N.; Fraser, G. T.; Lovas, F. J.; Suenram, R. D.; Fujitake, M. *J. Chem. Phys.* **1995**, *102*, 1114.
(184) Laurie, V. W. *Acc. Chem. Res.* **1970**, *3*, 331.
(185) Harris, D. O.; Engerholm, G. G.; Tolman, C. A.; Luntz, A. C.; Keller, R. A.; Kim, H.; Gwinn, W. D. *J. Chem. Phys.* **1969**, *50*, 2438.
(186) Lister, D. G.; MacDonald, J. N.; Owen, N. L. *Internal Rotation and Inversion: An Introduction to Large Amplitude Motions in Molecules*; Academic Press: San Francisco, 1978.
(187) Klopper, W.; Schütz, M. *Chem. Phys. Lett.* **1995**, *237*, 536.
(188) Sabo, D.; Bacic, Z.; Bürgi, T.; Leutwyler, S. *Chem. Phys. Lett.* **1995**, *244*, 283.
(189) Sabo, D.; Bacic, Z.; Graf, S.; Leutwyler, S. *Chem. Phys. Lett.* **1996**, *261*, 318.
(190) Blume, D.; Whaley, K. B. *J. Chem. Phys.* **2000**, *112*, 2218.
(191) Viant, M. R.; Brown, M. G.; Cruzan, J. D.; Saykally, R. J.; Geleijns, M.; van der Avoird, A. *J. Chem. Phys.* **1999**, *110*, 4369.
(192) Keutsch, F. N.; Saykally, R. J.; Wales, D. J. *J. Chem. Phys.* **2002**, *117*, 8823.
(193) Geleijns, M.; van der Avoird, A. *J. Chem. Phys.* **1999**, *110*, 823.
(194) Liedl, K. R.; Sekusak, S.; Kroemer, R. T.; Rode, B. M. *J. Phys. Chem. A* **1997**, *101*, 4707.
(195) Loerting, T.; Liedl, K. R.; Rode, B. M. *J. Chem. Phys.* **1998**, *109*, 2672.
(196) Hermansson, K.; Knuts, S.; Lindgren, J. *J. Chem. Phys.* **1991**, *95*, 7486.
(197) Huisken, F.; Kaloudis, M.; Kulcke, A. *J. Chem. Phys.* **1996**, *104*, 17.
(198) van Duijneveldt-van de Rijdt, J. G. C. M.; van Duijneveldt, F. B. *Chem. Phys.* **1993**, *175*, 271.
(199) Masella, M.; Flament, J. P. *Chem. Phys. Lett.* **1998**, *286*, 177.
(200) Coker, D. F.; Watts, R. O. *J. Phys. Chem.* **1987**, *91*, 2513.
(201) Low, G. R.; Kjaergaard, H. G. *J. Chem. Phys.* **1999**, *110*, 9104.
(202) Althorpe, S. C.; Clary, D. C. *J. Chem. Phys.* **1995**, *102*, 4390.
(203) van Thiel, M.; Becker, E. D.; Pimentel, G. C. *J. Chem. Phys.* **1957**, *27*, 486.
(204) Tursi, A. J.; Nixon, E. R. *J. Chem. Phys.* **1970**, *52*, 1521.
(205) Mann, B.; Neikes, T.; Schmidt, E.; Luck, W. A. P. *Ber. Bunsen.-Ges. Phys. Chem.* **1974**, *78*, 1236.
(206) Huong, P. V.; Cornut, J.-C. *J. Chim. Phys. PCB* **1975**, *72*, 534.
(207) Ayers, G. P.; Pullin, A. D. E. *Spectrochim. Acta A* **1976**, *32*, 1629.
(208) Fredin, L.; Nelander, B.; Ribbegard, G. *J. Chem. Phys.* **1977**, *66*, 4065.
(209) Bentwood, R. M.; Barnes, A. J.; Orville-Thomas, W. J. *J. Mol. Spectrosc.* **1980**, *84*, 391.
(210) Manceron, L.; Loutellier, A.; Perchard, J. P. *Chem. Phys.* **1985**, *92*, 75.
(211) Tso, T.-L.; Lee, E. K. C. *J. Phys. Chem.* **1985**, *89*, 1612.
(212) Engdahl, A.; Nelander, B. *J. Chem. Phys.* **1987**, *86*, 4831.
(213) Engdahl, A.; Nelander, B. *J. Mol. Struct.* **1989**, *193*, 101.
(214) Fajardo, M. E.; Tam, S. *J. Chem. Phys.* **2001**, *115*, 6807−6810.
(215) MacGillivray, L. R.; Atwood, J. L. *J. Am. Chem. Soc.* **1997**, *119*, 2592.
(216) Fröchtenicht, R.; Kaloudis, M.; Koch, M.; Huisken, F. *J. Chem. Phys.* **1996**, *105*, 6128.
(217) Nauta, K.; Miller, R. E. *Science* **2000**, *287*, 293.
(218) Suzuki, S.; Blake, G. A. *Chem. Phys. Lett.* **1994**, *229*, 499.
(219) Liu, K.; Elrod, M. J.; Loeser, J. G.; Cruzan, J. D.; Pugliano, N.; Brown, M. G.; Rzepiela, J.; Saykally, R. J. *Faraday Discuss.* **1994**, *97*, 35.
(220) Brown, M. G.; Viant, M. R.; McLaughlin, R. P.; Keoshian, C. J.; Michael, E.; Cruzan, J. D.; Saykally, R. J.; Geleijns, M.; van der Avoird, A. *J. Chem. Phys.* **1999**, *111*, 7789.
(221) Keutsch, F. N.; Karyakin, E. N.; Saykally, R. J.; van der Avoird, A. *J. Chem. Phys.* **2001**, *114*, 3988.
(222) Keutsch, F. N.; Fellers, R. S.; Viant, M. R.; Saykally, R. J. *J. Chem. Phys.* **2001**, *114*, 4005.
(223) Keutsch, F. N.; Brown, M. G.; Petersen, P. B.; Saykally, R. J.; Geleijns, M.; van der Avoird, A. *J. Chem. Phys.* **2001**, *114*, 3994.
(224) Brown, M. G.; Keutsch, F. N.; Braly, L. B.; Saykally, R. J. *J. Chem. Phys.* **1999**, *111*, 7801.
(225) Luzar, A.; Chandler, D. *Phys. Rev. Lett.* **1996**, *76*, 928.
(226) Luzar, A.; Chandler, D. *Nature* **1996**, *379*, 55.
(227) Xantheas, S. S. Personal communication.
(228) Keutsch, F. N.; Fellers, R. S.; Brown, M. G.; Viant, M. R.; Petersen, P. B.; Saykally, R. J. *J. Am. Chem. Soc.* **2001**, *123*, 5938.
(229) Vernon, M. F.; Krajnovich, D. J.; Kwok, H. S.; Lisy, J. M.; Shen, Y. R.; Lee, Y. T. *J. Chem. Phys.* **1982**, *77*, 47.
(230) Page, R. H.; Frey, J. G.; Shen, Y. R.; Lee, Y. T. *Chem. Phys. Lett.* **1984**, *106*, 373.
(231) Coker, D. F.; Miller, R. E.; Watts, R. O. *J. Chem. Phys.* **1985**, *82*, 3554.
(232) Wuelfert, S.; Herren, D.; Leutwyler, S. *J. Chem. Phys.* **1987**, *86*, 3751.
(233) Paul, J. B.; Provencal, R. A.; Chapo, C.; Roth, K.; Casaes, R.; Saykally, R. J. *J. Phys. Chem. A* **1999**, *103*, 2972.
(234) Paul, J. B.; Provencal, R. A.; Chapo, C.; Petterson, A.; Saykally, R. J. *J. Chem. Phys.* **1998**, *109*, 10201.
(235) Paul, J. B.; Collier, C. P.; Saykally, R. J.; Scherer, J. J.; O'Keefe, A. *J. Phys. Chem. A* **1997**, *101*, 5211.

(236) Scherer, J. J.; Voelkel, D.; Rakestraw, D. J.; Paul, J. B.; Collier, C. P.; Saykally, R. J.; O'Keefe, A. *Chem. Phys. Lett.* **1995**, *245*, 273.
(237) Dykstra, C. E. *Chem. Phys. Lett.* **1999**, *299*, 132.
(238) Arunan, E.; Emilsson, T.; Gutowsky, H. S. *J. Am. Chem. Soc.* **1994**, *116*, 8418.
(239) Pribble, R. N.; Zwier, T. S. *Faraday Discuss.* **1994**, *97*, 229.
(240) Fredericks, S. Y.; Pedulla, J. M.; Jordan, K. D.; Zwier, T. S. *Theor. Chem. Acc.* **1997**, *96*, 51.
(241) Gruenloh, C. J.; Carney, J. R.; Arrington, C. A.; Zwier, T. S.; Fredericks, S. Y.; Jordan, K. D. *Science* **1997**, *276*, 1678.
(242) Gruenloh, C. J.; Carney, J. R.; Hagemeister, F. C.; Arrington, C. A.; Zwier, T. S.; Fredericks, S. Y.; Wood, J. T.; Jordan, K. D. *J. Chem. Phys.* **1998**, *109*, 6601.
(243) Gruenloh, C. J.; Carney, J. R.; Hagemeister, F. C.; Zwier, T. S.; Wood, J. T.; Jordan, K. D. *J. Chem. Phys.* **2000**, *113*, 2290.
(244) Barth, H.-D.; Buchhold, K.; Djafari, S.; Reimann, B.; Lommatzsch, U.; Brutschy, B. *Chem. Phys.* **1998**, *239*, 49.
(245) Tarakeshwar, P.; Kim, K. S.; Brutschy, B. *J. Chem. Phys.* **2001**, *114*, 1295.
(246) Palmer, P. M.; Chen, Y.; Topp, M. R. *Chem. Phys. Lett.* **2000**, *325*, 568.
(247) Maxton, P. M.; Schaeffer, M. W.; Felker, P. M. *Chem. Phys. Lett.* **1995**, *241*, 603.
(248) Gruenloh, C. J.; Hagemeister, F. C.; Carney, J. R.; Zwier, T. S. *J. Phys. Chem. A* **1999**, *103*, 503.
(249) Carney, J.; Zwier, T. S. *J. Phys. Chem. A* **1999**, *103*, 9943.
(250) Leutwyler, S.; Bürgi, T.; Schütz, M.; Taylor, A. *Faraday Discuss.* **1994**, *97*, 285.
(251) Roth, W.; Schmitt, M.; Jacoby, C.; Spangenberg, D.; Janzen, C.; Kleinermanns, K. *Chem. Phys.* **1998**, *239*, 1.
(252) Watanabe, T.; Ebata, T.; Tanabe, S.; Mikami, N. *J. Chem. Phys.* **1996**, *105*, 408.
(253) Connell, L. L.; Ohline, S. M.; Joireman, P. W.; Corcoran, T. C.; Felker, P. M. *J. Chem. Phys.* **1991**, *94*, 4668.
(254) Yoshino, R.; Hashimoto, K.; Omi, T.; Ishiuchi, S.-I.; Fujii, M. *J. Phys. Chem. A* **1998**, *102*, 6227.
(255) Matsumoto, Y.; Ebata, T.; Mikami, N. *J. Chem. Phys.* **1998**, *109*, 6303.
(256) Kisiel, Z.; Bialkowska-Jaworska, E.; Pszczólkowski, L.; Milet, A.; Struniewicz, C.; Moszynski, R.; Sadlej, J. *J. Chem. Phys.* **2000**, *112*, 5767.
(257) Struniewicz, C.; Korona, T.; Moszynski, R.; Milet, A. *Chem. Phys. Lett.* **2001**, *343*, 588.
(258) Wormer, P. E. S.; Groenenboom, G. C.; van der Avoird, A. *J. Chem. Phys.* **2001**, *115*, 3604.
(259) Packer, M. J.; Clary, D. C. *J. Phys. Chem.* **1995**, *99*, 14323.
(260) Florio, G. M.; Gruenloh, C. J.; Quimpo, R. C.; Zwier, T. S. *J. Chem. Phys.* **2000**, *113*, 11143.
(261) Bach, A.; Leutwyler, S. *Chem. Phys. Lett.* **1999**, *299*, 381.
(262) Zwier, T. S. *J. Phys. Chem. A* **2001**, *105*, 8827.
(263) Leforestier, C.; Gatti, F.; Fellers, R. S.; Saykally, R. J. *J. Chem. Phys.* **2002**, *117*, 8710.
(264) Benedict, W. S.; Gailar, N.; Pyler, E. K. *J. Chem. Phys.* **1956**, *24*, 1139.
(265) Reimers, J. R.; Watts, R. O. *Chem. Phys.* **1984**, *85*, 83.
(266) Wales, D. J.; Hodges, M. P. *Chem. Phys. Lett.* **1998**, *286*, 65.
(267) Lee, H. M.; Suh, S. B.; Lee, J. Y.; Tarakeshwar, P.; Kim, K. S. *J. Chem. Phys.* **2000**, *112*, 9759.
(268) Forney, D.; Jacox, M. E.; Thompson, W. E. *J. Mol. Spectrosc.* **1993**, *157*, 479.
(269) Herzberg, G. *Infrared and Raman spectra of polyatomic molecules*; Van Nostrand: New York, 1945.
(270) Ayotte, P.; Weddle, G. H.; Johnson, M. A. *J. Chem. Phys.* **1999**, *110*, 7129.
(271) Sakai, M.; Daigoku, K.; Ishiuchi, S.-I.; Saeki, M.; Hashimoto, K.; Fujii, M. *J. Phys. Chem. A* **2001**, *105*, 8651.

CR980125A